# The past and present trace metal budget of the Black Sea –

# A comparison of the Holocene and Eemian marine ingression

An der Fakultät für Mathematik und Naturwissenschaften

der Carl von Ossietzky Universität Oldenburg

zur Erlangung des Grades und Titels eines

Doktors der Naturwissenschaften (Dr. rer. nat.)

angenommene Dissertation

von Herrn Dipl.-Chem.

Sebastian Eckert

geboren am 22. August 1982 in Delmenhorst

Oldenburg, den 11.07.2014

Gutachter: Prof. Dr. Hans-Jürgen Brumsack
Zweitgutachter: Prof. Dr. Stefan Weyer
Tag der Disputation: 14.02.2014

# Abstract

The paleoenvironmental evolution of the Black Sea is closely linked to the ingression of Mediterranean seawater over the Bosporus sill after the Last Glacial Maximum. But this is not only true for the Holocene, but also for the Eemian interglacial.

In this work the temporal and spatial development of anoxic conditions in the Black Sea during both warm periods is reconstructed for the first time.

The rise of the Holocene suboxic chemocline, which divides oxic surface water from anoxic, sulfidic (euxinic) deep water was reconstructed by combining high-resolution geochemical records of bulk parameters (carbonate, total organic carbon, sulfur), redox-sensitive trace metals (e.g. Co, Cr, Cu, Fe, Mo, Ni, U and V), and an isotopic proxy ($\delta^{56}$Fe) from seven Holocene sediment cores in the Black Sea. Based on these data a single composite geochemical core log of the sapropelic sediment record was generated that serves as a reference archive for the entire basin. The Holocene proxy records reflect the changing depositional and redox conditions of the Black Sea and indicate a gradual rise of the chemocline until ca. 5.3 ka, when it reached the shelf. Trace metal and isotopic inventories document one major descent of the chemocline since the onset of brackish/marine conditions before the present stable situation was established.

A second composite geochemical profile was established for the Eemian interglacial on basis of geochemical data of two Eemian sapropels. In addition to the Holocene set of parameters, more isotopic proxies ($\delta^{97}$Mo, $\delta^{238}$U, $\delta^{13}$C) and organic markers for photic zone euxinia (isorenieratene derivatives) were determined for these samples. The Eemian proxy records indicate that anoxic to euxinic conditions persisted in the Black Sea basin during that time interval, too. Trace metal enrichments suggest a slightly different paleoenvironmental setting during both time periods, but a lithological classification analogous to the accepted unit classification of the Holocene sapropel could be developed. $\delta^{238}$U and $\delta^{97}$Mo values indicate an anoxic but not fully euxinic environment during the Eemian interglacial, while a euxinic water column has been established since the Holocene.

This study implies that episodes of repeated Black Sea sapropel formation are linked to interglacial periods and reflect the global sea level rise. Proxy records document the

ingression of Mediterranean seawater over the Bosporus sill into the basin, which caused the onset and gradual rise of the chemocline during both interglacials.

# Kurzfassung

Die Evolution der Umweltbedingungen des Schwarzen Meeres hängt stark von dem einfließenden Mittelmeerwasser ab, das seit dem Ende des letzten Hochglazials über den Bosporus in das Becken des Schwarzen Meeres fließt. Diese gilt nicht nur für das Holozän, sondern ebenso für die Eem-Warmzeit.

In dieser Arbeit wird zum ersten Mal die zeitliche und räumliche Entwicklung der anoxischen Bedingungen im Schwarzen Meer während beider Warmzeiten rekonstruiert.

Der Anstieg der holozänen suboxischen Chemokline, die das oxische Oberflächenwasser vom anoxischen (euxinischen) Tiefenwasser trennt, wurde anhand einer hochauflösenden, geochemischen Multiproxy-Analyse rekonstruiert. Hierfür wurden Summenparameter (Carbonat, gesamter organischer Kohlenstoff, Schwefel), redoxsensitive Spurenmetalle (z.B. Co, Cr, Cu, Fe, Mo, Ni, U und V) und das Fe-Isotopenverhältnis ($\delta^{56}$Fe) von sieben Sedimentkernen aus dem Holozänen Schwarzen Meer genutzt. Anhand dieser Daten konnte ein einheitliches geochemisches Sedimentprofil der Sapropelschichten generiert werden, das als Referenz für das gesamte anoxische Becken des Schwarzen Meeres dienen kann. Die holozänen Proxy-Daten reflektieren die sich ändernden Ablagerungs- und Redoxbedingungen im Schwarzen Meer und zeichnen den kontinuierlichen Anstieg der Chemokline bis vor ca. 5.300 Jahren mit dem Erreichen des Schelfs nach. Das Spurenmetall- und Fe-Isotopeninventar dokumentiert eine bedeutende Phase des Absinkens der Chemokline während des späten Holozäns, bevor nach dem Wiederanstieg der heutige stabile Zustand erreicht wurde.

Ein zweites geochemisches Profil des Eem-Sapropels aus dem letzten Interglazial konnte anhand der geochemischen Daten von zwei Sedimentkernen generiert werden. Zusätzlich zu bereits in den holozänen Proben bestimmten Parametern wurden weitere Isotopenverhältnisse ($\delta^{97}$Mo, $\delta^{238}$U, $\delta^{13}$C) und organische Biomarker (Isorenieratenderivate) bestimmt. Die Proxy-Daten im Eem-Sapropel zeigen, dass in diesem Zeitintervall ebenfalls anoxische Bedingungen und vergleichbare Elementanreicherung wie im Holozän vorherrschten. Spurenmetall-Anreicherungen legen eine leicht verschiedene Entwicklung der Ablagerungsbedingungen nahe.

Trotzdem konnte eine lithologische Charakterisierung der Eem-Sedimente, analog zu der im Holozän erfolgen. $\delta^{238}$U- und $\delta^{97}$Mo-Werte weisen auf etwas schwächere euxinische Bedingungen in der Wassersäule im Eem hin, während im Holozän voll-euxinische Bedingungen herrschen.

Diese Arbeit zeigt, dass die wiederholte Sapropelbildung im Becken des Schwarzen Meeres vom globalen Meeresspiegelanstieg in Warmzeiten gesteuert wird. Proxy-Daten dokumentieren den Einstrom von Mittelmeerwasser über den Bosporus in das Becken, durch den die Ausbildung und der graduelle Anstieg der Chemokline in beiden Warmzeiten verursacht wird.

# Inhaltsverzeichnis

# Abbildungsverzeichnis

# Tabellenverzeichnis

# 1. Einleitung

## 1.1. Motivation

Das Schwarze Meer als Lehrbuchbeispiel für ein anoxisches Becken bietet die Gelegenheit, komplexe biogeochemische Prozesse in situ zu erforschen. Seine besonderen biogeochemischen und topographischen Eigenschaften ermöglichen es Wissenschaftlern seit über sechs Jahrzehnten, die Bildung und Charakteristika von anoxischen Sedimenten und Wässern zu studieren. Das Hauptaugenmerk liegt dabei auf der Untersuchung der Sapropele. Diese organikreichen Sedimente stellen ein rezentes Analogon zu den mit Kohlenstoff angereicherten Schwarzschiefer-Vorkommen dar.

Anhand dieser Sapropele können sowohl primäre biogeochemische Prozesse in der Wassersäule als auch diagenetische Reaktionen in der Sedimentsäule rekonstruiert werden. In den rezenten Sapropelen, welche als geologisches Archiv genutzt werden können, findet sich die Geschichte des Übergangs des Schwarzen Meeres von einem abgeschlossenen, limnischen See zu dem jetzigen Binnenmeer.

Der Fokus dieser Arbeit liegt aber nicht nur auf der rezenten Geschichte des Schwarzen Meeres, welche in der Literatur schon mehrfach beschrieben wurde, sondern auf der geochemischen Rekonstruktion des vorherigen Interglazials, des Eem, und dem bisher noch nicht durchgeführten Vergleich der beiden Interglaziale für das Schwarze Meer. Von besonderem Interesse sind dabei die generelle geochemische Zusammensetzung der Eem-Sedimente sowie die Prozesse die zu der Bildung des Eem-Sapropels geführt haben.

Durch einen Vergleich des Holozän- und des Eem-Sapropels auf geochemischer Ebene können aus dem geologischen Archiv des vorherigen Interglazials Rückschlüsse für die jetzige Epoche gewonnenen werden.

## 1.2. Fragestellung

In dieser Arbeit sollen die Unterschiede und Gemeinsamkeiten zwischen dem jetzigen Holozän-Interglazial und dem vorangegangen Eem-Interglazial anhand von Sedimenten aus dem Schwarzen Meer auf geochemischer Ebene beleuchtet werden.

Hierzu wurden von den hier bearbeiteten acht Sedimentkernen, insbesondere von den Sapropelschichten, fast durchgängig und hochauflösend Proben entnommen und auf Haupt- und Spurenmetallgehalte analysiert. An ausgewählten Proben wurden die Isotopensignaturen von Eisen, Molybdän und Uran bestimmt. Zusätzlich wurden spezielle Biomarker (Isorenieratanderivate) an ausgewählten Proben gemessen.

Die Hauptfragen mit denen sich diese Arbeit beschäftigt sind: Wie sahen die Paläoumweltbedingungen während der beiden Warmzeiten auf geochemischer Ebene aus und sind sie vergleichbar? An welche Prozesse im Sediment und/oder in der Wassersäule sind diese Paläoumweltbedingungen gekoppelt und haben sie sich im Laufe der Jahrtausende verändert? Waren die Mechanismen, die zu einer Verbindung des Schwarzen Meeres mit dem Mittelmeer und damit mit den Weltozeanen geführt haben, dieselben oder gab es Unterschiede? Wie haben sich diese jeweiligen Verbindungen auf das Metallbudget des Sediments ausgewirkt?

Um diese Fragen beantworten zu können, wurden zuerst die Sapropele des Holozäns untersucht, da sie in der Literatur besser bekannt sind. Die Erkenntnisse zu Ablagerungs- und Bildungsprozessen wurden dann auf den bisher unbekannten Eem-Sapropel übertragen, nachdem dieser geochemisch klassifiziert wurde, um dadurch den Vergleich der beiden Interglaziale zu ermöglichen.

Ein wichtiger Unterpunkt ist hierbei der Prozess der hinter den authigenen Eisenanreicherungen im Sediment steht. Um diesen Punkt beantworten zu können, wurde der rezente Sapropel auf Haupt- und Spurenelemente analysiert, insbesondere auf die Elemente, welche mit Eisensulfiden assoziiert sind. Zudem wurden $\delta^{56/54}$Fe Werte bestimmt, um die chemische Herkunft (authigen/lithogen) der Eisengehalte zu präzisieren.

Die geochemischen Bedingungen innerhalb des Sediments zur Zeit dessen Ablagerung wurden durch verschiedene redoxsensitive Elemente (Fe, Mo, Re, U) und (teilweise) deren Isotope (Mo, U) rekonstruiert. Anhand von Molybdän-Anreicherungen können Einflussraten von Meerwasser in das limnische Schwarze Meer zu Beginn beider Warmzeiten abgeschätzt werden.

Diese Herangehensweise garantiert einen optimalen Vergleich beider Interglaziale auf geochemischer Ebene und ergänzt die bisherigen Erkenntnisse über das Verhalten von

Spurenmetallen in anoxischen Systemen, sowohl in rezenten (Ostsee-Tiefs, Mittelmeer, Cariaco Graben, Fjorde) als auch in fossilen Ablagerungen (Schwarzschiefer).

## 1.3. Das Schwarze Meer

### 1.3.1. Bathymetrie und Hydrologie

Das Schwarze Meer ist ein zwischen Osteuropa und Vorderasien gelegenes Binnenmeer (Abb. 1-1). Die einzige Verbindung des Schwarzen Meeres zum Atlantischen Ozean verläuft über den Bosporus, das Marmarameer, die Dardanellen und das Mittelmeer. Gespeist wird das Schwarze Meer durch mehrere Flüsse, darunter Donau, Dnepr, Don, Dnister, Kizilirmak, Yesilirmak und Sakarya. Das Volumen des Schwarzen Meeres beträgt 423.000 $km^3$ bei einer maximalen Tiefe von 2.206 m und einer Fläche von 534.000 $km^2$ (alle Angaben ohne Einbeziehung des Asowschen Meeres; ROSS et al., 1974). Der Anteil der Schelffläche beträgt dabei 30 % gegenüber 43 % für den Anteil des tiefen Beckens (DEGENS and ROSS, 1974). Die restlichen 27 % werden von den Hangflächen eingenommen. Die anoxische Wassersäule nimmt 73 % der Fläche und 90 % des Volumens ein (DEGENS and ROSS, 1974; WIJSMAN et al., 2001), das Schwarze Meer ist somit das größte anoxische Becken der Erde. Es besitzt zudem eine positive Wasserbilanz, da sich die Einträge über Flüsse (352 $km^3/a$), den Bosporus (305 $km^2/a$) und die Niederschläge (300 $km^2/a$) mit der Evaporation (353 $km^3/a$) und dem Ausströmen von Oberflächenwasser über den Bosporus (605 $km^3/a$) fast ausgleichen (ÖZSOY and ÜNLÜATA, 1997). Ein besonderes Merkmal des Schwarzen Meeres ist seine stratifizierte Wassersäule, mit anoxischem, sulfidhaltigem (euxinischem) Tiefenwasser und oxischem Oberflächenwasser. Diese beiden Wassermassen werden durch die sogenannte Chemokline getrennt, das ist eine 20-50 m starke suboxische Sprungschicht in ca. 150 m Wassertiefe (HUANG et al., 2000). Die Chemokline ist gleichzeitig auch eine Pyknokline (Dichtesprungschicht), welche das dichtere und höher salinare Tiefenwasser (Salinität von ca. 22) von dem brackischen Oberflächenwasser (Salinität von ca. 17) trennt (MURRAY et al., 1991). Diese Dichtesprungschicht verhindert die Durchmischung von sauerstoffreichem Oberflächenwasser mit dem darunterliegenden Tiefenwasser, was zu einem Sauerstoffdefizit führt und letztendlich zu den jetzigen anoxischen Bedingungen unterhalb der Chemokline.

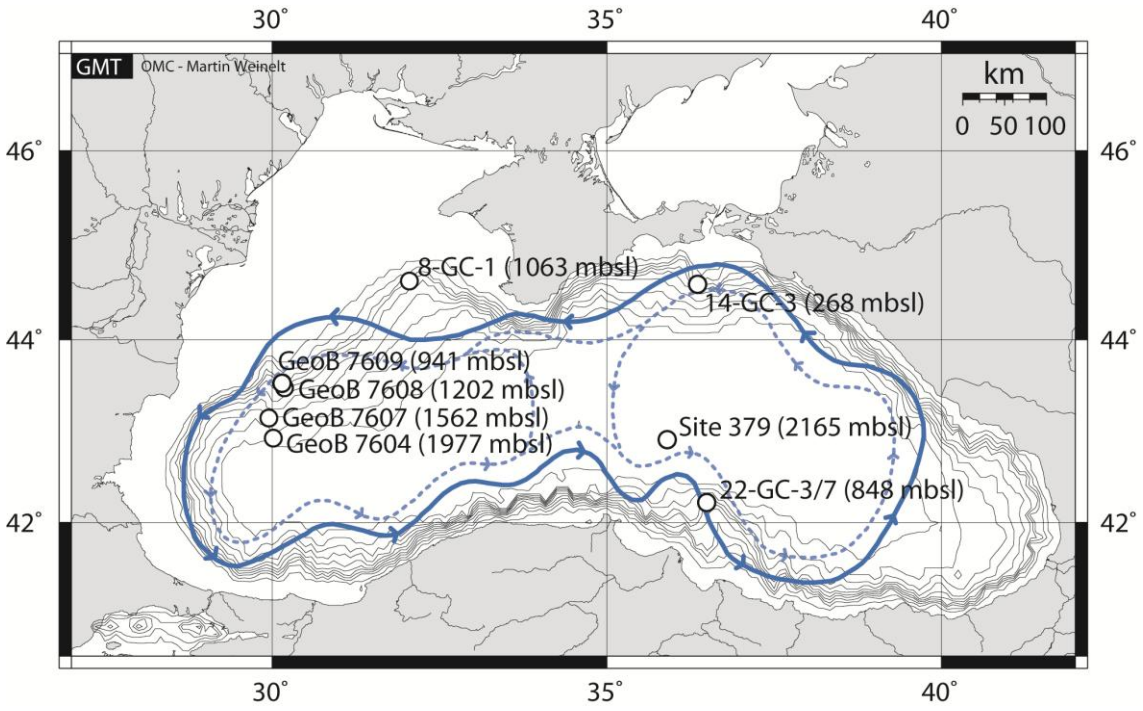


**Abb. 1-1** Karte des Schwarzen Meeres mit Kernlokationen
Tiefenangaben in meters below sea level (mbsl). In blau sind der Randstrom und der westliche sowie östliche Wirbelstrom (gestrichelt) eingezeichnet.

Die Strömungsverhältnisse im Schwarzen Meer werden hauptsächlich von einem 50 km breiten, zyklonalen Randstrom (engl. Rim Current) bestimmt (Abb. 1-1). Dieser Randstrom wird unterteilt in zwei große Wirbelströmungen (engl. gyre), den westlichen und den östlichen Wirbel. An seinen äußeren Rändern ist der Randstrom mit einer Vielzahl von kleineren, antizyklonalen Wirbeln (engl. eddies) verbunden, welche die Strömungsverhältnisse an den Küstengebieten maßgeblich beeinflussen (ÖZSOY and ÜNLÜATA, 1997). Angetrieben werden diese Strömungen durch ein Zusammenspiel von Wind, thermohaliner Zirkulation, Flusseinstrom, Meerwassereinstrom über den Bosporus und dem so genannten „Jebar“ Effekt, welcher den Einfluss von Baroklinität und lokaler Topographie auf die Strömung beschreibt (STANEV, 1990).

### 1.3.2. Lithostratigraphie

Die Lithostratigraphie der Sedimente, welche im Schwarzen Meer während des Holozäns abgelagert wurden, wird in drei Abschnitte (engl. unit) unterteilt (ROSS and DEGENS, 1974). Die Charakterisierung der einzelnen Units basiert hauptsächlich auf dem Verhältnis von organischem Kohlenstoff (engl. total organic carbon; TOC) und Carbonat ($CaCO_3$), welche noch durch die Sedimentfarbe und Schichtung ergänzt

werden und im Folgenden beschrieben wird (ARTHUR and DEAN, 1998; ARTHUR et al., 1994; HAY et al., 1991; JONES and GAGNON, 1994; ROSS and DEGENS, 1974).

Unit III ist die älteste Sedimentschicht des Holozäns. Der Ablagezeitraum umfasst das gesamte Weichsel-Glazial, wie die letzte Eiszeit in Nord- und Mitteleuropa genannt wurde (vgl. mit Würm-Glazial für den Alpenraum), und das frühe Holozän. Unit III besteht zum Hauptteil aus limnischen Tonsedimenten mit einem TOC-Gehalt kleiner 1 % und einem Carbonat-Gehalt kleiner 20 %, welche diagenetisch von schwarzen Eisensulfiden überprägt wurden. Die zeitliche Grenze von Unit III zu Unit II liegt im Durchschnitt bei 7.500 Jahren vor heute und ist lithostratigraphisch durch einen Wechsel von gräulichem, homogenem Sediment der Unit III zu schwarz-braun-grünem, feinlaminiertem Sediment zu erkennen. Unit II besitzt einen Carbonat-Gehalt zwischen 5 % und 15 % und ist angereichert an TOC (bis zu 20 %) und Spurenmetallen. Daher wird Unit II als Übergangssapropel von den glazialen zu den heutigen Umweltbedingungen im Schwarzen Meer klassifiziert. Unit II wird nochmals unterteilt in Unit IIa und Unit IIb, hierbei besteht der Unterschied in der dunkleren Farbe von Unit IIb, hervorgerufen durch ein TOC-Maximum. Unit IIb wird wiederum unterteilt in Unit $IIb_1$, in welcher das TOC-Maximum liegt und in Unit $IIb_2$, in welcher feine, helle Aragonit-Lagen oberhalb der Unit II/III-Grenze zu finden sind. Der Wechsel von dem Übergangssapropel (Unit II) zu dem rezenten Sapropel (Unit I) fand vor ca. 2.800 Jahren statt und ist aus lithostratigraphischer Sicht durch das Auftreten von sich abwechselnden hellen und dunklen Schichten im Submillimeter-Bereich (engl. varves) zu erkennen. Im Durchschnitt besteht Unit I aus 1-10 % TOC und 10-75 % $CaCO_3$. Dabei ist das organische Material hauptsächlich in den dunklen Tonschichten zu finden. Die hellen Lagen bestehen hauptsächlich aus biogenen Carbonaten, die aus Überresten von Hapthophyten-Schalen stammen, insbesondere von der Art *Emiliania huxleyi* aus der Ordnung der Coccolithophoriden.

Wie in Kap. 4 im Detail gezeigt wird, sind die Sedimente des Eem-Interglazials vergleichbar zu den holozänen Abschnitten aufgebaut. Analog zu Unit III beginnt das Eem mit gräulichen, homogenen Tonsedimenten-Lagen, welche der Saale- bzw. Riss-Eiszeit zugeordnet werden können und als Unit VI definiert wurden. Darüber lagert sich eine sapropelartige Sedimentschicht ab, ähnlich zu Unit I. Dieser Sapropel ist vergleichbar laminiert mit hellen, carbonatreichen Schichten (20-80 %) und schwarzen, TOC-reichen Schichten (1-10 %), welche mit Spurenmetallen angereichert sind.

### 1.4. Sapropelbildung aus geochemischer Sicht

Um solche organikreichen Sedimentschichten, wie Sapropele, ablagern und erhalten zu können, müssen bestimmte Bedingungen in der Sediment- und der darüber liegenden Wassersäule erfüllt werden. Die Abwesenheit von Sauerstoff und die dadurch verhinderte Oxidation der organischen Partikel, welche in der Wassersäule absinken, ist eine der Hauptbedingungen (DEGENS and ROSS, 1974). Aus diesem Grund sind Sapropele ein eindeutiges Indiz für eine anoxische Wassersäule. Ein zweiter, wichtiger Faktor ist eine erhöhte Zufuhr an Nährstoffen in das Oberflächenwasser und eine daraus resultierende gesteigerte Primärproduktion in der euphotischen Zone (CALVERT et al., 1987). Durch den dadurch entstehenden Überschuss an organischem Material in der Wassersäule, welches oxidiert wird, erhöht sich auch der Verbrauch an gelöstem Sauerstoff. In einem holomiktischen Becken würden diese tieferen, sauerstoffarmen Wasserschichten, welche durch die Oxidation und Remineralisierung von organischem Material an Nährstoffen angereichert sind, durch Konvektion mit sauerstoffreichem, aber nährstoffärmerem Oberflächenwasser vermischt werden. Dies führt zu einem Nährstofftransport in die oberen Wasserschichten und zu einer Oxidation der unteren Schichten. Würde diese Zirkulation gestoppt werden, würde auch die Oxidation des organischen Materials stark reduziert werden, was zu einer Ablagerung und Erhaltung im Sediment führen würde. Dies ist der Fall in einem meromiktischen Becken, in dem die Zirkulation nur den oberen Teil des Wasserkörpers betrifft und die Durchmischung der tieferen Wasserschichten verhindert wird.

Das Schwarze Meer hat einen Wechsel von einem holomiktischen zu einem meromiktischen Becken nach dem Ende des letzten Hochglazials (vor ca. 20.000 Jahren) durchlaufen. Zu Beginn des Holozäns war das Schwarze Meer ein limnischer See ohne Verbindung zum Mittelmeer (DEGENS and ROSS, 1974). Mit dem Einsetzen der globalen Erwärmung nach dem Weichsel-Glazial erhöhte sich die Zufuhr von nährstoffreichem Flusswasser in das Schwarze Meer, da die Flüsse durch das Schmelzwasser der zurückgehenden Gletscher gespeist wurden. Durch die Erhöhung der Temperatur, Sonneneinstrahlung und Nährstoffkonzentration im Oberflächenwasser konnte die Primärproduktion gesteigert werden. Das Abschmelzen der Gletscher hatte aber auch einen Anstieg des globalen Meeresspiegels zur Folge, was zu der Verbindung von Schwarzem Meer und Marmarameer, und somit zum Mittelmeer, über den Bosporus vor ca. 9.000 Jahren führte (SOULET et al., 2011).

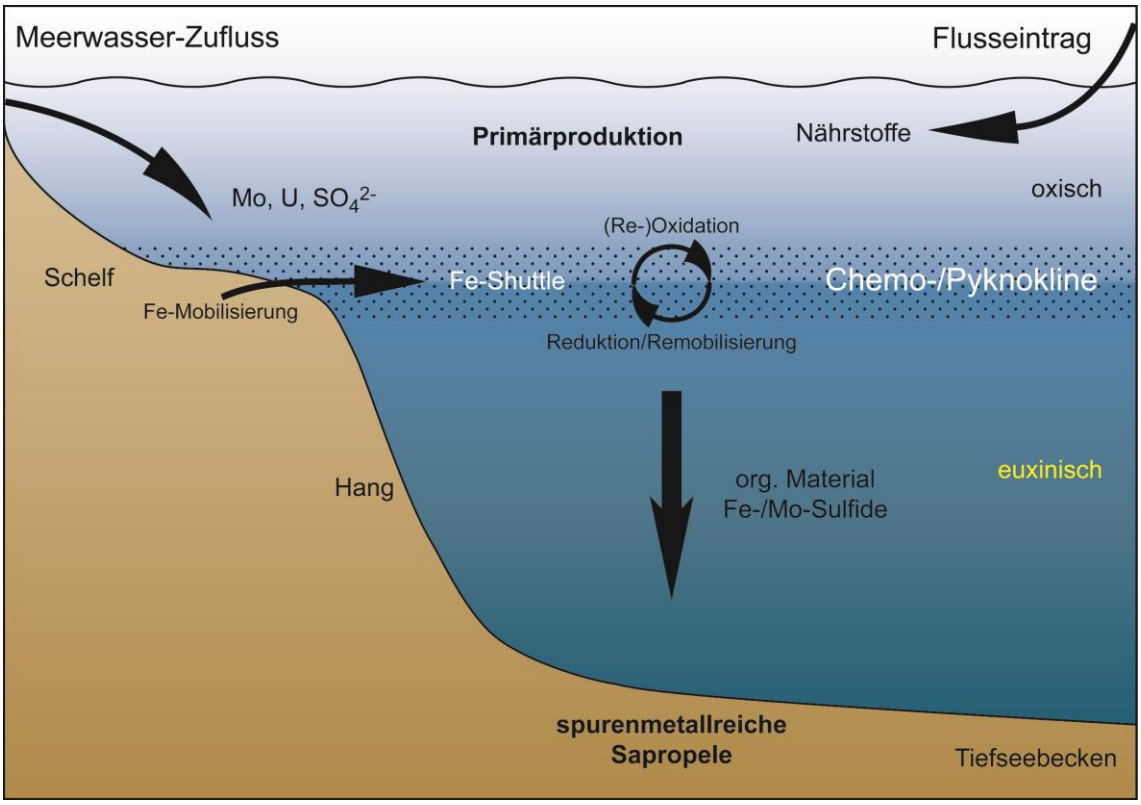


**Abb. 1-2** Schematische Darstellung der Wassersäulen-Prozesse im Schwarzen Meer.

Das einströmende Mittelmeer-Wasser hatte eine Stratifikation der Wassersäule zur Folge, da das dichtere Meerwasser sich am Boden des limnischen Beckens akkumulierte. Zwar gab es auch eine Durchmischung der marinen und limnischen Wasserkörper, welche zu den heutigen brackischen Bedingungen im Oberflächenwasser führte, aber die Ausbildung einer Pyknokline nahm mit der Menge an einströmendem Meerwasser zu (Abb. 1-2). Diese Pyknokline verhindert den Austausch von sauerstoffreichem Oberflächenwasser mit dem Tiefenwasser (DEGENS and ROSS, 1974). Die Kombination aus erhöhter Produktivität in der euphotischen Zone und der Stratifikation der Wassersäule erhöht das Erhaltungspotential des organischen Materials unterhalb der Pyknokline, da der Sauerstoff bei der Oxidation des organischen Materials verbraucht wird und nicht erneuert werden kann (Abb. 1-2). Aufgrund des Fehlens von gelöstem Sauerstoff als Elektronendonor verliert die aerobe Atmung zunehmend an Bedeutung bei der Remineralisierung des organischen Materials und mikrobiell-induzierte anaerobe Prozesse wie die Denitrifikation, Mangan-, Eisen- und Sulfat-Reduktion, sowie die Methanogenese treten mehr in den Vordergrund (FROELICH et al., 1979). Die Produkte dieser anaeroben Prozesse, insbesondere die bei der Sulfat-Reduktion entstehenden Sulfide, sorgen für eine massive Änderung der Wasserchemie

unterhalb der Pyknokline und spielen für die chemische Zusammensetzung der Sapropele eine entscheidende Rolle. Das sulfatreiche, marine Tiefenwasser bietet eine ausreichende Quelle an Substrat für die sulfatreduzierenden Bakterien, welche für die Anreicherung von gelöstem Sulfid in dem Tiefenwasser verantwortlich sind. Die durch die Trennung des oxischen Oberflächenwassers von dem anoxischen, sulfidreichen (euxinischen) Tiefenwasser ausgebildete Chemokline fällt mit der Pyknokline zusammen (Abb. 1-2). Die Chemokline dient als Übergangsphase von oxischen Bedingungen an der oberen Grenze zu euxinischen Bedingungen an der unteren Grenze (MURRAY et al., 1989).

Die Position der Chemokline und somit der anoxische Anteil des Schwarzen Meeres in der Wassersäule ist variabel mit der Zeit und kann anhand von Eisenanreicherungen in den Sapropelen des tiefen Beckens rekonstruiert werden, da in dieser Grenzschicht auch der so genannte „Eisen-Shuttle“ aktiv ist (LYONS and SEVERMANN, 2006; Abb. 1-2). Dieser Shuttle sorgt für den lateralen Transport von Eisen von den Schelfgebieten ins Beckeninnere, indem das im Sediment mikrobiell bzw. abiotisch reduzierte Eisen ($Fe^{2+}_{aq}$) in dem suboxischen Milieu der Chemokline gelöst bleibt (ANDERSON and RAISWELL, 2004; LEWIS and LANDING, 1991; LYONS and SEVERMANN, 2006; WIJSMAN et al., 2001; WILKIN et al., 1997). Dieses gelöste Eisen wird an der oberen Grenze zu Eisen(oxyhydr)oxiden oxidiert, welche ausfallen und in die suboxische Zone absinken, wo sie wieder reduziert und gelöst werden. Bilden sich größere Eisen(oxyhydr)oxid-Partikel können sie durch die suboxische Zone sinken und reagieren in den euxinschen Bedingungen zu Eisensulfiden, welche ausfallen und sich im Sediment ablagern. Parallel kann $Fe^{2+}_{aq}$ aus der Chemokline nach unten diffundieren und im sulfidischen Bereich ebenfalls Eisensulfid-Partikel bilden. Bei der Ablagerung von solchen authigenen Eisensulfiden werden auch andere sulfidbildende Spuren- und Schwermetalle (z.B. As, Co, Cu, Mo, Ni) mit gefällt (HUERTA-DIAZ and MORSE, 1992). Die Fällungsreaktionen (engl. scavening) führen zu einer starken Anreicherung von Spurenmetallen in den Sapropelen gegenüber dem geogenen Hintergrund.

Die stärkste Anreicherung in den Sedimenten des Schwarzen Meeres weist Molybdän auf, welches bis zu 100-fach gegenüber dem mittleren Tonschiefer (engl. average shale; AS) und der oberen, kontinentalen Kruste (engl. upper continental crust; UCC) angereichert ist, welche zur Vereinfachung den komplexen geogenen Hintergrund des Schwarzen Meeres repräsentieren. Solche hohen Anreicherungsfaktoren für Molybdän

dienen als Indikator für euxinische Bedingungen in einem marinen System. Als Quelle für das Molybdän dient das im Meerwasser gelöste $MoO_4^{2-}$, welches ab einem Schwellenwert von 11 µM in der Sulfidkonzentration (engl. action point of switch; APS) in einer Reaktionskaskade sukzessiv über die Thiomolybdat-Spezies quantitativ zu Molybdänsulfid reagiert ($MoO_xS_{4-x;}$ x = 0 – 4) (ERICKSON and HELZ, 2000; HELZ et al., 1996). Das Molybdänsulfid wird dann in einer Fe-Mo-S Trägerphase im Sediment abgelagert (HELZ et al., 2011). Hierbei sind neben der Sulfid-Konzentration auch noch das verfügbare, reaktive Eisen und ein geeigneter pH-Wert (< 8) die limitierenden Faktoren. In der Literatur wurde häufiger eine Korrelation von Molybdän und TOC beschrieben, welche auf die Komplexierung bzw. *scavenging* von Thiomolybdaten durch das absinkende organische Material zurückzuführen sein soll (ALGEO and LYONS, 2006; ALGEO et al., 2007). Neuesten Erkenntnisse zufolge (HELZ et al., 2011) besteht nur ein indirekter Zusammenhang zwischen Mo und TOC, da beide an die Biogeochemie des Eisens gekoppelt sind. Eisen ist ein wichtiger Bestandteil der Stickstofffixierung während der Primärproduktion von organischem Material. Zusätzlich sedimentieren Eisensulfide (inkl. der Fe-Mo-S Verbindungen) und organisches Material gemeinsam ab, was in einer Vergesellschaftung von Fe, Mo, TOC, S und mit diesen assoziierten Elementen im Sediment resultiert.

Ein weiteres interessantes Element in anoxischen Sedimenten ist Uran, welches auch als Proxy für Änderungen im redox-chemischen Milieu genutzt wird. Uran ist im oxischen Meerwasser als Uranylcarbonat-Anion ($U^{VI}O_2(CO_3)_3^{4-}$) gelöst und weist ein konservatives Verhalten innerhalb der Wassersäule auf. Unter suboxischen und anoxischen Bedingungen kann Uran oberflächenkatalysiert zu $U^{IV}O_2$ reduziert werden. Im Gegensatz zu Fe und Mo ist die Geochemie des Urans nicht vom gelösten Sulfid in der Wassersäule abhängig, sondern nur von der Oberfläche von Partikeln (z.B. Minerale, organisches Material, Detrius, etc.). Dabei wirken zwar sulfatreduzierende Bakterien reduktionsfördernd, aber die eigentliche Reduktion des Urans ist von der Sulfat-Reduktion und dem Eisen-Shuttle entkoppelt (KLINKHAMMER and PALMER, 1991). Da die Uran-Reduktion oberflächenkatalysiert abläuft bieten die Sapropele des Schwarzen Meeres eine ideale Sedimentmatrix zur näheren Untersuchung dieses Reduktionsprozesses, da die Matrix aus Tonmineralen, Carbonaten und organischem Material zusammengesetzt ist, welche jeweils spezifische Oberflächeneigenschaften zur Verfügung stellen. Die Zusammensetzung des Sediments variiert je nach lithologischer

Unit in den Anteilen ihrer Komponenten, so dass man eine Abhängigkeit des Urans von einer Komponente über die Units hinweg verfolgen kann. Somit ist Uran zwar ein von Fe und Mo unabhängiger redoxsensitiver Proxy, kann aber von der Sedimentmatrix beeinflusst werden (s. Kap. 5).

Ein Sedimentarchiv besteht in der Regel nicht nur aus primären Signalen aus der Wassersäule, sondern es können in älteren Sapropel-Schichten diagenetische Veränderungen, wie z.B. Überprägungen durch Eisensulfide oder Oxidationseffekte durch Turbidite auftreten, welche die primären Signale verfälschen können (NERETIN et al., 2004). Bei der Überprägung mit Eisensulfiden wird Fe unter suboxischen/anoxischen Bedingungen im Sediment gelöst und diffundiert im Porenwasser in die Richtung, in der euxinische Bedingungen vorliegen. Dort fällt das Fe als Eisensulfid wieder aus. In den Sedimenten des Schwarzen Meeres wird das Fe in den glazialen Tonen der Unit III gelöst und diffundiert Richtung Sediment-Wasser-Grenze. Das mikrobiell gebildete Sulfid aus der Wassersäule diffundiert in die Tiefe und an der Grenzschicht fallen Eisensulfide in den Porenräumen des Sediments aus. Da die Grenzschicht dieses $Fe^{2+}_{aq}/S^{2-}_{aq}$ Gradienten in die Tiefe wandert, sind Überprägungen von rezenten, euxinischen Sedimenten mit Eisensulfiden nicht möglich. Im Fall der Sedimente vom Schwarzen Meer befindet sich diese Grenzschicht in ca. 3-4 m Tiefe und somit in Unit III (NERETIN et al., 2004). Turbidite, die oxische Sedimentlagen in anoxische Sedimentarchive transportieren, verursachen eine Oxidation der dortigen redoxsensitiven Elemente, da spontan ein Sauerstoffgradient entsteht. Dies hat zur Folge, dass Elemente, welche unter anoxischen Bedingungen im Sediment angereichert sind, z.B. Uran, durch den im Turbidit enthaltenen Sauerstoff bzw. oxidierte Element-Spezies oxidiert werden und somit im Porenwasser gelöst werden. Dort diffundiert die oxidierte Spezies in Richtung anoxische Bedingungen wo sie wieder reduziert wird und ein nicht-primäres Anreichungssignal erzeugt (THOMSON et al., 1998).

Diese komplexe Ablagerungschemie von Fe und Mo beeinflusst auch die Isotopenzusammensetzung von Fe- und Mo-Verbindungen im Sediment. Eine Isotopensignatur kann als Proxy für bestimmte Prozesse dienen, welche sich auf die (Paläo-)Umwelt auswirken, wie z.B. die Änderung der Redoxbedingungen oder eine authigene Anreicherung des jeweiligen Elements (BARLING et al., 2001; POULSON et al., 2006; SEVERMANN et al., 2006; SEVERMANN et al., 2008). Die Isotopensignatur des

Eisens ($\delta^{56/54}$Fe) in den Sapropelen des Schwarzen Meeres zeigen einen niedrigen $\delta^{56/54}$Fe-Wert (~-0,3 ‰) in den eisenreichen Sapropel-Schichten gegenüber dem geogenen Hintergrund (~0,07 ‰; SEVERMANN et al., 2008). Dies ist ein gutes Beispiel für die massenabhängige Isotopenfraktionierung in natürlichen, authigenen Prozessen und Redoxreaktionen, weil bei dem gesamten Durchlaufen des Eisen-Shuttles immer das leichtere Fe-Isotop bevorzugt reagiert. Da sowohl bei Fe als auch Mo die massenabhängige Isotopenfraktionierung gegenüber der massenunabhängigen Fraktionierung überwiegt, werden in jeder physikalischen und chemischen Reaktion die leichteren Isotope bevorzugt (BIGELEISEN and MAYER, 1947). Demzufolge sinkt das Verhältnis des schwereren Isotops zu dem leichteren Isotop des Analyten in einem Reaktionsprodukt gegenüber dem Ausgangsverhältnis in den Edukten. Um die Isotopenverhältnisse untereinander besser zu vergleichen, werden sie auf ein Standardverhältnis normiert und in der folgenden Delta-Schreibweise (s. Formel 1) veröffentlicht. Hierbei steht $^{s/l}$E für die schweren (s) und leichten (l) Isotope eines Elements (E).

$$\delta^{s/l}E = \left( \frac{{}^{s}E/{}_{l}E\,_{Probe}}{{}^{s}E/{}_{l}E\,_{Standard}} - 1 \right) \cdot 1000 \qquad (1)$$

Eine Kopplung von authigenen Eisenanreicherungen mit niedrigen $\delta^{56/54}$Fe-Werten ist daher ein Indikator für einen aktiven Eisen-Shuttle auf den Schelfgebieten des Schwarzen Meeres und einer damit verbundenen Chemokline in der euphotischen Zone (s. Kap. 3).

Die Isotopensignatur von Molybdän in Sedimenten ($\delta^{98/95}$Mo) eines euxinischen Beckens mit ausreichend hoher Sulfid-Konzentration sollte der Signatur der Wassersäule entsprechen (~2,3 ‰), da Mo, wie oben beschrieben, unter diesen Bedingungen quantitativ aus der Wassersäule ins Sediment überführt wird. Ist dies nicht der Fall und der $\delta^{98/95}$Mo-Wert im Sediment ist niedriger als der Wassersäulen-Wert, kann nicht von einer vollständigen quantitativen Fällung von Mo ausgegangen werden. Somit können keine vollständig euxinischen Bedingungen in der Wassersäule vorhanden sein, welche ein vollständiges Durchlaufen der Thiomolybdat-Reaktionskaskade begünstigen.

Im Gegensatz zu den Isotopen von Fe und Mo fraktionieren die Isotope des U nicht massenabhängig. Diese massenunabhängige Fraktionierung wird hauptsächlich durch den *nuklear field shift* (NFS) hervorgerufen (BIGELEISEN, 1996; FUJII et al., 2006; SCHAUBLE, 2007). Dies ist ein thermodynamischer Effekt, der durch die Architektur und Elektronendichte der Atomkerne von Elementen mit einer Ordnungszahl größer 40 hervorgerufen wird. Die thermodynamischen Effekte, welche die massenabhängige Fraktionierung beeinflussen, nehmen mit der Masse des Atoms (und steigender Temperatur) ab, wohingegen der NFS nicht von der Masse des Atoms beeinflusst wird, sondern durch die Anordnung von Neutronen und Protonen in dem Atomkern und die Verteilung der Valenzelektronen in der zum Atom gehörenden Elektronenhülle (BIGELEISEN, 1996). Hierbei ist die Verteilung der Neutronen der einzelnen Isotope entscheidend, da die Atomkern-Architektur eines Isotops mit einer ungeraden Anzahl an Neutronen die Elektronenhülle stärker beeinflusst als die von Isotopen mit einer geraden Anzahl von Neutronen (engl. odd-even staggering; BIGELEISEN, 1996). Im Beispiel von Uran (Ordnungszahl 92) erhält man daher eine stärkere Fraktionierung zwischen $^{235}U$ und $^{238}U$ als zwischen $^{234}U$ und $^{238}U$, obwohl zwischen dem zuletzt genannten Isotopenpaar eine größere Massendifferenz zu finden ist.

Die Fraktionierung zwischen den einzelnen U-Isotopen in einem natürlichen System, angezeigt durch $\delta^{238/235}U$, kann weitere Indizien über die in dem System vorherrschenden Redoxbedingungen liefern und dient somit als gute Ergänzung und Verifizierung zu $\delta^{56/54}Fe$ und $\delta^{98/95}Mo$ (WEYER et al., 2008).

## 1.5. Ein geochemischer Vergleich der lithologischen Schichten im Schwarzen Meer

Anhand der Elementzusammensetzung der einzelnen Sedimentschichten können nicht nur Aussagen über die Redoxbedingungen zur Zeit der Ablagerung oder Herkunft der lithogenen Komponenten gemacht werden, es ist zudem möglich eine Bilanz aufzustellen, welche die Umweltsituationen während der Ausbildung der Sedimentschichten genauer beschreiben kann als der geochemische Parameter per se. Ein zusätzlicher Vergleich von An- oder Abreicherungen gegenüber dem geogenen Hintergrund des Systems kann authigene Prozesse anzeigen (BRUMSACK, 1989b;

BRUMSACK, 2006a). Hierfür erweist sich der Anreicherungsfaktor (engl. enrichment factor; EF) als hilfreiches Werkzeug.

$$\mathrm{EF} = \frac{\mathrm{Element}/\mathrm{Al}_{\mathrm{Probe}}}{\mathrm{Element}/\mathrm{Al}_{\mathrm{Hintergrund}}} \quad (2)$$

Um die jeweilige An- oder Abreicherung des Analyten zu bestimmen wird das Element/Al-Verhältnis des Analyten in der Probe durch das Element/Al Verhältnis des geogenen Hintergrunds dividiert. Werte größer 1 zeigen eine Anreicherung des Analyten an, Werte kleiner 1 folglich eine Abreicherung (BRUMSACK, 2006a).

### 1.5.1. Terrigene Elementproxies

Als Proxies für den terrigenen Einfluss auf eine Sedimentschicht dienen Al, Cr, K, Mg, Rb, Ti und Zr, welche in Ton- und Schwermineralen vorkommen und durch verschiedene Verwitterungsprozesse über die Flüsse in die Meeresbecken eingetragen werden.

Der Gehalt an Aluminium als Proxy für Tonminerale, welche aus verwitterten Alumosilikaten stammen, liegt in allen sechs lithologischen Units unterhalb des Wertes für den gemittelten Tonschiefer von 16,7 % (WEDEPOHL, 1991). Dies deutet auf eine Verdünnung durch eine authigene/biogene Sedimentfraktion hin. Die stärkste Verdünnung ist in Unit I zu sehen, gefolgt von Unit V und Unit II, wohingegen die Al-Gehalte von Unit III und VI am nächsten zum gemittelten Tonschiefer liegen (s. Tab. 1-1). Anderseits kann die Verdünnung durch eine terrigene Sedimentfraktion mit Hilfe der Normierung auf Al kompensiert werden. Dadurch werden authigene Signale gegenüber dem Hintergrund hervorgehoben. Aus diesem Grund werden im Folgenden die Element/Al Verhältnisse verwendet, um die Unterschiede bzw. Gemeinsamkeiten zwischen den einzelnen Units zu beschreiben.

Der Einfluss durch Schwerminerale, seien sie verwittert oder eingetragen, wird durch die Element/Al Verhältnisse von Cr, Rb, Ti und Zr repräsentiert. Hier zeigen sich nur marginale Unterschiede zwischen den Units, was auf eine recht konstante Zusammensetzung der Hintergrundsedimentation des Schwarzen Meeres auf einer räumlichen und zeitlichen Ebene schließen lässt (s. Tab. 1-1).

Die leicht erhöhten Cr/Al und Ti/Al Werte in Unit V und VI der Station 22 lassen einen erhöhten äolischen Eintrag von Sahara-Staub an der anatolischen Küste im Vergleich zum Gesamtbecken vermuten (MOLLER et al., 2012; WEHAUSEN and BRUMSACK, 1999). Die unterschiedlichen Mg/Al im Vergleich zu den konstanten K/Al Werte in den verschiedenen Units deuten auf einen Wechsel zwischen Illit- (K-Anreicherung) und Chlorit-dominiertem (Mg-Anreicherung) Flusseintrag im Laufe der Zeit hin (WEHAUSEN and BRUMSACK, 1999; s. Tab. 1-1).

**Tab. 1-1** Gemittelte Elementgehalte, Element/Al-Verhältnisse und Anreicherungsfaktoren (EF) der unterschiedlichen lithographischen Sedimentschichten.

| | **Avg. Black Sea Unit I (n = 314)** | | | **Avg. Black Sea Unit II (n = 342)** | | | **Avg. Black Sea Unit III (n = 564)** | | | **Site 22 Unit V (n = 157)** | | | **Site 22 Unit VI (n = 49)** | | | **Avg. Shale** | |
|---|---|---|---|---|---|---|---|---|---|---|---|---|---|---|---|---|---|
| | [wt. %] | element/Al | EF | [wt. %] | element/Al | EF | [wt. %] | element/Al | EF | [wt. %] | element/Al | EF | [wt. %] | element/Al | EF | [wt. %] | element/Al |
| **$SiO_2$** | 25,0 ± 11,9 | 2,8 ± 0,2 | 0,90 | 36,5 ± 9,8 | 2,9 ± 0,6 | 0,93 | 43,9 ± 10,3 | 2,7 ± 0,2 | 0,87 | 29,5 ± 9,1 | 2,7 ± 0,2 | 0,87 | 36,0 ± 8,7 | 2,7 ± 0,1 | 0,87 | 58,9 | 3,1 |
| **$TiO_2$** | 0,36 ± 0,17 | 0,051 ± 0,002 | 0,96 | 0,51 ± 0,13 | 0,050 ± 0,004 | 0,95 | 0,61 ± 0,15 | 0,047 ± 0,004 | 0,89 | 0,43 ± 0,16 | 0,054 ± 0,004 | 1,02 | 0,54 ± 0,10 | 0,052 ± 0,004 | 0,98 | 0,78 | 0,053 |
| **$Al_2O_3$** | 7,9 ± 3,7 | | | 11,4 ± 2,6 | | | 14,6 ± 3,6 | | | 8,9 ± 3,0 | | | 12,1 ± 3,2 | | | 16,7 | |
| **$Fe_2O_3$** | 3,8 ± 1,3 | 0,7 ± 0,2 | 1,28 | 4,7 ± 1 | 0,6 ± 0,1 | 1,03 | 6,0 ± 1,5 | 0,5 ± 0,1 | 0,92 | 4,4 ± 1,4 | 0,7 ± 0,1 | 1,28 | 5,6 ± 1,1 | 0,6 ± 0,1 | 1,10 | 6,9 | 0,5 |
| **MgO** | 1,9 ± 0,8 | 0,30 ± 0,11 | 1,69 | 2,6 ± 0,7 | 0,28 ± 0,15 | 1,58 | 3,0 ± 0,6 | 0,25 ± 0,07 | 1,41 | 2,5 ± 0,9 | 0,32 ± 0,05 | 1,80 | 3,4 ± 0,3 | 0,33 ± 0,06 | 1,86 | 2,6 | 0,18 |
| **CaO** | 23,9 ± 9,8 | 6,6 ± 6,7 | 37,10 | 9,6 ± 5,7 | 1,4 ± 1,9 | 7,87 | 11,0 ± 9,7 | 1,7 ± 2,8 | 9,56 | 22,9 ± 9,4 | 5,0 ± 5,7 | 28,11 | 18,8 ± 8,0 | 2,4 ± 1,3 | 13,49 | 2,2 | 0,2 |
| **$Na_2O$** | 2,9 ± 1,3 | 0,67 ± 0,52 | 4,99 | 3,1 ± 1,3 | 0,44 ± 0,29 | 3,28 | 1,4 ± 0,5 | 0,15 ± 0,08 | 1,12 | 1,1 ± 0,2 | 0,18 ± 0,06 | 1,34 | 0,9 ± 0,1 | 0,11 ± 0,02 | 0,82 | 1,6 | 0,13 |
| **$K_2O$** | 1,4 ± 0,6 | 0,28 ± 0,02 | 0,83 | 2,0 ± 0,4 | 0,28 ± 0,01 | 0,83 | 2,6 ± 0,7 | 0,28 ± 0,02 | 0,83 | 1,5 ± 0,5 | 0,27 ± 0,02 | 0,80 | 2,1 ± 0,7 | 0,27 ± 0,02 | 0,80 | 3,6 | 0,34 |
| **$P_2O_5$** | 0,14 ± 0,02 | 0,019 ± 0,011 | 2,41 | 0,17 ± 0,06 | 0,015 ± 0,011 | 1,90 | 0,12 ± 0,02 | 0,007 ± 0,002 | 0,89 | 0,18 ± 0,10 | 0,019 ± 0,014 | 2,41 | 0,11 ± 0,04 | 0,007 ± 0,001 | 0,89 | 0,16 | 0,008 |
| **S** | 1,5 ± 0,5 | 0,46 ± 0,28 | 20,33 | 1,7 ± 0,6 | 0,31 ± 0,16 | 13,70 | 0,5 ± 0,6 | 0,08 ± 0,09 | 3,54 | 1,2 ± 0,3 | 0,26 ± 0,08 | 11,49 | 0,9 ± 0,2 | 0,16 ± 0,09 | 7,07 | 0,2 | 0,02 |
| **TOC** | 4,3 ± 1,8 | 1,59 ± 1,05 | 70,27 | 9,3 ± 6,4 | 1,87 ± 1,59 | 82,65 | 0,8 ± 0,2 | 0,15 ± 0,14 | 6,63 | 3,9 ± 2,0 | 0,91 ± 0,36 | 40,22 | 0,4 ± 0,1 | 0,06 ± 0,01 | 2,65 | 0,2 | 0,02 |
| **TIC** | 5,2 ± 2,0 | 2,18 ± 1,98 | | 1,8 ± 1,4 | 0,40 ± 0,60 | | 2,4 ± 2,2 | 0,61 ± 0,96 | | 4,8 ± 2,0 | 1,53 ± 1,88 | | 3,6 ± 1,9 | 0,64 ± 0,44 | | | |
| | [ppm] | | | [ppm] | | | [ppm] | | | [ppm] | | | [ppm] | | | [ppm] | |
| **As** | 14 ± 6 | 4,1 ± 2,4 | 3,62 | 16 ± 8 | 2,8 ± 1,8 | 2,48 | 17 ± 15 | 2,5 ± 2,6 | 2,21 | 55 ± 13 | 12 ± 5 | 10,61 | 20 ± 13 | 4 ± 3 | 3,54 | 10 | 1,1 |
| **Ba** | 647 ± 1036 | 192 ± 284 | 2,93 | 586 ± 451 | 105 ± 92 | 1,60 | 386 ± 122 | 54 ± 27 | 0,82 | 292 ± 61 | 69 ± 32 | 1,05 | 315 ± 56 | 50 ± 4 | 0,76 | 580 | 66 |
| **Bi** | 0,20 ± 0,09 | 0,065 ± 0,021 | 4,42 | 0,29 ± 0,05 | 0,054 ± 0,013 | 3,67 | 0,33 ± 0,08 | 0,045 ± 0,011 | 3,06 | 0,23 ± 0,09 | 0,051 ± 0,008 | 3,47 | 0,27 ± 0,08 | 0,037 ± 0,002 | 2,52 | 0,13 | 0,015 |
| **Cd** | 0,71 ± 0,33 | 0,28 ± 0,17 | 19,04 | 0,60 ± 0,39 | 0,11 ± 0,09 | 7,48 | 0,27 ± 0,19 | 0,038 ± 0,035 | 2,58 | 0,46 ± 0,22 | 0,12 ± 0,08 | 8,16 | 0,23 ± 0,04 | 0,033 ± 0,005 | 2,24 | 0,13 | 0,015 |
| **Co** | 22 ± 9 | 6,7 ± 4,5 | 3,12 | 18 ± 7 | 3,3 ± 1,7 | 1,54 | 17 ± 8 | 2,2 ± 0,9 | 1,02 | 17 ± 6 | 3,8 ± 0,7 | 1,77 | 18 ± 6 | 2,8 ± 0,3 | 1,30 | 19 | 2,1 |
| **Cr** | 62 ± 37 | 14 ± 5 | 1,38 | 91 ± 34 | 15 ± 4 | 1,47 | 118 ± 40 | 15 ± 3 | 1,47 | 89 ± 43 | 18 ± 5 | 1,77 | 124 ± 23 | 20 ± 2 | 1,96 | 90 | 10 |
| **Cs** | 3,5 ± 2,0 | 1,05 ± 0,37 | 1,69 | 5,4 ± 1,2 | 0,98 ± 0,08 | 1,58 | 7,5 ± 1,8 | 1,02 ± 0,07 | 1,64 | 4,7 ± 1,7 | 1,08 ± 0,09 | 1,74 | 6,9 ± 1,7 | 0,97 ± 0,04 | 1,56 | 5,5 | 0,62 |
| **Cu** | 52 ± 18 | 15 ± 7 | 2,95 | 73 ± 38 | 14 ± 10 | 2,75 | 45 ± 12 | 6 ± 3 | 1,18 | 57 ± 17 | 13 ± 3 | 2,55 | 42 ± 6 | 7 ± 1 | 1,38 | 45 | 5 |
| **Mn** | 456 ± 90 | 134 ± 62 | 1,39 | 393 ± 144 | 67 ± 27 | 0,70 | 694 ± 173 | 102 ± 62 | 1,06 | 864 ± 785 | 362 ± 323 | 3,76 | 1012 ± 193 | 174 ± 59 | 1,81 | 850 | 96 |
| **Mo** | 37 ± 20 | 10 ± 6 | 67,99 | 77 ± 53 | 15 ± 13 | 101,99 | 6 ± 9 | 0,8 ± 1,4 | 5,44 | 53 ± 37 | 12 ± 9 | 81,59 | 5 ± 4 | 0,9 ± 0,8 | 6,12 | 1,3 | 0,1 |
| **Nb** | 5,1 ± 2,9 | 1,5 ± 0,3 | 0,74 | 6,9 ± 2,2 | 1,2 ± 0,2 | 0,59 | 8,7 ± 3,5 | 1,2 ± 0,5 | 0,59 | 6,9 ± 2,7 | 1,6 ± 0,1 | 0,79 | 8,9 ± 2,7 | 1,3 ± 0,3 | 0,64 | 18 | 2,0 |
| **Ni** | 63 ± 30 | 17 ± 7 | 2,21 | 97 ± 45 | 17 ± 9 | 2,21 | 83 ± 40 | 11 ± 4 | 1,43 | 89 ± 35 | 19 ± 4 | 2,47 | 98 ± 16 | 16 ± 2 | 2,08 | 68 | 8 |
| **Pb** | 16 ± 9 | 4,3 ± 2,4 | 1,73 | 16 ± 4 | 2,6 ± 0,7 | 1,04 | 18 ± 5 | 2,3 ± 0,4 | 0,92 | 15 ± 7 | 3,3 ± 1,8 | 1,33 | 14 ± 5 | 2,2 ± 0,3 | 0,88 | 22 | 2,5 |
| **Rb** | 63 ± 29 | 15 ± 1 | 0,95 | 88 ± 21 | 15 ± 1 | 0,95 | 122 ± 35 | 16 ± 2 | 1,01 | 67 ± 23 | 14 ± 1 | 0,88 | 88 ± 25 | 14 ± 1 | 0,88 | 140 | 16 |
| **Re** | 0,039 ± 0,019 | 0,016 ± 0,011 | 14,14 | 0,072 ± 0,030 | 0,014 ± 0,007 | 12,38 | 0,020 ± 0,030 | 0,003 ± 0,006 | 2,65 | 0,059 ± 0,063 | 0,014 ± 0,011 | 12,38 | n.d. ± n.d. | n.d. ± n.d. | | 0,010 | 0,001 |
| **Sb** | 1,6 ± 0,3 | 0,56 ± 0,28 | 3,30 | 2,2 ± 0,9 | 0,40 ± 0,15 | 2,36 | 1,6 ± 1,1 | 0,23 ± 0,19 | 1,36 | 1,1 ± 0,6 | 0,25 ± 0,07 | 1,47 | 1,3 ± 0,9 | 0,22 ± 0,19 | 1,30 | 1,5 | 0,17 |
| **Sc** | 7,7 ± 4,0 | 2,4 ± 0,3 | 1,63 | 11,9 ± 2,6 | 2,2 ± 0,3 | 1,50 | 15 ± 4 | 2,0 ± 0,3 | 1,36 | 10 ± 4 | 2,3 ± 0,2 | 1,56 | 16 ± 3 | 2,3 ± 0,2 | 1,56 | 13 | 1,5 |
| **Sr** | 890 ± 389 | 350 ± 358 | 10,31 | 446 ± 430 | 91 ± 135 | 2,68 | 234 ± 114 | 43 ± 54 | 1,27 | 1357 ± 1175 | 418 ± 699 | 12,32 | 300 ± 81 | 53 ± 23 | 1,56 | 300 | 34 |
| **Tl** | 0,45 ± 0,15 | 0,15 ± 0,05 | 1,95 | 0,81 ± 0,23 | 0,15 ± 0,06 | 1,95 | 0,65 ± 0,16 | 0,09 ± 0,02 | 1,17 | 0,45 ± 0,17 | 0,10 ± 0,02 | 1,30 | 0,62 ± 0,18 | 0,09 ± 0,01 | 1,17 | 0,68 | 0,08 |
| **U** | 11 ± 6 | 4,2 ± 4,1 | 10,03 | 11 ± 5 | 2,1 ± 1,4 | 5,02 | 3 ± 2 | 0,5 ± 0,4 | 1,19 | 16 ± 13 | 3,9 ± 4,0 | 9,32 | 3 ± 1 | 0,5 ± 0,3 | 1,19 | 3,7 | 0,4 |
| **V** | 109 ± 36 | 29 ± 9 | 1,97 | 175 ± 57 | 31 ± 15 | 2,11 | 133 ± 32 | 17 ± 1 | 1,16 | 124 ± 35 | 27 ± 5 | 1,84 | 117 ± 23 | 19 ± 1 | 1,29 | 130 | 15 |
| **W** | 0,6 ± 0,4 | 0,18 ± 0,06 | 0,88 | 1,1 ± 0,5 | 0,21 ± 0,08 | 1,03 | 1,5 ± 0,9 | 0,23 ± 0,18 | 1,13 | 1,1 ± 0,2 | 0,21 ± 0,03 | 1,03 | 1,1 ± 0,2 | 0,17 ± 0,02 | 0,83 | 1,8 | 0,20 |
| **Y** | 24 ± 21 | 7,6 ± 7,6 | 1,64 | 19 ± 3 | 3,3 ± 0,7 | 0,71 | 21 ± 4 | 2,8 ± 0,5 | 0,60 | 18 ± 9 | 4,0 ± 1,3 | 0,86 | 18 ± 5 | 2,8 ± 0,2 | 0,60 | 41 | 4,6 |
| **Zn** | 88 ± 73 | 29 ± 37 | 2,70 | 81 ± 13 | 14 ± 3 | 1,30 | 91 ± 22 | 12 ± 1 | 1,12 | 66 ± 20 | 14 ± 1 | 1,30 | 75 ± 17 | 11,8 ± 0,4 | 1,10 | 95 | 10,7 |
| **Zr** | 73 ± 27 | 19 ± 3 | 1,05 | 95 ± 24 | 16 ± 3 | 0,88 | 107 ± 27 | 14 ± 3 | 0,77 | 75 ± 30 | 16 ± 2 | 0,88 | 97 ± 20 | 15 ± 1 | 0,83 | 160 | 18 |
| | **(n = 42)** | | | **(n = 53)** | | | **(n = 39)** | | | **(n = 25)** | | | **(n = 8)** | | | | |
| **La** | 16 ± 5 | 5,4 ± 1,7 | 1,19 | 19 ± 4 | 3,4 ± 0,4 | 0,75 | 27 ± 7 | 3,6 ± 0,6 | 0,80 | 19 ± 11 | 4,1 ± 1,3 | 0,91 | 26 ± 9 | 3,5 ± 0,4 | 0,77 | 40 | 4,5 |
| **Ce** | 32 ± 11 | 11 ± 3 | 1,02 | 38 ± 8 | 7 ± 1 | 0,65 | 54 ± 15 | 7 ± 1 | 0,65 | 34 ± 17 | 8 ± 2 | 0,74 | 51 ± 17 | 7 ± 1 | 0,65 | 95 | 11 |
| **Pr** | 3,6 ± 1,2 | 1,2 ± 0,4 | 1,09 | 4,3 ± 0,8 | 0,8 ± 0,1 | 0,73 | 6,1 ± 1,6 | 0,8 ± 0,1 | 0,73 | 4,4 ± 2,8 | 0,9 ± 0,3 | 0,82 | 5,9 ± 2,0 | 0,8 ± 0,1 | 0,73 | 9,7 | 1,1 |
| **Nd** | 14 ± 4 | 5,0 ± 1,6 | 1,13 | 17 ± 3 | 3,1 ± 0,4 | 0,70 | 23 ± 6 | 3,2 ± 0,5 | 0,73 | 17 ± 11 | 3,7 ± 1,3 | 0,84 | 23 ± 7 | 3,1 ± 0,3 | 0,70 | 39 | 4,4 |
| **Sm** | 2,9 ± 0,8 | 1,0 ± 0,4 | 1,21 | 3,3 ± 0,6 | 0,6 ± 0,1 | 0,73 | 4,6 ± 1,1 | 0,6 ± 0,1 | 0,73 | 3,6 ± 2,6 | 0,8 ± 0,3 | 0,97 | 4,4 ± 1,4 | 0,6 ± 0,1 | 0,73 | 7,3 | 0,8 |
| **Eu** | 0,71 ± 0,18 | 0,25 ± 0,10 | 1,38 | 0,82 ± 0,14 | 0,15 ± 0,02 | 0,83 | 1,1 ± 0,2 | 0,15 ± 0,02 | 0,83 | 0,85 ± 0,65 | 0,18 ± 0,08 | 0,99 | 1,0 ± 0,3 | 0,14 ± 0,01 | 0,77 | 1,6 | 0,18 |
| **Gd** | 2,8 ± 0,7 | 1,0 ± 0,7 | 1,26 | 3,1 ± 0,6 | 0,6 ± 0,1 | 0,76 | 4,0 ± 0,9 | 0,6 ± 0,1 | 0,76 | 3,5 ± 2,7 | 0,8 ± 0,3 | 1,01 | 4,0 ± 1,2 | 0,56 ± 0,03 | 0,71 | 7,0 | 0,79 |
| **Tb** | 0,45 ± 0,11 | 0,16 ± 0,07 | 1,18 | 0,53 ± 0,11 | 0,10 ± 0,02 | 0,74 | 0,68 ± 0,15 | 0,09 ± 0,03 | 0,66 | 0,55 ± 0,44 | 0,12 ± 0,06 | 0,88 | 0,61 ± 0,17 | 0,084 ± 0,004 | 0,62 | 1,2 | 0,136 |
| **Dy** | 2,7 ± 0,6 | 0,97 ± 0,40 | 1,56 | 3,0 ± 0,5 | 0,56 ± 0,10 | 0,90 | 3,8 ± 0,8 | 0,51 ± 0,07 | 0,82 | 3,3 ± 2,6 | 0,70 ± 0,34 | 1,13 | 3,5 ± 0,9 | 0,49 ± 0,01 | 0,79 | 5,5 | 0,62 |
| **Ho** | 0,54 ± 0,13 | 0,20 ± 0,08 | 1,10 | 0,64 ± 0,12 | 0,12 ± 0,02 | 0,66 | 0,79 ± 0,16 | 0,11 ± 0,02 | 0,61 | 0,64 ± 0,49 | 0,14 ± 0,06 | 0,77 | 0,70 ± 0,18 | 0,097 ± 0,002 | 0,54 | 1,6 | 0,181 |
| **Er** | 1,6 ± 0,4 | 0,57 ± 0,23 | 1,29 | 1,9 ± 0,3 | 0,35 ± 0,07 | 0,79 | 2,2 ± 0,5 | 0,30 ± 0,05 | 0,68 | 1,9 ± 1,4 | 0,41 ± 0,18 | 0,93 | 2,0 ± 0,5 | 0,28 ± 0,01 | 0,63 | 3,9 | 0,44 |
| **Tm** | 0,23 ± 0,07 | 0,081 ± 0,031 | 1,19 | 0,30 ± 0,05 | 0,056 ± 0,012 | 0,83 | 0,34 ± 0,08 | 0,046 ± 0,008 | 0,68 | 0,27 ± 0,19 | 0,060 ± 0,024 | 0,88 | 0,30 ± 0,07 | 0,042 ± 0,001 | 0,62 | 0,6 | 0,068 |
| **Yb** | 1,5 ± 0,4 | 0,52 ± 0,20 | 1,24 | 1,8 ± 0,3 | 0,34 ± 0,06 | 0,81 | 2,1 ± 0,5 | 0,29 ± 0,04 | 0,69 | 1,8 ± 1,2 | 0,40 ± 0,16 | 0,96 | 2,0 ± 0,5 | 0,28 ± 0,01 | 0,67 | 3,7 | 0,42 |
| **Lu** | 0,23 ± 0,07 | 0,081 ± 0,031 | 1,02 | 0,32 ± 0,06 | 0,060 ± 0,014 | 0,76 | 0,34 ± 0,08 | 0,046 ± 0,008 | 0,58 | 0,27 ± 0,18 | 0,059 ± 0,022 | 0,75 | 0,30 ± 0,07 | 0,041 ± 0,001 | 0,52 | 0,7 | 0,079 |

### 1.5.2. Biogene Elementproxies

Anhand von biogenen Elementproxies lassen sich Aussagen über das Vorhandensein von Organismen-Überresten in einer Sedimentschicht und somit über den Grad der Paleoprimärproduktion in der Wassersäule treffen. Weiterhin können die Sedimentfraktionen (Carbonate, Opal/Quarz, TOC) definiert und auf biogene Genese zurückgeführt werden. Beispiele von biogenen Elementproxies sind u.a. die Bestandteile von biogenem Calcit/Aragonit (Ca, Mg, Sr), partikuläre organische Materialien (POM bzw. TOC), sowie Übergangsmetalle (Cd, Cu, Ni, V, Zn), die mit den funktionellen Gruppen der organischen Komponenten im Sediment komplexieren können (TRIBOVILLARD et al., 2006). Weitere Indikatoren für eine biogene Sedimentfraktion sind Barium, welches von Phytoplankton metabolisiert und als Baryt in das Sediment eingelagert wird, sowie Phosphor und Schwefel. Beide letztgenannten Elemente sind häufig in natürlichen, organischen Verbindungen vertreten.

Wie schon in Kapitel 1.3.2 erwähnt wurde, enthalten Unit I, II und V einen erhöhten Anteil an TOC, welcher auf eine erhöhte Primärproduktivität in den Ablagerungsintervallen bei einem ausreichend hohen Erhaltungpotenzial schließen lässt. Unit I und V beinhalten zudem biogene Carbonate, welche von Coccolithen stammen und somit ein direkter Beweis für eine Hapthophyten-Gesellschaft in der euphotischen Zone während der Ablagerung der Sedimentschicht sind (HAY et al., 1991). Sämtliche Element/Al Verhältnisse der geochemischen Proxies für biogene Carbonate und POM sind in den drei Units gegenüber dem Hintergrund (repräsentiert durch AS) angereichert (s. Tab. 1-1).

Auch Phosphor und Schwefel sind in den Sapropelen angereichert, wobei man diese beiden Elemente als Produktivitätsproxies kritisch betrachten muss, da das Signal des Schwefels aus organischen Quellen unter euxinischen Bedingungen von dem anorganischen Sulfid-Schwefel überlagert wird und Phosphor unter euxinischen Bedingungen zu $PO_4^{3-}{}_{aq}$ remobilisiert wird und keine Adsorption an Fe-/Mn-Oxiden stattfinden kann (DELLWIG et al., 2010; MÄRZ et al., 2008; TRIBOVILLARD et al., 2006; und darin enthaltene Zitate).

Barium ist ebenfalls in den Sapropelen gegenüber den glazialen Sedimenten angereichert. Aber diese Anreicherungen müssen nicht unbedingt ein Produktivitätssignal widerspiegeln, da auch Baryt ($BaSO_4$), das die dominante

Ablagerungsspezies des Ba im Sediment darstellt, unter euxinischen, im speziellen unter sulfatreduzierenden Bedingungen mobilisierbar ist (BRUMSACK, 1989b; BRUMSACK and GIESKES, 1983; HENKEL et al., 2012; KENISON FALKNER et al., 1993; TORRES et al., 1996; WELDEAB et al., 2003a). Diese Mobilisierung des Ba findet nur unterhalb der $SO_4^{2-}/S^{2-}$-Grenze im Porenwasser statt, meistens in Bereichen der aktiven Methanogenese, wenn die Sulfatkonzentration genügend gering ist um Baryt in Lösung zu bringen. Daher kann nicht unbedingt davon ausgegangen werden, dass die Ba-Signale in Unit V von primärer Natur sind im Gegensatz zu den Ba-Signalen in Unit I und II, welche höchstens leicht überprägt sein können durch Ba aus Unit III, welches nach oben diffundiert ist.

### 1.5.3. Authigene Elementproxies

Im Bezug auf die generelle, chemische Zusammensetzung unterscheiden sich die Sapropele des Holozän-Interglazials nicht sehr von dem Sapropel des Eem-Interglazials. In beiden Zeiträumen herrschten anoxische bis euxinische Bedingungen in der Wassersäule, so dass organik- und spurenmetallreiche Sedimente abgelagert wurden. Die Anreicherungen der Elemente in den Sapropelen sind untereinander gut vergleichbar ebenso die Signatur von Fe- und Mo-Isotopen. Dennoch scheint die Ablagerungsgeschichte des Schwarzen Meeres in den beiden Warmzeiten unterschiedlich zu sein. Während für die Verbindung von Schwarzem Meer und Marmarameer im Holozän sowohl über ein abruptes, flutartiges Szenario (RYAN et al., 2003; RYAN et al., 1997), als auch über ein graduelles Einfluss-Modell (AKSU et al., 2002; IVANOVA et al., 2007; MAJOR et al., 2002; YANKO-HOMBACH et al., 2007) diskutiert wird, deuten die in Kap. 4 vorgestellten geochemischen Daten des Eem-Sapropels auf ein graduelles Einfluss-Modell von (Marmara-)Meerwasser in das Schwarze Meer hin.

Wie in Kap. 1.4 beschrieben hängt die Anreicherung der Elemente Fe und Mo in den Sedimenten hauptsächlich von Prozessen in der Wassersäule ab. Die nach Formel 1 normierten Isotopensysteme dieser Elemente sind ein Maß für Quantität dieser Prozesse (insbesondere für die Bildung von Sulfiden), welche diese Elemente aus der Wassersäule in das Sediment des Beckens transportieren. Die Anreicherung dieser beiden Elemente zeigen euxinische Bedingungen an und anhand von Bilanzrechnungen

lassen sich Meerwassereinstromraten zur Zeit der Verbindung des Schwarzen Meeres mit dem Marmarameer rekonstruieren (s. Kap. 3.3).

Zu der Gruppe der redoxsensitiven Metalle gehören nicht nur Fe und Mo, sondern, wie oben schon erwähnt, auch U und als Ergänzung Re. Die Besonderheit dieser beiden Proxies ist, dass U von der Sulfidbildung unbeeinflusst bleibt und somit nur anoxische Bedingungen anzeigt, während Re aufgrund seiner Chemie nur geeignet ist den suboxischen Übergangsbereich in der Sedimentsäule anzuzeigen (COLODNER et al., 1995; COLODNER et al., 1993; CRUSIUS et al., 1996; CRUSIUS and THOMSON, 2000; HELZ and DOLOR, 2012; MORFORD et al., 2012). Im Fall des Schwarzen Meeres ist Re stark in den Sapropelen angereichert, was auf anoxische Bedingungen hindeutet. Bildet man das Re/Mo-Verhältnis lässt sich zudem anhand eines Peaks feststellen, ab wann die euxinischen Bedingungen einsetzten. Dieser Peak ist in den unteren Units II und V zu finden und kommt dadurch zustande, dass Re-Verbindungen schon unter suboxischen/anoxischen Bedingungen abgelagert werden, aber Mo unter diesen Bedingungen noch in gelöster Form in der Wassersäule verbleibt. Sinkt das Re/Mo-Verhältnis nach einem Peak wieder ab, signalisiert das eine Anreicherung von Mo im Sediment, welche höchstwahrscheinlich durch eine Überschreitung der Sulfidkonzentration über den APS zu erklären ist.

Bei der Ablagerung der partikulären Fe-Mo-S-Phasen tritt zudem noch das *scavenging* von einigen Elementen auf, die im Kap. 1.5.2 als biogene Proxies genannt werden, aber aufgrund dieses *scavenging* Effektes nicht nur organisch, sondern auch anorganisch gebunden werden können. Zu diesen Elementen gehören Übergangsmetalle, die leicht Sulfide bilden wie z.B. Cd, Co, Cu, Ni und Zn. Diese Elemente werden in das $FeS_x$-Gerüst eingebaut und in das Sediment transportiert (HUERTA-DIAZ and MORSE, 1990; HUERTA-DIAZ and MORSE, 1992; TRIBOVILLARD et al., 2006).

Aber nicht nur Elementanreicherungen können als Proxy dienen, auch aus Abreicherungen von bestimmten Elementen in den Sedimenten können sich Schlüsse über das System ziehen lassen. Ein gutes Beispiel dafür ist Mn, das im oxischen System schwerlösliches $MnO_2$ bildet, welches unter reduzierenden Bedingungen zu $MnO_4^{2-}{}_{aq}$ reagiert (CALVERT and PEDERSEN, 1993). Eine Abreicherung an Mn zeigt somit reduzierende Bedingungen an. Ausnahmen zeigen jedoch, dass es bei einem Überschuss von Mn in einer anoxischen Wassersäule unter bestimmten Vorrausetzungen zu der

Ausfällung von Mn-Sulfiden oder -Carbonaten kommen kann (KONOVALOV et al., 2004; PAKHOMOVA et al., 2007). Vorrausetzungen dafür sind, dass das gelöste Mn nicht aus dem Becken entweichen kann, es also keinen oder nur einen sehr geringen Austausch der Wassersäule gibt. Weitere Vorrausetzungen sind pH-Wert, Eh-Wert, Alkalinität und Sulfidkonzentration in dem Becken. Oxidierte Mn-Phasen übernehmen in einem stratifizierten System, wie dem Schwarzen Meer, auch noch die Aufgabe des Transportes von Spurenelementen per *scavenging* in das Sediment. Dabei heften sich Spurenelemente an die $MnO_2$ bzw. MnOOH-Partikel und werden durch die Chemokline in das Tiefenwasser transportiert. Unter den dortigen reduzierenden Bedingungen löst sich die Mn-Phase auf und setzt die Spurenmetalle frei.

Im Falle der hier vorgestellten Sapropele finden sich erhöhte Mn/Al-Verhältnisse in Bereichen mit erhöhtem Carbonat-Gehalt, wie z.B. Unit I oder der obere Teil von Unit V bzw. Unit IV (s. Tab. 1-1). Die TOC-reichen Sapropellagen hingegen weisen Mn/Al-Verhältnisse auf, welche niedriger sind als der detritische Hintergrund (hier: AS). Dies bedeutet, dass Mn während der Sapropelablagerung mobilisiert wurde. Das ist ein weiteres Indiz für die reduzierenden Bedingungen im Schwarzen Meer.

### 1.5.4. Seltene Erden

Die Verteilung der Seltenen Erden (engl. rare earth elements; REE) in den einzelnen Sedimentschichten des Schwarzen Meeres zeigt eine Gruppierung der glazialen Sedimentschichten (Unit III und VI) und der interglazialen Sedimentschichten (Unit I, II und V) an (s. Abb. 1-3 und Tab. 1-1). Unit I hebt sich noch durch geringere, normierte Gehalte von den anderen Units ab. Normiert man die Gehalte der Seltenen Erden auf Chondritgehalte (nach NAKAMURA, 1974) wird eine negative Eu-Anomalie in allen Units sichtbar (s. Abb. 1-3A). Diese Eu-Anomalie geht auf innerkrustale Differenzierungs- und Fraktionierungsprozesse zurück, die dafür sorgen, dass die Oberkruste an Eu verarmt und die Unterkruste an Eu angereichert wird. Über die Verwitterung von der Oberkruste (Muttergestein) zu Tonsedimenten wird diese negative Eu-Anomalie an den geogenen Hintergrund der Sedimente des Schwarzen Meeres vererbt (TAYLOR and MCLENNAN, 1985).

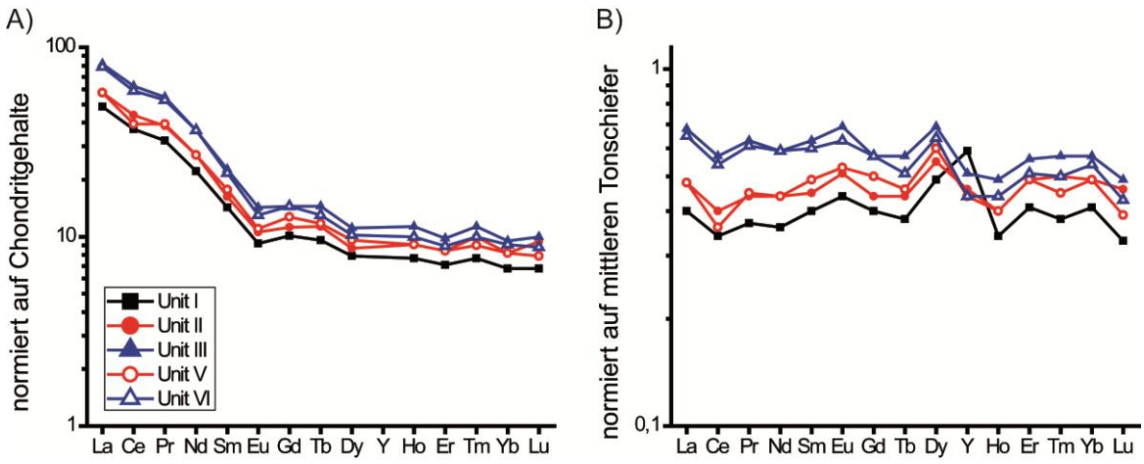


**Abb. 1-3** Verteilung der Selten Erden in den verschiedenen Units.
A) Häufigkeit der Selten Erden normiert auf Chondritgehalte nach NAKAMURA (1974); B) Gehalte der Selten Erden normiert auf den mittleren Tonschiefer.

Bei der Normierung auf den mittleren Tonschiefer (WEDEPOHL, 1991) ist eine negative Ce-Anomalie zu erkennen (s. Abb. 1-3B). Diese negative Ce-Anomalie resultiert aus den chemischen Eigenschaften der gelösten, dreiwertigen Seltenen Erden unter oxischen Bedingungen, wie sie im Atlantik und dem Oberflächenwasser des Mittelmeeres, sowie des Schwarzen Meeres vorherrschen, zu $REE^{IV}$ oxidiert zu werden (SHOLKOVITZ et al., 1994). Die oxidierten Seltenen Erden adsorbieren vornehmlich an Partikeloberflächen (biogene Carbonate, Tonmineralien, POM) oder bilden schwerlösliche Oxide, welche im Sediment abgelagert werden, wodurch das Meerwasser verarmt und das Sediment die Seltenen Erden Signatur der Wassersäule widerspiegelt (PLANAVSKY et al., 2010). Nachdem dieses an Seltenen Erden verarmte Meerwasser über den Bosporus in das Schwarze Meer einfließt, werden die darin verbliebenen Seltenen Erden Partikel beim Durchdringen der suboxischen Chemokline mobilisiert und verbleiben in der Wassersäule. Somit wird nur ein geringer Anteil der Seltenen Erden im Sediment des Schwarzen Meeres abgelagert, wodurch die auf AS normierten Gehalte generell < 1 sind (s. Abb. 1-3B). Besonders deutlich wird dies bei Ce, aufgrund von dessen Redox- und Adsorptionseigenschaften (SHOLKOVITZ et al., 1994).

Die Y-Anreicherung in Unit I gegenüber den restlichen Units ist wahrscheinlich durch eine höhere Partikeldichte in der Wassersäule und eine hochliegende Chemokline zu erklären, da Y gegenüber den Seltenen Erden eine geringere Partikelreaktivität hat (BAU et al., 1997). Dies hat zur Folge, dass Y nicht dermaßen dem durch das Redoxpotential gesteuerten Adsorptions-/Desorptionszyklus unterliegt, wie die Seltenen Erden (BAU et

al., 1997). Folglich wurden während der Ablagerung von Unit I mehr Seltenen Erden mobilisiert als Y, wodurch sich in den normierten Gehalten ein positive Y-Anomalie herausgebildet hat.

# 2. Autorenanteil an den hier vorgestellten Publikationen

Kapitel 3: Establishment of euxinic conditions in the Holocene Black Sea

Der Verlauf der Chemokline im Schwarzen Meer wurde anhand geochemischer Daten rekonstruiert. Hierbei hat Sebastian Eckert die Analysen der Haupt und Spurenelemente von sechs Sedimentkernen unter der Betreuung von Dr. Bernhard Schnetger durchgeführt. Der Sedimentkern 14-GC-3 wurde von Henning Fröllje im Rahmen einer Bachelorarbeit analysiert. Die Fe-Isotopendaten wurden von Dr. Silke Severmann ermittelt. Sebastian Eckert hat die Daten ausgewertet, interpretiert und mit allen Koautoren diskutiert. Das Manuskript wurde federführend von Sebastian Eckert unter Mithilfe aller Koautoren verfasst.

Kapitel 4: The Eemian and Holocene marine ingressions into the Black Sea: A geochemical comparison

Ein Eem-Sapropel aus dem Schwarzen Meer wurde geochemisch charakterisiert und dessen Ablagerungsgeschichte mit dem Holozän-Sapropel verglichen. Die Laborprobenahme und die Analyse der Haupt- und Spurenelemente der Eem-Sapropele wurden von Sebastian Eckert unter der Betreuung von Dr. Bernhard Schnetger durchgeführt. Die Mo- und U-Isotopenverhältnisse wurden von Sebastian Eckert unter der Anleitung von Prof. Dr. Stefan Weyer ermittelt. Die Fe-Isotopendaten stammen von Dr. Silke Severmann. Die Extraktion und Quantifizierung der Isorenieratenderivate, sowie die Bestimmung der Kohlenstoffisotopenverhältnisse wurden von Sebastian Eckert unter der Anleitung von Dr. Jürgen Köster durchgeführt. Prof. Dr. Helge Arz hat den Kern 22-GC-3 und das Altersmodell zur Verfügung gestellt. Sebastian Eckert hat die Daten ausgewertet, interpretiert und mit allen Koautoren diskutiert. Das Manuskript wurde von Sebastian Eckert unter Mithilfe aller Koautoren verfasst.

Kapitel 5: The dependency of uranium on sedimentary carbonate content in the Holocene Black Sea

In dieser Arbeit wurde gezeigt, dass die Assoziation von U und Carbonat unter reduzierenden Bedingungen in natürlichen Sedimenten möglich ist. Die geochemische

Analytik der hier genutzten Proben wurde von Sebastian Eckert unter Betreuung von Dr. Bernhard Schnetger durchgeführt. Sebastian Eckert hat die Daten ausgewertet, insbesondere mittels Cluster-Analyse, interpretiert und mit allen Koautoren diskutiert. Das Manuskript wurde von Sebastian Eckert unter Mithilfe aller Koautoren verfasst.

Kapitel 6: Manganese-rich brown layers in Arctic Ocean sediments: Composition, formation mechanisms, and diagenetic overprint

Diese Arbeit befasst sich mit der diagenetischen Umlagerung von Mn in arktischen Sedimenten. Hierbei haben Dr. Christian März und Sebastian Eckert die Probenahme und die Porenwasseranalysen durchgeführt. Sebastian Eckert war an der Interpretation der Daten, sowie bei der Diskussion und Erstellung des Manuskripts, welches von Dr. Christian März verfasst wurde, beteiligt. Die Arbeit wurde wie folgt publiziert:

März C., Stratmann A., Matthiessen J., Meinhardt A.-K., Eckert S., Schnetger B., Vogt C., Stein R., Brumsack H.-J. (2011): Manganese-rich brown layers in Arctic Ocean sediments: Composition, formation mechanisms, and diagenetic overprint. *Geochim. Cosmochim. Acta* **75** (23), 7668-7687.

# 3. Establishment of euxinic conditions in the Holocene Black Sea

Authors:

Sebastian Eckert, Mikrobiogeochemie, Institut für Chemie und Biologie des Meeres (ICBM), Carl von Ossietzky Universität, 26111 Oldenburg

Hans-Jürgen Brumsack, Mikrobiogeochemie, Institut für Chemie und Biologie des Meeres (ICBM), Carl von Ossietzky Universität, 26111 Oldenburg

Silke Severmann, Department of Earth and Planetary Sciences, and Institute of Marine and Coastal Science, Rutgers University, New Brunswick, NJ 08901, USA

Bernhard Schnetger, Mikrobiogeochemie, Institut für Chemie und Biologie des Meeres (ICBM), Carl von Ossietzky Universität, 26111 Oldenburg

Christian März, Mikrobiogeochemie, Institut für Chemie und Biologie des Meeres (ICBM), Carl von Ossietzky Universität, 26111 Oldenburg

Henning Fröllje, Mikrobiogeochemie, Institut für Chemie und Biologie des Meeres (ICBM), Carl von Ossietzky Universität, 26111 Oldenburg

Published in Eckert, S., Brumsack, H.-J., Severmann, S., Schnetger, B., März, C., and Fröllje, H., 2013. Establishment of euxinic conditions in the Holocene Black Sea. *Geology* **41**, 431-434.

## Abstract

The paleoenvironmental evolution of the Black Sea is closely linked to the ingression of Mediterranean seawater over the Bosporus sill after the Last Glacial Maximum. We have reconstructed the temporal and spatial development of the Black Sea suboxic chemocline, which divides oxic surface water from anoxic, sulfidic (euxinic) deep water. By combining high-resolution geochemical records of bulk parameters (carbonate, total organic carbon, sulfur), trace metals (Cu, Mo, V), and an isotopic proxy ($\delta^{56}Fe$) from seven sediment cores in the Black Sea, we generated a single composite geochemical core log that serves as a reference archive for the entire basin. Our proxy records reflect the changing depositional and redox conditions of the Black Sea and permit us to estimate the inflow budget of Mediterranean seawater throughout the Holocene. Our data indicate a gradual rise of the chemocline until ca. 5.3 ka, when suboxic waters flooded the shelf for the first time. Trace metal and isotopic inventories document one major descent of the chemocline since the onset of brackish/marine conditions before the present stable situation was established.

## 3.1. Introduction

The Black Sea is an enclosed marine basin where the ingression of Mediterranean seawater over the shallow Bosporus sill is causing stratification of the water column. The stable pycnocline coincides with the chemocline, and stagnant sulfidic deep water favors the deposition of organic-rich sediments (sapropels). There is an ongoing debate whether the seawater ingression into the basin during the Holocene sea-level rise occurred catastrophically in one single step (the Great Flood; RYAN et al., 1997), or more gradually over a longer time period (AKSU et al., 2002; DEGENS and ROSS, 1974; YANKO-HOMBACH et al., 2007). The suboxic chemocline, separating oxic surface from sulfidic deep water, is currently at ~150 m water depth (HUANG et al., 2000). Its vertical migration ultimately governs the redox development in the Black Sea. Using metal abundances (Fe and Mo) and Fe isotopes ($\delta^{56}$Fe), we unravel the Holocene history of the chemocline and provide evidence for the temporal and spatial development of euxinic conditions in this type location of a restricted basin (BRUMSACK, 2006a; CALVERT and PEDERSEN, 1993).

Sedimentary enrichment of Fe has been observed in sapropels from the Black Sea and other restricted basins (e.g., ANDERSON and RAISWELL, 2004). The most widely accepted explanation for these characteristic enrichments implies the lateral transfer of reactive Fe from suboxic shelf sediments to the sulfidic water column of euxinic basins, where it is sequestered into syngenetic pyrite (CANFIELD et al., 1996; WIJSMAN et al., 2001; WILKIN et al., 1997). In this model, microbially induced diagenetic reactions within the suboxic shelf sediments cause mobilization of reactive Fe with a light Fe isotope composition, which is laterally conveyed in the suboxic chemocline. Strong support for this Fe shuttle model comes from the covariation between bulk sedimentary Fe/Al ratios and Fe isotope composition (SEVERMANN et al., 2008). Euxinic sediments with elevated Fe/Al ratios have lower $\delta^{56}$Fe values due to the basinward transport of isotopically light Fe.

Water column studies show elevated concentrations of dissolved and particulate Fe within the chemocline (LEWIS and LANDING, 1991), corroborating the model of enhanced lateral Fe transfer along this oxygen-depleted interface (LYONS and SEVERMANN, 2006). Consequently, the efficiency of the Fe shuttle is linked to the depth of the chemocline and therefore the surface area of either slope or shelf sediments

intercepting with suboxic waters (ANDERSON and RAISWELL, 2004). Changing sea level may exert additional control on the vertical migration of the chemocline (ARTHUR and SAGEMAN, 2005).

In the Black Sea sediments, Mo is a tracer for both seawater inflow and water column redox conditions. While Mo is the most abundant trace metal in oxic seawater, it may undergo significant drawdown under euxinic conditions (BERTINE, 1972). At dissolved sulfide concentrations $> 11\ \mu M$, Mo is transformed into highly particle-reactive thiomolybdates or Mo-Fe-S nanominerals that are quantitatively scavenged from the water column (ERICKSON and HELZ, 2000; HELZ et al., 2011). Low deep-water Mo concentrations (NEUBERT et al., 2008) document the almost complete transfer of the water column Mo inventory to the sedimentary pool. Thus, sedimentary Mo records of restricted basins broadly reflect the amount of inflowing seawater and at the same time serve as euxinia proxies under marine conditions, independent from the Mo removal pathway via sulfide or organic matter (ALGEO, 2004; ALGEO and LYONS, 2006; BRUMSACK, 1989b; HELZ et al., 2011).

### 3.2. Samples and Methods

Instead of showing individual sediment cores, we combine high-resolution data sets from seven sites throughout the basin (Abb. 3-4 in the GSA Data Repository) in a composite geochemical core log (CGCL) that serves as a reference for the entire Black Sea (Abb. 3-1 and Abb. 3-6). This approach is based on the assumption that water column processes in the Black Sea occurred synchronously on a basinwide scale, only influenced by variations in local sedimentation rate. All cores originate from the euxinic part of the water column. GeoB gravity cores follow a transect through the western basin (R/V *Meteor* expedition M51/4); cores from station 8, 14, and 22 were recovered in the northwestern part of the basin and off the eastern Anatolian coast (R/V *Meteor* expedition M72/5). A single composite core instead of seven cores illustrates basinwide similarities and highlights ubiquitous environmental changes in the geological record of the Black Sea after seawater ingression. Unit boundaries are based on lithological and geochemical criteria. Mean ages of the unit boundaries were taken from data in the literature (for details, see the Data Repository). For constructing the CGCL, we further considered distinct geochemical characteristics such as Mo, total organic carbon (TOC),

and Fe maxima. Based on these adjustment points, core depths were normalized to a reference depth scale. CGCL depicts the averaged and normalized vertical element distribution in Black Sea sediments.

Major and trace elements were analyzed by X-ray fluorescence and inductively coupled plasma–optical emission spectrometry. TOC and total sulfur (TS) were measured by coulometry and infrared spectrometry. Iron isotope compositions, reported here as $^{56}Fe/^{54}Fe$ delta notation normalized to average igneous rocks ($\delta^{56}Fe$), were determined by multicollector–inductively coupled plasma–mass spectrometry (Thermo Scientific NEPTUNE). For further details on samples and methodology, see the Data Repository.

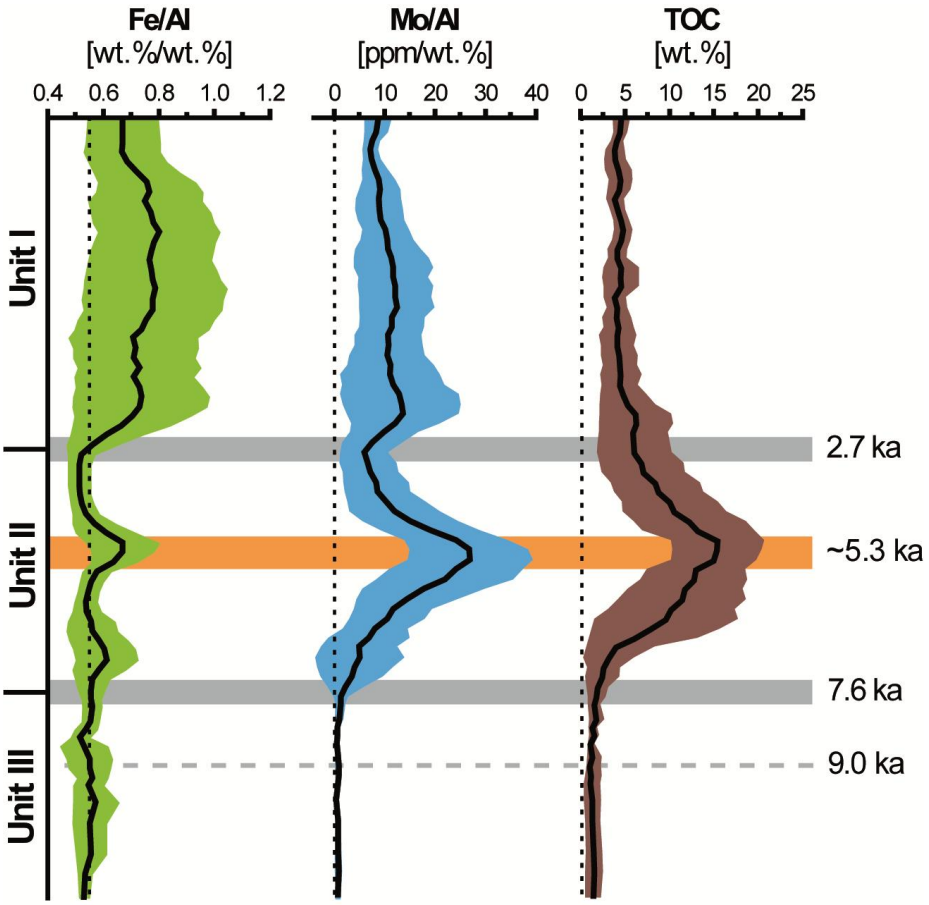


**Abb. 3-1** Composite geochemical core logs of Fe/Al, Mo/Al, and total organic carbon comprising data of seven cores (see text and Samples and Methods discussion); colored areas reflect standard deviation; vertical dashed lines are average shale values (WEDEPOHL, 1991); horizontal dashed line displays first ingression of Mediterranean seawater (ca. 9.0 ka; SOULET et al., 2011); horizontal gray bars depict unit boundaries; beige bar depicts first establishment of shelf suboxia (ca. 5.3 ka).

### 3.3. Results and Discussion

Common features observed in all Black Sea sediment cores are distinct Fe enrichments (Fe/Al > 0.55; WEDEPOHL, 1991) in the Holocene section. According to the Fe shuttle hypothesis, these enrichments may be explained by the impingement of suboxic chemocline waters on the broad Black Sea shelf. Suboxia on the shelf caused diagenetic mobilization of Fe with low $\delta^{56}$Fe values and its trapping in euxinic basin sediments (LYONS and SEVERMANN, 2006; SEVERMANN et al., 2008). In turn, during chemocline descent, Fe/Al ratios should be significantly lower (and $\delta^{56}$Fe values higher) in basin sediments (Abb. 3-2 and Abb. 3-3).

An initial Fe enrichment coinciding with the unit II-III boundary (ca. 7.6 ka) is characterized by light Fe isotope values (Abb. 3-1 and Abb. 3-2). This boundary documents the onset of anoxia in Black Sea bottom waters, followed by a chemocline rise and the expansion of euxinic conditions (ARTHUR and DEAN, 1998; DEGENS and ROSS, 1974). Synchronously increasing TOC and Mo/Al values reflect the transition from limnic (oxic) to marine (anoxic and/or euxinic) conditions, increasing productivity, changing redox conditions, and a growing Mo inventory as seawater entered the Black Sea basin.

The onset of marine conditions at the unit II-III boundary led to significant postdepositional overprinting. Following the inflow of seawater into the basin, $HS^-$ accumulated in euxinic unit II sediments and started migrating downward into limnic unit III sediments. Here it reacted with oxide-bound Fe, creating opposing gradients of $Fe^{2+}_{aq}$ and $HS^-$. The sulfidization front, currently located well below the sapropel, is marked by a distinct band of diagenetic FeSx precipitates (NERETIN et al., 2004). Continuous supply of sulfide from bacterial sulfate reduction in the sapropel forms an effective barrier to upward-migrating $Fe^{2+}_{aq}$. Mass balance calculations confirm the downward movement of the reaction front (JØRGENSEN et al., 2004). Consequently, a diagenetic origin of the Fe enrichment observed in unit II can be excluded.

Further upcore, a prominent Fe enrichment at ca. 5.3 ka is observed in the central part of unit II, coinciding with maxima in TOC, Mo/Al, and light Fe isotopes (Abb. 3-1, Abb. 3-2, and Abb. 3-6). This Fe/Al peak documents the first establishment of a fully expanded euxinic water column in the Black Sea (Abb. 3-1), where the chemocline impinged on the shelf with its much larger surface area compared to the slope, causing

an intensified shuttling of Fe with a low $\delta^{56}$Fe signature (Abb. 3-1, Abb. 3-2, and Abb. 3-3B). Increasing Mo/Al ratios record the growing Mo reservoir fed by continuing seawater inflow, and an increasing Mo drawdown owing to the expansion of euxinic water masses. The TOC maximum reflects higher surface productivity, but is also affected by improved organic matter preservation in a sulfidic water column (CALVERT and PEDERSEN, 1993).

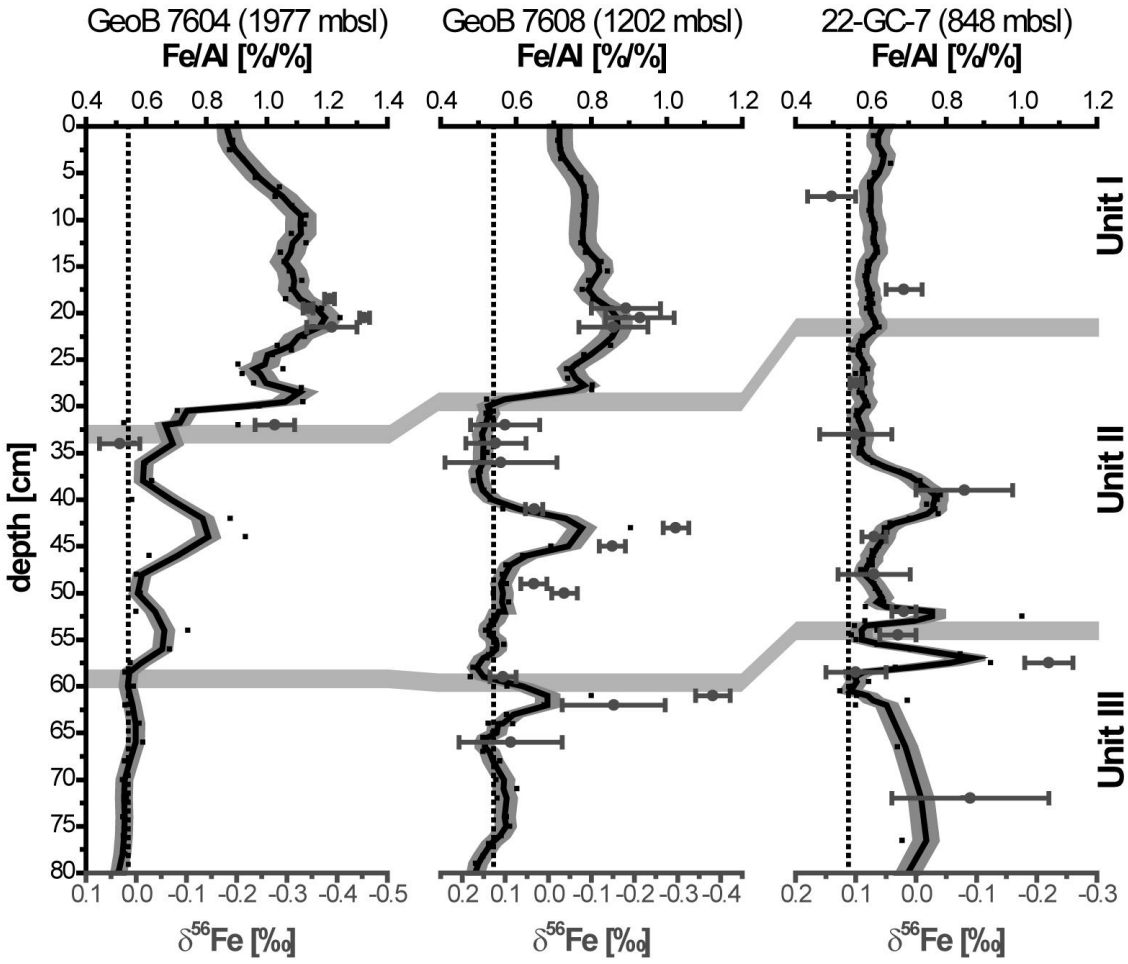


**Abb. 3-2** Depth profiles of Fe/Al and $\delta^{56}$Fe
Fe/Al (black dots−measured data; solid lines−two-point average smoothing; gray areas−standard deviation of the measurement) and $\delta^{56}$Fe (large dark gray dots; note inverted scale) for gravity cores GeoB 7604, GeoB 7608, and 22-GC-7. Vertical dashed lines show average shale Fe/Al ratio of 0.55 (WEDEPOHL, 1991); error bars represent 2σ standard deviation; gray horizontal bars are unit boundaries; mbsl−meters below sea level.

We estimate the past seawater influx into the Black Sea from the gradual Mo increase between the unit II-III boundary and the Mo peak in unit II (for details, see the Data Repository). Based on today's deepwater salinity of 22, the Mediterranean seawater inflow increased from < 10 $km^3$/a at the onset of Mo enrichment at ca. 8 ka (PIPER and

CALVERT, 2011) to 350 $km^3/a$ at the Mo maximum in unit II, which is comparable to the present 305 $km^3/a$ inflow (ÖZSOY and ÜNLÜATA, 1997). A simple budget calculation demonstrates that the water column of the Holocene Black Sea was replenished at least twice during deposition of unit II to account for the Mo enrichment in the sapropel. This is in line with a renewal time of 935 a for Black Sea deep waters (ÖSTLUND, 1974). Our data imply an initial rise of the chemocline from the deep basin (~2200 m water depth) to the shelf break (~200 m water depth) over a period of ~2 ka. The respective chemocline rise of ~1 m/a agrees well with our assumed seawater influx of ~1 $m^3 \cdot m^{-2} \cdot a^{-1}$.

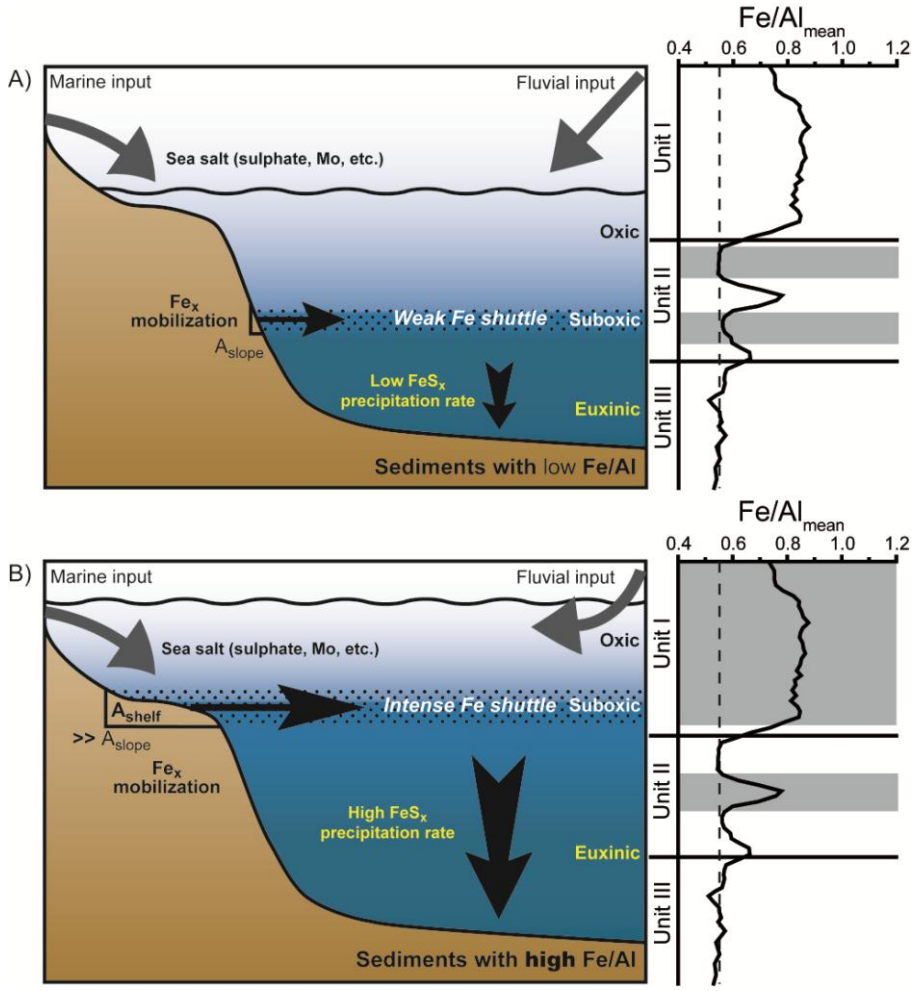


**Abb. 3-3** Scheme of chemocline evolution in Holocene Black Sea.
A: Chemocline rises above sediment surface and impinges slope, where small amounts of reactive iron ($Fe_x$) are mobilized, precipitate as sulfide in euxinic water column, and accumulate in basin sediments. B: Chemocline reaches shelf for first time, where large quantities of $Fe_x$ are mobilized, which are transported in suboxic waters, precipitate as sulfides, and accumulate in sapropels, as reflected by high Fe/Al ratios. After this stage, chemocline oscillates back to slope (A) before its final ascent to the shelf during deposition of unit I. During chemocline descent, Fe shuttle mechanism is shut off. Vertical dashed line reflects average shale Fe/Al ratio of 0.55 (WEDEPOHL, 1991); gray areas in vertical profiles highlight intervals deposited during corresponding chemocline mode.

The return to very low Fe/Al and relatively heavy Fe isotope values in the upper unit II (Abb. 3-1 and Abb. 3-2) documents the descent of the chemocline. Slope sediments previously sulfidized by direct contact with euxinic waters could not serve as a source for dissolved Fe, so the Fe shuttle was shut off (Abb. 3-3A). At the same time, Mo/Al ratios gradually decrease from maximum values in unit II to lower values at the base of unit I (Abb. 3-1), either due to stronger hydrographic restriction or increased river input and freshening of the Black Sea basin (REPETA, 1993; VAN DER MEER et al., 2008). While our geochemical data do not allow us to distinguish between these two processes, decreased seawater input due to a shoaling of the Bosporus sill by tectonic activity or a local sea-level regression seems very plausible (BRÜCKNER et al., 2010). Despite diminished seawater input, euxinic conditions still persisted in the deeper water column, as documented by the decreasing but still relatively high TOC and Mo/Al values (Abb. 3-1). Mo removal from the euxinic water column outbalanced its replenishment by deep-water renewal.

Elevated Fe/Al ratios with light $\delta^{56}$Fe values in unit I, similar to the peak seen in unit II (Abb. 3-1 and Abb. 3-2), indicate the recurring rise of the chemocline to its present location on the shelf break (Abb. 3-3B). Surface productivity, organic matter preservation (TOC profiles in Abb. 3-1), and chemocline depth (as documented by relatively invariant Fe/Al and $\delta^{56}$Fe; Abb. 3-2) are fairly stable throughout unit I with some minor fluctuations ~200–300 a ago (LYONS et al., 1993; REPETA, 1993). Unit I represents the stable marine stage of the Black Sea basin, with a rather constant and balanced inflow and outflow of marine and brackish waters.

Our data strongly suggest a variable efficiency of the Fe shuttle mechanism. In unit I sediments, an excess Fe fraction of 22 % explains the Fe/Al CGCL. A simple inventory calculation demonstrates that the Fe shuttle mechanism does not significantly deplete the Fe pool in Black Sea shelf sediments (see the Data Repository). Based on our average unit I $\delta^{56}$Fe value of –0.25 ‰, isotope mass balance calculations suggest an Fe shuttle contribution of ~36 %. This value is in broad agreement with the previous value.

The Black Sea chemocline oscillation reported here agrees with earlier studies on syngenetically formed pyrite framboids (WILKIN and ARTHUR, 2001) and biomarkers, which suggest that the chemocline was located below the photic zone during deposition of unit III, upper unit II, and unit I, but intersected with the photic zone during

deposition of lower unit II (HUANG et al., 2000; REPETA, 1993). Our results confirm these studies, as we find low Fe/Al ratios in units III and upper unit II, but higher Fe/Al ratios in lower units II and unit I (Abb. 3-1).

### 3.4. Conclusion

Our high-resolution composite geochemical core log and Fe isotope data demonstrate that the establishment of the chemocline and euxinic conditions in the Black Sea water column did not occur in one single step. High-resolution Fe/Al records show that within unit II, ca. 5.3 ka, suboxic waters spread over large areas of the shelf for the first time, initiating the transfer of Fe from the shelf toward the basin by the Fe shuttle mechanism. In parallel, the gradual sedimentary Mo increase documents that Mediterranean seawater inflow was comparable to today. After this first fully euxinic stage, a prominent chemocline drop and concomitant decrease in Fe/Al ratios and Mo inventory is observed, due either to hydrographic restriction or increased fluvial input. With the onset of unit I ca. 2.7 ka, the Fe shuttle was reestablished, and the chemocline reached its present position. We show that sedimentary archives in anoxic systems like the Black Sea precisely record basinwide changes in water column processes. Similar budget calculations may be important for the interpretation of trace metal records in ancient anoxic settings.

*Acknowledgements:*

This study was supported through grants from the German Research Foundation (DFG, Deutsche Forschungsgemeinschaft) to Brumsack (Br 775/15 and 775/26). We thank the crew members of R/V *Meteor* expeditions M51/4 and M72/5, and Tim Lyons and two anonymous reviewers for thoughtful reviews.

## 3.5. Data Repository

### 3.5.1. Sample preparation and analysis

Trace metal and major element analyses were performed at the ICBM, Oldenburg (Germany), according to the following protocol:

Sediment samples were freeze-dried and ground with an agate planetary ball mill before being analyzed by X-Ray Fluorescence (XRF) for major and minor elements, by infrared (IR) spectroscopy for total carbon (TC) and total sulfur (TS) and by $CO_2$-Coulometry for total inorganic carbon (TIC). The amount of total organic carbon (TOC) was calculated as the difference between TC and TIC.

For XRF analysis 0.7 g of dried and ground sample were mixed with 4.2 g $Li_2B_4O_7$ and 1.0 g $(NH_4)_2NO_3$ (oxidizing agent) and fused to borate glass beads at 1350 °C in platinum crucibles. These beads were analyzed with a Philips PW-2400 WD-XRF spectrometer (calibrated with 53 geostandards and checked for accuracy by random measurements of acid digested samples using an iCap 6000 Inductively Coupled Plasma Optical Emissions Spectrometer).

For TC and TS analyses a given amount of dried and ground sample (50-100 mg) was mixed with $V_2O_5$ (oxidizing agent) and combusted in an $O_2$ stream. The resulting $CO_2$ and $SO_2$ were measured with an ELTRA CS-500 IR-spectrometer. For TIC analysis 5 ml 2 M $HClO_4$ were added to 50-100 mg of dried and ground sample, and the evolving $CO_2$ was measured in a coulometric cell (UIC CM-5012; carrier gas: $N_2$).

All analytical results were cross-checked by parallel analysis of in-house and international reference materials (olivine basalt GSR-3, carbonate rock GSR-6). The relative standard deviations (RSDs) for our XRF-measurements are < 5 % for major and < 8 % for trace elements, while the RSDs for TC, TIC and hence TOC are < 1 % and for TS < 5 %.

Because carbonate and organic carbon contents vary significantly in Black Sea sediments, we use element/Al ratios to compensate for dilution effects. In the following, the Fe/Al and Ca/Al ratios are given as [wt. %/wt. %], while the trace metal/Al ratios are defined as [ppm/wt. %]. The original data will be published in PANGAEA (www.pangaea.de; doi in progress).

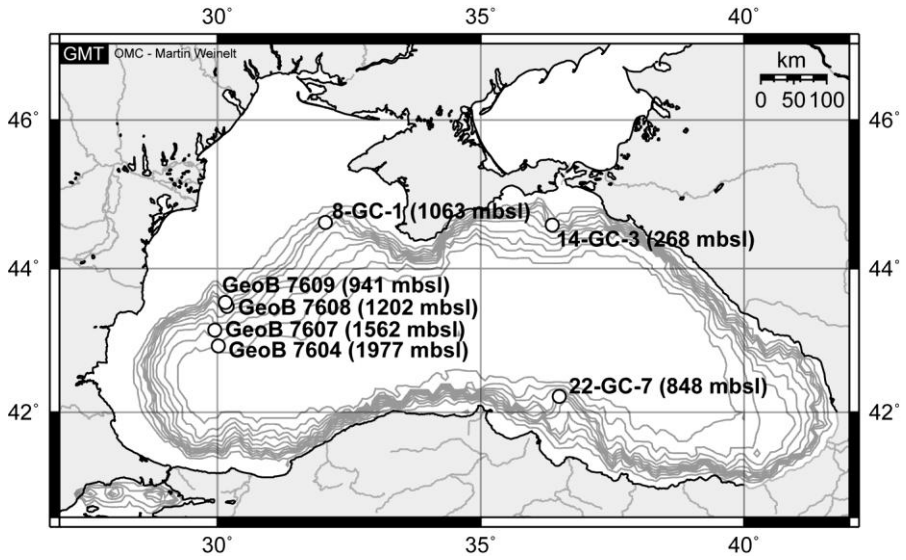


**Abb. 3-4** Map of the Black Sea with sampling locations. Sampling depths are noted in brackets (created by OMC: http://www.aquarius.geomar.de/make_map.html; OMC copyright: M. Weinelt).

### 3.5.2. Iron isotope analysis

Samples for iron isotope analysis were processed at the Institute of Marine and Coastal Sciences, Rutgers University, USA. Dried sediments were fully digested by standard acid digestion techniques ($HF-HNO_3-HCl$) and iron was purified by passing sample solutions through an anion exchange resin, using standard protocol (SEVERMANN et al., 2006). Iron isotope measurements were performed at the Woods Hole Oceanographic Institute ICP facility, Massachusetts, USA, using a Thermo Fisher Neptune multiple-collector ICP mass spectrometer, following the procedure of Arnold et al. (2004a). Purified samples were introduced into the mass spectrometer as 200–500 ppb iron solutions, mixed with equal amounts of copper standard of known isotope composition (NIST-976 copper isotope standard), which was measured simultaneously for mass bias correction. Bracketing standards were measured after every second sample for additional mass bias control. Isotope ratios of $^{56}Fe/^{54}Fe$ and $^{57}Fe/^{54}Fe$ are reported using standard delta notation. Measured ratios are normalized relative to igneous rocks, which have an average isotope composition of $\delta^{56}Fe = 0 \pm 0.10$ ‰ (2σ) (BEARD et al., 2003). On this scale the isotope composition of the international iron isotope reference material IRMM-014 is -0.09 ‰ for $\delta^{56}Fe$. The average external precision for $\delta^{56}Fe$ was typically better than ± 0.10 ‰ (2σ) for all samples. Several standard reference materials of known isotope composition, including SDO-1 (Devonian black shale) BIR-1 (basalt)

and SCo-1 (Upper Cretaceous silty marine shale) were measured routinely for each sample batch, and values agreed well with previous measurements and published values.

### 3.5.3. Constructing the composite geochemical core log (CGCL)

All cores used for the construction of the CGCL originate from the euxinic section of the water column in different parts of the Black Sea. The four GeoB cores follow a transect through the western basin, the cores from sites 8, 14, and 22 were recovered in the north-western part and off the eastern Anatolian coast (Abb. 3-4). Several major element and metal proxies in these seven gravity cores (Abb. 3-4 and Abb. 3-5) were combined to a single composite core log (Abb. 3-2 and Abb. 3-6) following a three-step procedure:

1) The depth scale of each core was adjusted to a reference core by linear interpolation between five adjustment points chosen based on litho-/chemostratigraphic similarities: a) Unit II/III and b) Unit I/II boundaries (on the basis of lithology, TOC and CaCO3 profiles, according to ARTHUR and DEAN, 1998; ROSS and DEGENS, 1974), c) Fe/Al peaks, d) Mo maxima and e) TOC maxima. This was done to compensate for variations in sedimentation rate respectively dilution.

2) Proxy data were combined and mean values plus standard deviations were calculated for each interpolated 1 cm depth interval by a MATLAB routine.

3) The resulting composite profiles underwent a two-point-average smoothing to remove part of the scatter.

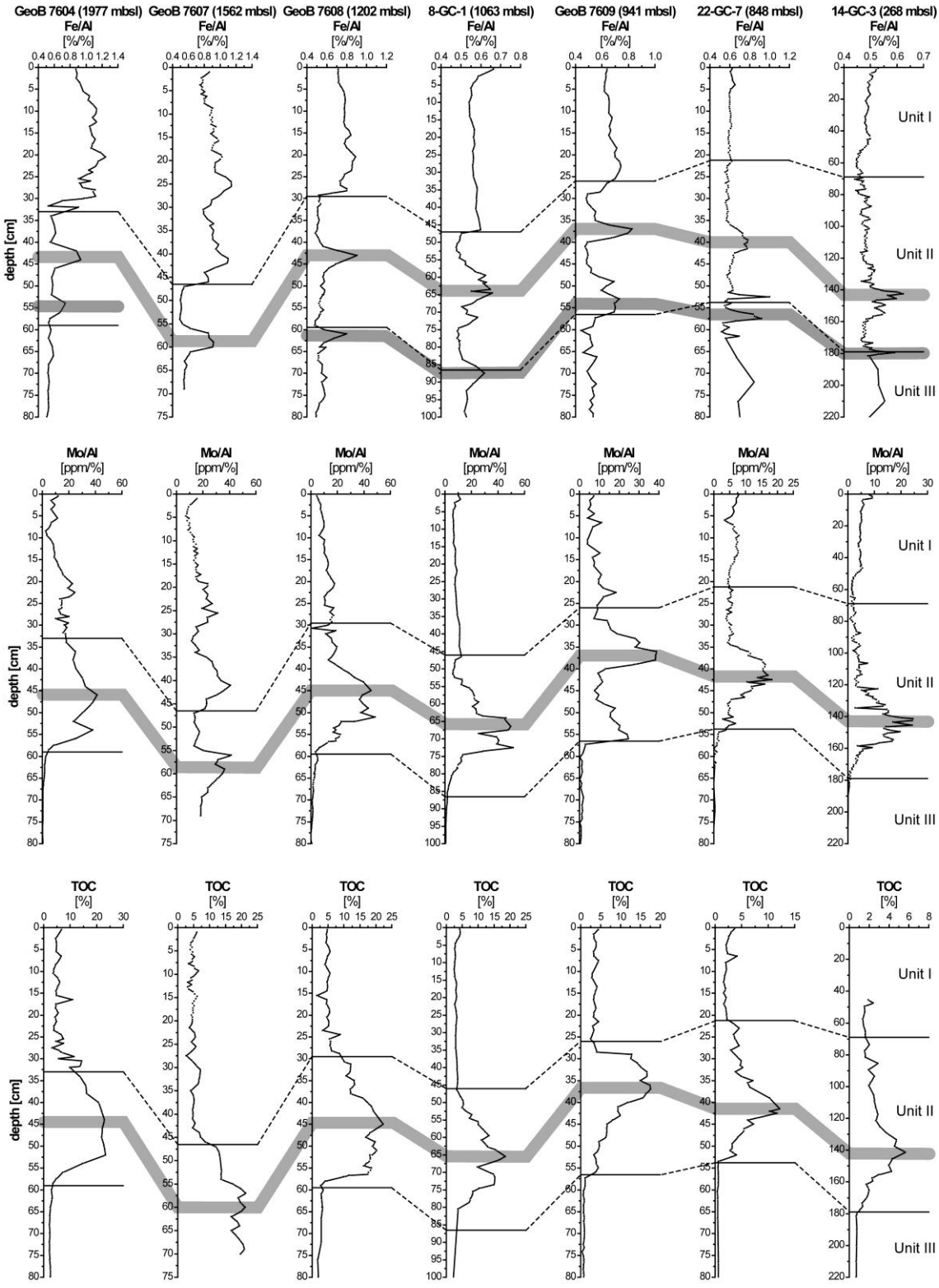


**Abb. 3-5** Depth profiles of Fe/Al, Mo/Al and TOC for the sampling locations shown in Abb. 3-4. The horizontal lines indicate the unit boundaries. The shaded bars highlight ubiquitous signals in the geochemical records. The original data will be published in PANGAEA (www.pangaea.de; doi in progress).

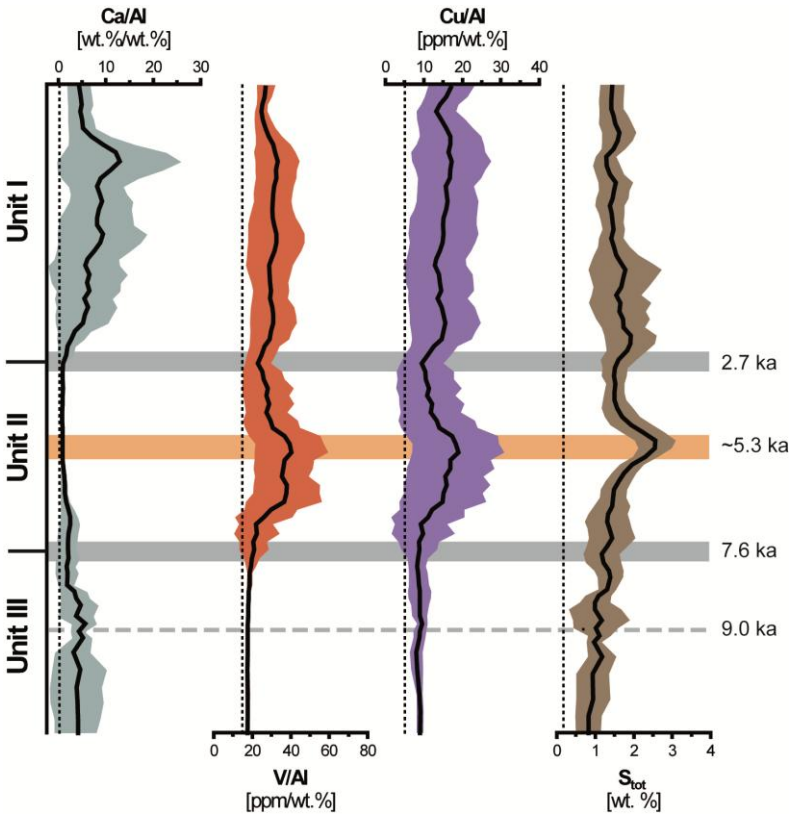


**Abb. 3-6** Composite geochemical core logs (CGCL) of Ca/Al, Cu/Al, V/Al, and $S_{tot}$. The vertical distribution patterns are based on element data of seven cores (see text and method section). The colored areas show the standard deviations. The vertical dashed lines represent average shale values. The dashed horizontal line displays the first ingression of Mediterranean seawater into the Black Sea basin (9.0 ka; SOULET et al., 2011). The beige bar depicts first establishment of shelf suboxia (~5.3 ka). The grey horizontal bars show the unit boundaries. The Ca/Al profile parallels the establishment of coccolithophorida communities in Unit I after completion of the limnic/marine transition. Cu/Al, V/Al, and $S_{tot}$ display the development of euxinic conditions in the sedimentary archive, as do Fe/Al, Mo/Al, and TOC data. TOC indicates an increase in productivity and/or preservation during the transition phase (Unit II).

The age model of the CGCL is based on the average thickness of each unit and the average ages of the Unit I/II and Unit II/III boundaries as defined by lithological and geochemical criteria from the literature in seven cores across the Black Sea (ARTHUR and DEAN, 1998; BAHR et al., 2006; BAHR et al., 2005; JONES and GAGNON, 1994; LAMY et al., 2006; MAJOR et al., 2002; ROSS and DEGENS, 1974; VERLEYE et al., 2009; see also Tab. 3-1). The mean ages of around 2.7 ka for the Unit I/II and 7.6 ka for the Unit II/III boundaries are valid for the whole basin because relatively rapid paleoenvironmental changes (as indicated by distinctive peaks in the geochemical records) occur at different sampling locations. The chronology of core GeoB 7608 (Abb. 3-4), which is also incorporated in our CGCL, was established by Bahr et al. (2006; 2005).

**Tab. 3-1** Age model for Black Sea basin sediments using average boundary ages from the literature.

| Age Unit I/II boundary [cal. kyr BP] | Age Unit II/III boundary [cal. kyr BP] | References |
|---|---|---|
| 2,044 ± 7 | 7,869 ± 237 | Arthur & Dean (1998) |
| | 7,607 ± 40 | Bahr et al. (2005, 2006) |
| 2,720 ± 160 | 7,540 ± 130 | Jones & Gagnon (1994) |
| 2,760 ± 35 | 7,995 ± 55 | Lamy et al. (2006) |
| 3,330 ± 108 | 7,160 ± 108 | Major et al. (2002) |
| 3,090 ± 140 | 7,090 ± 180 | Ross & Degens (1974) |
| 3,050 ± 35 | 8,140 ± 50 | Verleye et al. (2009) |
| 2,760 ± 287 | 7,607 ± 316 | Median |

### 3.5.4. Inventory calculation based on Mo enrichment

We assume an anoxic water column of 2,000 m depth with an average Mo concentration of 4 µg/l (equivalent to an absolute Mo content of 8 g/m²) (NÄGLER et al., 2011), while the average Mo concentration of oxic seawater (salinity: 35) is ~10 µg/l (MARTIN and WHITFIELD, 1983). The Black Sea Unit II sapropel is on average 30 cm thick, has a density of 1.5 g/cm³, a porosity of 60 %, and an average Mo content of 80 mg/kg, leading to a total Mo content ($P_{Mo\,t}$) of 14 g/m². Thus, roughly twice the water column Mo inventory was incorporated into the basinwide Unit II sapropel. Consequently, assuming quantitative Mo removal, the water column Mo inventory had to be replenished at least twice over the duration of the sapropel formation (see also Tab. 3-2).

**Tab. 3-2** Parameters used for calculation of budgets.

| | |
|---|---|
| **Sedimentary parameters** | |
| Black Sea basin area | $A_{BS}$ = 413,000 km² |
| Avg. density | $\rho$ = 1.5 t/m³ |
| Avg. porosity | $\Phi$ = 60 % |
| Mass of 1 cm sediment layer | $m = \rho \cdot 0.01\ m^3 \cdot (1 - \Phi) = 0.006$ t |
| $Fe_{total}$ content of the sapropel in 1 cm interval | $Fe_t$ [mg/kg] |
| $Fe_{total}$ content of 1 cm layer per m² | $C_{Fe}$ [g] = $Fe_t \cdot m$ |
| $Mo_{total}$ content of the sapropel in 1 cm interval | $Mo_t$ [mg/kg] |
| $Mo_{total}$ content of 1 cm layer per m² | $C_{Mo}$ [g] = $Mo_t \cdot m$ |
| Avg. sedimentation rate of Unit I | $SR_I$ = 0.0155 cm/yr → 1 cm = 65 yr |
| Avg. sedimentation rate of Unit II | $SR_{II}$ = 0.0065 cm/yr → 1 cm = 154 yr |
| **Water column parameters** | |
| Anoxic water column | $d_{wc}$ = 2000 m |
| Avg. Mo concentration | $Mo_{aq}$ = 4 µg/l |
| Mo content per m² | $P_{Mo\ aq} = (Mo_{aq} \cdot d_{wc}) / 0.001\ m^2 = 8$ g/m² |
| Inflowing seawater Mo concentration (salinity of 22) | $Mo_{sw}$ = 6.7 µg/l |
| Seawater inflow estimates | $F_{SW}$ [km³/yr] = $[(C_{Mo} / Mo_{sw}) / (1/SR)] \cdot A_{BS}$ |
| **Sapropel parameters** | |
| Avg. thickness of Unit II sapropel layers | $d_{sap}$ = 30 cm |
| Correction factors for the average sedimentation rate of Unit I and II | $f_I$ = 1.9 and $f_{II}$ = 1.3 |
| Absolute Fe content of the Black Sea sapropel | $M_{Fe} = (f_I \cdot \Sigma C_{Fe\ Unit\ I} + f_{II} \cdot \Sigma C_{Fe\ Unit\ II}) \cdot A_{BS} = 6.8 \cdot 10^9$ t |
| Avg. Mo content in the Unit II sapropels | $Mo_{t2}$ = 80 mg/kg |
| Mo content per m² | $P_{Mo\ t} = [\rho \cdot (1 - \Phi) \cdot d_{sap}] \cdot Mo_{t2} = 14$ g/m² |

Estimates of past seawater inflow over the Bosporus sill into the Black Sea are based on the Mo contents in each 1-cm interval of the CGCL. The sedimentary parameters (porosity, density, Mo content and sediment thickness) are taken from the calculation above. At an average sedimentation rate of 0.0065 cm/a for Unit II sediments, each 1-cm interval of the CGCL corresponds to about 150 a. The sedimentary parameters and the Mo contents may be used to calculate the total Mo inventory of each basin-wide

sediment layer, which is equivalent to a specific volume of seawater required to provide the total amount of Mo. We assume a dilution of the inflowing Mediterranean seawater equivalent to today's Black Sea deep water salinity (22), resulting in a Mo concentration in the water column of about 6.7 µg/l. Dividing the total Mo inventory in a basin-wide sediment interval by this Mo concentration results in the volume of seawater required per m² per year. To compare with today's situation, the seawater inflow of 305 km³/a has to be divided by the anoxic basin area of approx. 300,000 km², resulting in 1.0 m/a water exchange (ÖZSOY and ÜNLÜATA, 1997). Multiplication by the Black Sea basin area (413,000 km²) leads to the total influx of seawater ($F_{SW}$) into the Black Sea per year (see also Tab. 3-2).

### 3.5.5. Inventory calculations for Fe enrichment in shelf sediments

To estimate the excess Fe content ($Fe_x$) in the deep basin sediments we calculated the $Fe_x$ after eq. 3 for every cm interval of the CGCL.

$$Fe_x = Fe - \left(Al \times \frac{Fe}{Al_{bg}}\right) \quad (3)$$

where Fe and Al are the iron and aluminum contents, respectively, in the sample and $Fe/Al_{bg} = 0.51$ is the minimum Fe/Al ratio of all Unit III samples with a total sulfur content < 0.1 % (n = 230), representing the iron background value excluding an overprinting by diagenetic Fe sulfides. In a second step, the percentage of the $Fe_x$ fraction relative to the total Fe was calculated. To eliminate scatter, a two-point-average smoothing was applied to the data, resulting in Abb. 3-7. This simple inventory calculation shows that 14-27 % (mean value: 22 %) of the Fe in the Fe-enriched sapropel sediments must originate from elsewhere.

The accumulation rates of total Fe in the basin sediment were calculated by using the Fe content per 1-cm interval of the CGCL, the sediment properties from above, and an average sedimentation rate of 0.0155 cm/a (65 a/cm) for Unit I. The calculations were performed by using the same method as for the Mo budget.

The Fe inventory of the basin sapropel ($M_{Fe}$) was calculated by integrating the total Fe contents per m² at 1-cm intervals in the CGCL for Units I and II separately. To correct for the dilution by the spatially varying sedimentation rates in the Black Sea basin during deposition of both units, accumulation rates were multiplied by factors of 1.3 and 1.9 for Unit I and II, respectively. These modified accumulation rates were multiplied by the Black Sea basin area to estimate the total amount of Fe enriched in the sapropel layer ($M_{Fe}$ = 6.8 x $10^9$ t; see also Tab. 3-2). The estimated excess Fe fraction (1.8 x $10^9$ t) of this iron inventory represents 17 % of the $Fe_x$ from the average Holocene Black Sea sediments, and 22 % of the Fe enriched layer in Unit I and II. A simple inventory calculation shows that shelf sediments provide enough Fe to explain the enrichments in the deep basin sapropel: We calculated from Fe/Al ratios that the sapropel contains on average ~22 % $Fe_x$. Multiplying this excess Fe with the basin-to-shelf area ratio (170,000 km²/140,000 km² = 1.21) results in ~27 % of $Fe_x$ that must have been mobilized from the shelf. We investigated three cores from the suboxic shelf with an average Fe concentration of 3 wt. %. Since sediment accumulation rates are at least four times higher on the shelf compared to the basin, we calculate a maximum loss of ~0.2 wt. % of the shelf Fe inventory due to the Fe shuttle model. Owing to the locally variable Fe content of Black Sea shelf sediments, this loss may be insignificant.

In addition to the Fe inventory, the fraction $f$ of mobilized $Fe_x$ was calculated by Fe isotope mass balance, using equation (4) transposed to $f_{Fe_x}$ :

$$\delta^{56}Fe_{total} = f_{Fe_x} \times \delta^{56}Fe_x + \left(1 - f_{Fe_x}\right) \times \delta^{56}Fe_{weath} \qquad (4)$$

$\delta^{56}Fe_x$ was calculated following the equation of Severmann et al. (2008) for samples with Fe enrichment, and separately for samples with Fe/Al background values. $\delta^{56}Fe_{weath} \approx 0 \pm 0.05$ ‰ is the average Fe isotope composition of weathering input diluting the Fe enrichments. On the basis of equation (2), the $\delta^{56}Fe_{total}$ value of the Fe/Al peaks may be explained by a 36 % contribution of $Fe_x$ mobilized from the shelf sediments. This value is in line with the overall calculated $Fe_x$ fraction of > 20 %.

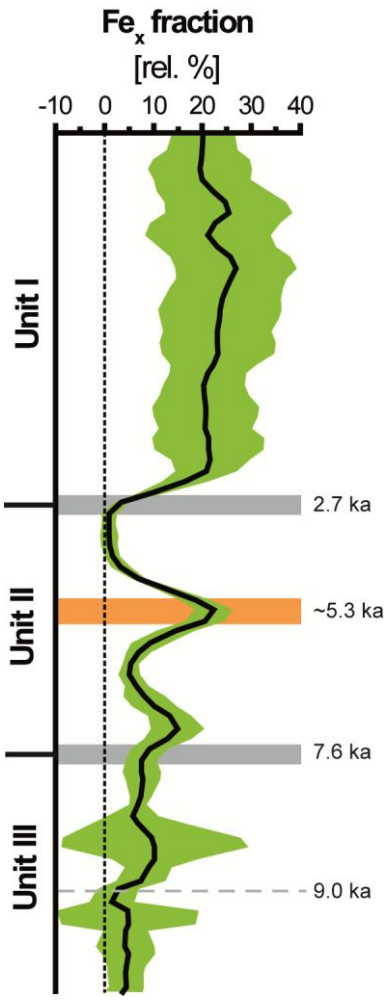


**Abb. 3-7** Percentage of the $Fe_x$ fraction relative to total Fe in CGCL.
The green area shows the standard deviation; the vertical dashed line shows the zero % $Fe_x$ fraction, negative values are due to diagenetic Fe mobilization. This plot is based on the Fe/Al background value of 0.51 for Unit III samples with low S contents, thus excluding diagenetic Fe sulfide overprinting. The dashed horizontal line displays the first ingression of Mediterranean seawater into the Black Sea basin (9.0 ka). The beige bar depicts first establishment of shelf suboxia (~5.3 ka). The grey horizontal bars show the unit boundaries.

# 4. The Eemian and Holocene marine ingressions into the Black Sea: A geochemical comparison

Authors:

Sebastian Eckert, Mikrobiogeochemie, Institut für Chemie und Biologie des Meeres (ICBM), Carl von Ossietzky Universität, 26111 Oldenburg

Bernhard Schnetger, Mikrobiogeochemie, Institut für Chemie und Biologie des Meeres (ICBM), Carl von Ossietzky Universität, 26111 Oldenburg

Stefan Weyer, Institut für Mineralogie, Leibniz Universität Hannover, 30167 Hannover

Silke Severmann, Department of Earth and Planetary Sciences, and Institute of Marine and Coastal Science, Rutgers University, New Brunswick, NJ 08901, USA

Jürgen Köster, Mikrobiogeochemie, Institut für Chemie und Biologie des Meeres (ICBM), Carl von Ossietzky Universität, 26111 Oldenburg

Helge Arz, Leibniz Institut für Ostseeforschung, Warnemünde (IOW), 18119 Rostock

Hans-Jürgen Brumsack, Mikrobiogeochemie, Institut für Chemie und Biologie des Meeres (ICBM), Carl von Ossietzky Universität, 26111 Oldenburg

to be submitted to *Geochim. Cosmochim. Acta*

## Abstract

During R/V *Meteor* expedition M72/5 in 2007, two gravity cores (22-GC-7/3) were recovered, which contain a sapropel of presumably Eemian age 7 m beneath the recent (Holocene) one. Both sapropels were sub-sampled on a millimeter scale and analyzed for major and trace elements. Additionally, selected samples of the Eemian sapropel were analyzed for isotopic proxies ($\delta^{56}$Fe, $\delta^{97}$Mo, $\delta^{238}$U, $\delta^{13}$C) and organic markers for photic zone euxinia (isorenieratene derivatives). Total organic and inorganic carbon in the Eemian sapropel were used to establish a lithological classification analogous to the accepted unit classification of the Holocene sapropel. Comparable enrichments in redox-sensitive elements (e.g. Co, Cr, Cu, Fe, Mo, Ni, U and V) indicate that both sapropels were deposited under anoxic to euxinic conditions. Trace metal enrichments suggest a slightly different paleoenvironmental setting during both time periods. $\delta^{238}$U and $\delta^{97}$Mo values indicate an anoxic but not fully euxinic environment during the Eemian interglacial, while in the Holocene a euxinic water column has been fully established. Element enrichment patterns of the Eemian sapropel are comparable to those of the Holocene sapropel from the same location, as well as to those of the age-equivalent *S5* sapropel from the Mediterranean Sea. Paleoproductivity proxies (e.g. TOC, P, Cu and Ni) document increased deposition and/or preservation of organic matter during the interglacial periods in the Black Sea. Our study implies that repeated sapropel formations are linked to interglacial periods and reflect the global sea level rise followed by marine ingression over the Bosporus sill into the Black Sea basin.

## 4.1. Introduction

The Black Sea forms the textbook example of a restricted marine basin with a permanently stratified water column and anoxic to euxinic deep water masses (ROSS and DEGENS, 1974). During the Holocene, the Black Sea changed from an oxic limnic/brackish lake to the modern anoxic, restricted marine basin. The impact of this change on Black Sea sediments is well discussed in previous works (ARTHUR and DEAN, 1998; ARTHUR et al., 1994; BAHR et al., 2006; BAHR et al., 2005; BAHR et al., 2008; CALVERT, 1990; CALVERT and KARLIN, 1998; CALVERT and PEDERSEN, 1993; HAY et al., 1991; JONES and GAGNON, 1994; LAMY et al., 2006; ROSS and DEGENS, 1974; WIJSMAN et al., 2001; WILKIN and ARTHUR, 2001; WILKIN et al., 1997; ECKERT et al., 2013) and shortly summarized below:

At the end of the last glacial (Würm/Weichselian) the Eurasian ice shields declined, leading to increasing melt water discharge, river runoff and a rising sea level in all ocean basins including the Black Sea. The melt water eroded the Black Sea hinterlands, expanded the drainage area of the Black Sea, and increased the fluvial sediment supply to the basin. This increase in fluvial input triggered primary production due to higher nutrient delivery. At about 9 ka the Marmara Sea level rose above the Bosporus sill (SOULET et al., 2011), which lead to the ingression of denser Mediterranean seawater through the Sea of Marmara into the Black Sea basin (DEGENS and ROSS, 1974; GIOSAN et al., 2009; PIPER and CALVERT, 2011 and references therein). A pycnocline and a stratified water column developed. This pycnocline forms a physical barrier preventing mixing of oxygenated surface water masses with sulfide-containing (euxinic) deep water masses. At the same time a suboxic chemocline developed with gradually declining oxygen and increasing sulfide concentrations. Due to the elevated rain of organic matter from the photic zone and euxinic conditions in large parts of the water column, the degradation of organic matter (OM) is slowed down and its preservation is enhanced, resulting in the deposition of an organic carbon (OC) rich sapropel layer (CALVERT et al., 1987). These OC-rich sediments form the key feature of the transition from limnic to today's brackish environmental conditions in the Black Sea.

At DSDP Site 379 (Leg 42B) an older sapropelic layer of presumably Eemian age (USHER and SUPKO, 1978) was for the first time discovered in the Black Sea at 99 meters below sea floor (mbsf) (Abb. 4-1). The Eemian interglacial in Europe, which

divides the Riss/Saalian glacial from the Würm/Weichselian glacial, spans from 130 to 114 ka and corresponds to the Mikulino (Russia) and Sangamon (North America) interglacial and further to marine oxygen isotope stage (MIS) 5e (TURON, 1984). This interglacial was warmer than the Holocene, although shorter in duration, and had a higher global sea level than today (FIELD et al., 1994; KOPP et al., 2009; MCMANUS et al., 1994; RUDDIMAN et al., 1984; TURNER, 2000). Climate variability during the Eemian was smaller in scale compared to the Holocene (e.g. Younger Dryas, Bølling/Allerød), but the mid-Eemian cold event (approx. 122 ka) forms a key feature of many northern hemisphere sedimentary archives (KARABANOV et al., 2000). While the development of the Eemian in polar regions, on the northern/central European continent, and in the Mediterranean Sea (*S5* sapropel) is well studied (CANE et al., 2002; MOLLER et al., 2012; ROHLING et al., 2006; SANGIORGI et al., 2006; TRIANTAPHYLLOU et al., 2010; WELDEAB et al., 2003a), there exists almost no geochemical information about this prominent time interval for the Black Sea region.

Enrichments in Fe, Mo, and U are often used for paleoenvironmental reconstruction of organic carbon-rich sediments (BRUMSACK, 1989a; BRUMSACK, 2006b; TRIBOVILLARD et al., 2006). In this work we combine elemental with novel isotope proxies ($\delta^{56}$Fe, $\delta^{97}$Mo, $\delta^{238}$U) and results of organic geochemical analyses. Euxinic sediments are often enriched in Fe due to authigenic $FeS_x$ precipitation in a euxinic water column. Therefore, Fe may be a valuable proxy for the reconstruction of paleoenvironmental conditions (LYONS and SEVERMANN, 2006; WIJSMAN et al., 2001; WILKIN et al., 1997).

Iron is deposited in deep basin sediments via the shelf to basin Fe shuttle (LYONS and SEVERMANN, 2006; WIJSMAN et al., 2001). In this model Fe is in a first step mobilized from the shelf/slope sediments by microbial reduction, in a second step laterally transported via the suboxic chemocline to the central basin, where it is in a third step finally deposited as authigenic Fe sulfide. Thus, the vertical fluctuation of the chemocline from the deep basin sediment-water interface to the shelf break is reflected in Fe/Al depth profiles. High ratios indicate a shallow chemocline where large parts of the shelf are bathed in suboxic waters. Low ratios are indicative for a chemocline located below the shelf break and oxic water masses prevailing on the shelf, which are inhibiting Fe mobilization.

When the shelf to basin Fe shuttle does exist in a restricted basin the chemocline position is traced by Fe enrichments (or Fe/Al ratios) in the geological record (ECKERT et al., 2013).

Fe mobilization and redistribution within previously deposited lacustrine and brackish sediments may mask the primary distribution pattern. For the Holocene Black Sea sapropel this can be ruled out, because continuous resupply of sulfide owing to microbial sulfate reduction forms an effective barrier to prevent the upward migration of $Fe^{2+}_{aq}$ into the Holocene sequence. The downward migrating $Fe^{2+}_{aq}/HS^{-}_{aq}$ boundary thus prevents the diagenetic overprint of Fe enrichments in overlying Holocene sediments (NERETIN et al., 2004). On the other hand the speed of the downward diffusing redox front is too slow and the lacustrine sediment package is too thick for affecting the Eemian sapropel.

The isotopic composition of Fe in the sediment may be used as further evidence in favor of the Fe shuttle model, because the heavy $^{56}Fe$ isotopes are discriminated in all physical/chemical reactions and the light $^{54}Fe$ isotopes are preferentially mobilized due to mass-dependent fractionation (BEARD et al., 2003). The complete reaction cascade from microbial mobilization within the shelf sediments to $FeS_x$ precipitation in the deep basin favors the light Fe isotope leading to low $\delta^{56}Fe$ values in the sediment layers where excess Fe is deposited while the chemocline was located at shallow depths (SEVERMANN et al., 2008).

Molybdenum is highly enriched in seawater (10 µg/l) compared to freshwater (0.5 µg/l) (MARTIN and WHITFIELD, 1983). Under euxinic conditions, Mo is essentially quantitatively removed from the water column, due to the thiomolybdate cascade reaction ($MoO_xS_{4-x}$; x = 0-3) to Mo sulfide in environments with dissolved sulfide concentration above the action point of switch (APS, $HS^-$ > 11 µM; ERICKSON and HELZ, 2000; HELZ et al., 1996) and/or Mo-Fe-S precipitation (HELZ et al., 2011). Therefore Mo is a useful proxy for the intrusion of marine waters into a limnic system under euxinic conditions. By contrast, under oxic, non-sulfidic conditions Mo will not serve as a proxy for saltwater intrusion, because a precipitation mechanism is lacking.

Uranium, the second most abundant trace metal in seawater, is redox-sensitive and therefore may as well serve as paleoenvironmental proxy, even though its chemical

behavior differs from Mo especially under anoxic condition (KLINKHAMMER and PALMER, 1991; TRIBOVILLARD et al., 2006). Uranium reduction must be catalyzed by particle surfaces, e.g. surfaces of minerals or bacteria. Thus, elevated U concentrations can be used as proxy for anoxic conditions within the sediment.

The isotope systems of Mo and U are considered to be applicable tools to improve the reconstruction of paleoredox conditions. Mo and U isotopes fractionate to a different extent between oxic and anoxic to euxinic environments, as shown by different $\delta^{98}$Mo and $\delta^{235}$U values (ARNOLD et al., 2004a; BARLING et al., 2001; MONTOYA-PINO et al., 2010; NÄGLER et al., 2011; NÄGLER et al., 2005; NEUBERT et al., 2008; POULSON et al., 2006; WEYER et al., 2008).

The isorenieratene derivatives are biomarkers for green sulfur bacteria (GSB, *Chlorobiaceae*). This group of bacteria does not only require sunlight for photosynthetic respiration, but also dissolved sulfide as electron donor. GSB therefore serve as a proxy for water column euxinia in the photic zone (HUANG et al., 2000; KOOPMANS et al., 1996; REPETA, 1993; REPETA and SIMPSON, 1991; SINNINGHE DAMSTÉ et al., 1993).

The carbon isotopic composition of bulk organic matter ($\delta^{13}C_{TOC}$) may be used to roughly distinguish between a dominating terrestrial ($\delta^{13}C_{TOC}$ ~ -27 ‰) or marine origin ($\delta^{13}C_{TOC}$ ~ -20 ‰) of the organic matter (WESTERHAUSEN et al., 1993).

Here we present the first geochemical study of an Eemian sediment core from the Black Sea, which was recovered during *Meteor* expedition M72/5 at 8 mbsf. Besides the high-resolution analysis of major and minor elements we studied the isotopic ratios of Fe, Mo, and U, isorenieratene derivatives and $\delta^{13}C$ in selected samples.

The dataset is used to identify similarities and differences between the Holocene and Eemian paleoenvironmental conditions in the Black Sea basin with special attention to a) processes in the water column, b) the development of the marine ingression from the Mediterranean Sea over the Bosporus sill and c) the influence of melt water pulses for the fluvial input into the basin.

## 4.2. Material and methods

### 4.2.1. Sampling

Sediment cores used for this study were sampled north of the Anatolian coast in the south-eastern Black Sea at 848 mbsl (meter below sea level) (Abb. 4-1). Sampling was accomplished by a gravity corer (GC) and a parallel Multicorer (MUC) during R/V *Meteor* expedition M72/5. The 9.57 cm long gravity core 22-GC-7 was cut into one-meter sections on board, stored in a cold-storage room and was continuously sub sampled in the laboratory at the ICBM in Oldenburg, Germany. The sub-sampling intervals for 22-GC-7 were 0.5 cm for the Holocene sapropel, 5-10 cm for the glacial clay sediment layers and 0.2-0.6 cm for the older (here referred to as Eemian) sapropel. From a parallel core at the same site, 22-GC-3, only the Eemian sapropel was sub-sampled at 0.5 cm intervals. Core 22-MUC-2 was continuously sub-sampled in 1-5 cm intervals directly on board and was cold-stored as well. Additionally core 11 of DSDP Leg 42B site 379 (USHER and SUPKO, 1978) was re-sampled from the archive half at the IODP Bremen Core Repository. The samples were freeze-dried and ground with an agate mortar and stored in PE-vials.

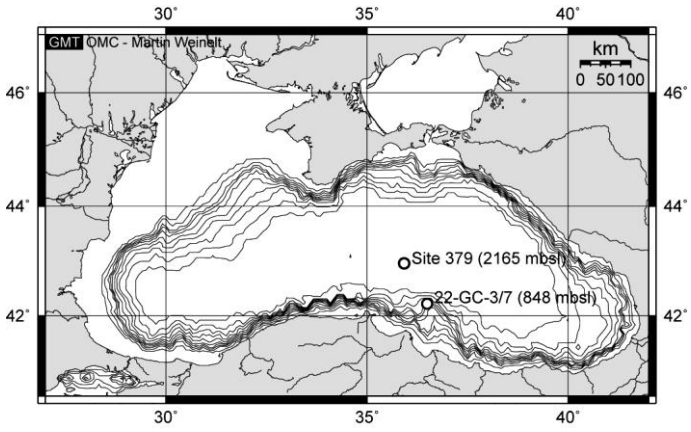


**Abb. 4-1** The Black Sea topography with sampling locations of DSDP Leg 42B Site 379 and M72/5 Site 22
(created by OMC; copyright: M. Weinelt).

### 4.2.2. Geochemical analysis

Major and minor elements were analyzed by wavelength dispersive X-ray fluorescence spectrometry (WD-XRF), inductively coupled plasma optical emission spectrometry (ICP-OES) and high resolution ICP mass spectrometry (HR-ICP-MS). $\delta^{56}Fe$, $\delta^{97}Mo$ and $\delta^{238}U$ were determined by multi-collector (MC-)ICP-MS. Total carbon (TC) and total sulfur (TS) were measured by IR-spectroscopy and total inorganic carbon (TIC) by $CO_2$-coulometry.

#### 4.2.2.1. Trace metal analysis

For XRF analysis 0.7 g of dried and ground sample were mixed with 4.2 g $Li_2B_4O_7$ and 1.0 g $(NH_4)_2NO_3$ (oxidizing agent) and fused to borate glass beads (modified after SCHNETGER et al., 2000). These beads were measured with a Philips PW-2400 WD-XRF spectrometer (calibrated with 53 geostandards).

For ICP-OES/MS analysis 100 mg of dried and ground sample were oxidized with 1 ml $HClO_4$ in closed PTFE beakers (PDS-6) at 180 °C. After cooling, 3 ml HF were added and the mixture was re-heated to 180 °C for 12 h. After digestion the acids were evaporated on a hotplate at 180 °C. Residues were re-dissolved and fumed off three times with 3 ml diluted HCl (6 M), and taken up with 1 ml $HNO_3$ and 10 ml $H_2O$. The solution was again heated at 180 °C for 8 h. The digestions were finally diluted with $HNO_3$ (2 % v/v) for ICP-OES (1:250) and HR-ICP-MS (1:2500) measurements. $HNO_3$ and HCl were purified by subboiling distillation; $HClO_4$ and HF had Merck Suprapur® quality; 18 MΩ water was used for dilution. For ICP-OES analysis all sample solutions were spiked with Sc as internal standard. For HR-ICP-MS analysis Be and In were used as internal standards. The HR-ICP-MS measurements were done with a Thermo Scientific Element 2 instrument according to a modified version of the method of SCHNETGER (1997). For ICP-OES measurements a Thermo Scientific iCap 6300 instrument with radial plasma and Cetac AS520 autosampler were used.

#### 4.2.2.2. Carbon and sulfur analysis

For the TC and TS analyses 50-100 mg of dried and ground sample was mixed with $V_2O_5$ (oxidizing agent) and burned in an $O_2$ stream. The resulting $CO_2$ and $SO_2$ were measured with an ELTRA CS-500 IR-spectrometer.

For the TIC analysis 5 ml 2 M $HClO_4$ was added to 50-100 mg dried and ground sample, and the carbonate carbon escaping from the sample as $CO_2$ was measured in a coulometric cell (UIC CM-5012; carrier gas: $N_2$). The carbonate content in the samples was calculated from TIC values. The percentage of total organic carbon (TOC) was calculated by the difference of TC and TIC.

The results of the above-mentioned analysis methods are confirmed by measurements of in-house and international standards (see as well BABU et al., 1999). These measurements show a pooled relative standard deviation (RSD) of < 1 % for TC and TIC, < 5 %for TS. Accuracy and precision for major, minor and trace elements measured by ICP-OES/MS and XRF are presented in supplemental Tab. 4-3.

The element enrichments are mainly presented as element to aluminum ratios in wt. %/wt. % for major elements and ppm/wt. % for minor and trace elements.

Excess values of elements are calculated as follows (BRUMSACK, 2006b):

$$El_{xs} = El_t - (Al_{smp} \times El/Al_{bg}) \quad (1)$$

where $El_t$ is the total absolute content of the element in the sample, $Al_{smp}$ is the aluminum content of the sample and $El/Al_{bg}$ describes the element to aluminum ratio of the lithogenic background. In this work average shale was used as a reference (WEDEPOHL, 1991).

Enrichment factors (EF) are calculated as described by eq. 2, using average shale values for normalization.

$$EF_{\text{avg. shale}} = \frac{(El/Al)_{\text{sample}}}{(El/Al)_{\text{avg. shale}}}, \quad (2)$$

where El/Al is the element to aluminum ratios of the sample and the average shale reference, respectively.

#### 4.2.2.3. Metal isotope ratio analysis

For the determination of metal isotope ratios, aliquots of the above mentioned acid digestions were used.

Uranium isotope ratios, reported as $\delta^{238}U$ have been analyzed according to the method described in WEYER et al. (2008) at the Institute of Geosciences, University of Frankfurt a.M. To separate U from the sediment matrix a chromatographic extraction method with Eichrom® UTEVA resin in PE-columns was used. To measure the U isotopes quantitatively a $^{233}U+^{236}U$ double spike (WEYER et al., 2008) was added to all samples. Delta values ($\delta^{238}U$) are reported relative to the reference material CRM-112A (mean $^{238}U/^{235}U = 137.863 \pm 0.019$ (2σ); n = 32) for normalization by means of standard-sample bracketing. The accuracy of $\delta^{238}U$ was determined by repeated measurements of reference materials IRMM-184 and REIMEP-18A (Tab. 4-4).

The determination of $\delta^{97}Mo$ and $\delta^{98}Mo$ was done after a modified method of BARLING et al. (2001). Purification of Mo from the sample matrix was achieved by a two-column ion exchange separation in BioRad™ PolyPrep columns. The first column, containing an anionic exchange resin (Dowex® 1X8; 100-200 mesh), was used to separate Mo, which forms anionic complexes, from Zr and other matrix elements. The second column, a cationic exchange resin (BioRad™ 50W-X8; 200-400 mesh), was used to remove Fe from the Mo fraction. For mass bias correction the Mo solutions were spiked with Zr (Specpure Lot: 700193E) to a Mo:Zr concentration ratio of 2:1. The delta notations for $^{97}Mo/^{95}Mo$ and $^{98}Mo/^{95}Mo$ were calculated relative to a Specpure® Mo plasma standard (Lot #802309E) for normalization by means of the bracketing method (mean $^{97}Mo/^{95}Mo = 0.06229 \pm 0.00005$ (2σ); mean $^{98}Mo/^{95}Mo = 1.52518 \pm 0.00019$ (2σ); n = 29). The accuracy of $\delta^{97}Mo$ and $\delta^{98}Mo$ was determined by repeated measurements of reference material SDO-1 and a gravimetrically prepared Mo standard (Grav-Mo-STD, BARLING et al., 2001) (Tab. 4-4).

The Mo and U isotopes measurements were done with a Thermo Scientific Neptune MC-ICP-MS at the Steinmann Institute, University of Bonn. Instrument parameters of the U isotopes measurements are published in WEYER et al. (2008). The measurements have a twofold pooled standard deviation (2σ) of 0.07 ‰ for $\delta^{97}Mo$, 0.12 ‰ for $\delta^{98}Mo$ and 0.11 ‰ for $\delta^{238}U$. Because of the better accuracy of $\delta^{97}Mo$ values compared to

$\delta^{98}$Mo values, the former ones were used for interpretation. Where required $\delta^{97}$Mo values were calculated in $\delta^{98}$Mo for comparison.

Determination of Fe isotope ratios, expressed as $\delta^{56}$Fe, was done at the Woods Hole Oceanographic Institute ICP facility, Massachusetts, USA. The Fe in the sample solutions was purified by passing the samples through anion exchange resin, using the protocol published in SEVERMANN et al. (2006). Iron isotope measurements were performed using a Thermo Fisher Neptune MC-ICP-MS, following the procedure of ARNOLD et al. (2004b). Purified samples were mixed with equal amounts of copper standard of known isotope composition (NIST-976 copper isotope standard), which was measured simultaneously for mass bias correction. Bracketing standards were measured after every second sample for additional mass bias control. Isotope ratios of $^{56}$Fe/$^{54}$Fe are reported using standard delta notation. Measured ratios are normalized relative to igneous rocks, which have an average isotope composition of $\delta^{56}$Fe = 0 ± 0.10 ‰ (2σ) (BEARD et al., 2003). On this scale the isotope composition of the international Fe isotope reference material IRMM-014 is -0.09 ‰ for $\delta^{56}$Fe. The average external precision for $\delta^{56}$Fe was typically better than ± 0.10 ‰ (2σ) for all samples. Several standard reference materials of known isotope composition, including SDO-1 (a Devonian black shale), BIR-1 (a basalt), MAG-1 (a marine mud) and SCo-1 (an Upper Cretaceous marine silty shale) were measured routinely for each sample batch, and values agree well with previous measurements and published values.

#### 4.2.2.4. Organic markers for photic zone euxinia and $\delta^{13}$C

For organic geochemical analyses 2-13 g of freeze-dried sediment was extracted by accelerated solvent extraction (ASE) with dichloromethane (DCM)/methanol (MeOH) (9:1 v/v). The extracts were further separated by column chromatography using alumina into apolar and polar fractions by elution with *n*-hexane/DCM (9:1 v/v) and DCM/MeOH (1:1 v/v), respectively (according to KOOPMANS et al., 1996). For quantitative analysis androstane and 5α-androstan-3β-ol standards were added. An aliquot of the polar fraction was derivatized with N-methyl-N-(trimethylsilyl)trifluoroacetamide (MSTFA). A second aliquot of the polar fraction was desulfurized with Raney-Ni (after SINNINGHE DAMSTÉ et al., 1988). Before

desulfurization another standard (2,3-dimethyl-5-(1',1'-$d_2$-hexadecyl)thiophene) was added to the polar samples for quantification. The released hydrocarbons were purified by column chromatography using alumina with *n*-hexane/DCM (9:1 v/v) and were subsequently hydrogenated with $PtO_2/H_2$.

The obtained fractions were analyzed using an Agilent 6890 gas chromatograph equipped with a flame ionization detector and a fused silica capillary column (J&W DB-5 HT, 30 m × 0.25 mm, film thickness 0.1 µm). Samples were injected at an initial temperature of 60 °C for 2 min and then heated with 3 °C/min to 350 °C which was held isothermally for 15 min.

Gas chromatography-mass spectrometry was carried out on a Thermo Scientific TSQ Quantum GC mass spectrometer coupled to a Thermo Scientific Trace GC Ultra gas chromatograph. The mass spectrometer operated at 70 eV with a scan time of 0.5 s and a mass range of *m/z* 50 – 650. The gas chromatograph was operated under the same analytical conditions mentioned above.

The isorenieratene derivatives in the apolar and in the desulfurized and hydrogenated polar fraction were tentatively identified based on their mass spectra, and distributions were examined by mass chromatograms of the most diagnostic ions of isorenieratene derivatives. The quantification of these compounds was performed on the gas chromatograms of the samples. The difference in the retention times of the GC-MS and GC-FID instruments are adjusted by an in-house reference material measured on both instruments.

In preparation of the $\delta^{13}C$ measurements of the bulk TOC of the extracted samples the residual carbonate must be removed by repetitive addition of 2 M subboiling-distilled HCl and evaporation at 90 °C. The samples, blanks, and standards (IVA 3802151, $\delta^{13}C_{VPDB}$ = -26.07 ‰) were measured by EA-IRMS (Thermo Finnigan MAT 252) at 80 eV.

## 4.3. Results

### 4.3.1. Stratigraphy

The full sequence of lithological units in this work is inferred from the two cores from site 22 (Abb. 4-2). The top part of the MUC was used to compensate for the consolidation of ca. 6 cm in the gravity cores. The correction is based on the comparison of elemental depth profiles of MUC and GC. The classification of the individual units is based on different authors (ARTHUR and DEAN, 1998; ARTHUR et al., 1994; HAY et al., 1991; ROSS and DEGENS, 1974). Chemically, Unit I is defined as a laminated sediment layer with TOC contents of 1-10 % and a $CaCO_3$ contents of 10-75 %, Unit II contains 1-20 % TOC and 5-15 % $CaCO_3$. The Unit I/II boundary is characterized by an initial peak in the $CaCO_3$ depth profile. This peak represents the first occurrence of *Emiliania huxleyi* after the Black Sea paleoenvironment changed from limnic to brackish/marine (HAY et al., 1991). Unit $II_a$ has a lower TOC content than Unit $II_{b1}$, which exhibits the highest TOC concentration. Unit $II_{b2}$ is distinguished from Unit $II_{b1}$ by an aragonite layer ($CaCO_3$ peak) at the bottom of this unit. Units I and II represent the Holocene, whereas Unit III, characterized by TOC contents < 1 %, is of Pleistocene age. We introduce the new additional units Unit IV to VI. Unit IV marks the transition from glacial clay to the Eemian sapropel and in this case comprises a turbidite layer. Unit V represents the Eemian sapropel, which exhibits several similarities to Units I and II. Unit VI is analogous to Unit III. In this work $CaCO_3$ is replaced by Ca*, which represents the Ca content corrected for apatite. Owing to the lack of sample material we could only analyze selected samples for $CO_2$ compared to Ca analyses by XRF. Ca* correlates very well with the $CaCO_3$ content ($r^2 = 0.9955$) and therefore our approach seems reasonable. The results of our geochemical classification for core 22-GC-7 are shown in Abb. 4-3.

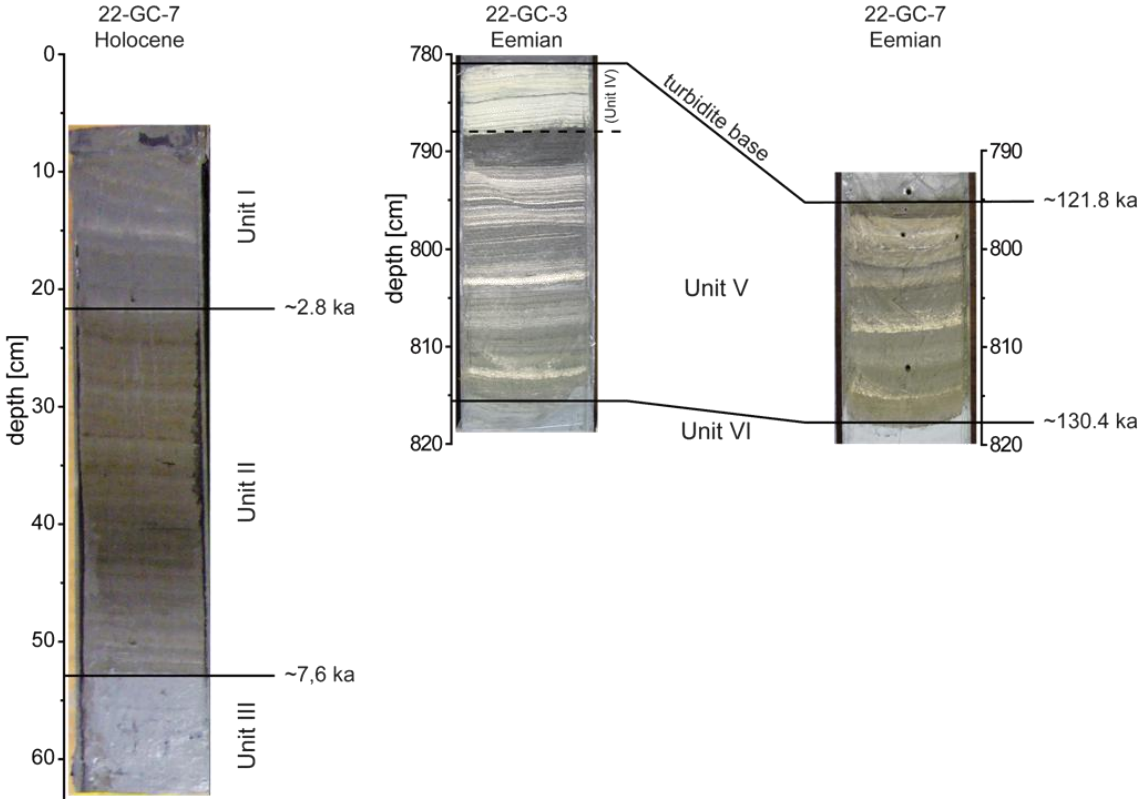


**Abb. 4-2** Lithostratigraphy of site 22.
The depth scale of the gravity core was corrected with help of the MUC samples to ensure to start the stratigraphy with the sediment surface. Comparison of core photos of the Holocene sapropel and the Eemian sapropel.

The top 21 cm of core 22-GC-7 (Unit I) consist of laminated dark greenish gray, TOC-rich clay layers with white coccolith bands (Abb. 4-2). Below Unit I follows a finely laminated dark greenish to black layer (Unit II), with elevated TOC and decreasing carbonate contents, extending down to 53.5 cm. Unit II is subdivided into three subunits: Unit $II_a$ (21-34 cm) has a lighter color and a lower TOC content compared to Unit $II_b$ (34-53.5 cm), which has a TOC maximum in Unit $II_{b1}$ (34-45 cm) and an aragonite layer in Unit $II_{b2}$ (45-53.5 cm). Unit III is represented by a thick interval of gray clay ranging from 53.5 cm to 797 cm. These clay layers are light gray at the top and dark gray below, and are occasionally interrupted by black Fe sulfide layers ($FeS_x$; e.g. pyrite, greigite, Fe monosulfides). In the interval 263-302 cm a diagonal band of black $FeS_x$ of later diagenetic origin (NERETIN et al., 2004) intersects the clay. The uppermost top of the following Unit IV, which records the transition from anoxic/marine to oxic/limnic conditions, was possibly cut off by a turbidite and therefore might be incomplete and the transition from Unit IV to III might be not fully documented in these cores.

The turbidite is present in both cores. We define its base by distinct peaks in Si/Al, Ti/Al, and Zr/Al ratios (WEHAUSEN and BRUMSACK, 1999), which reflect grain sorting effects. The turbidite affected Unit IV in core 22-GC-7 to a larger degree than in core 22-GC-3 because only from core 22-GC-3 a finely laminated, white coccolith marl was recovered at 780.5-787.5 cm depth, which we assign to represent the lowermost section of Unit IV of Eemian age.

The Eemian sapropel is finely laminated as well and - in analogy to Unit II - was sub-divided into Unit $V_a$ (22-GC-7: 797-799 cm, 22-GC-3 787.5-790.5 cm), a brownish, TOC-rich clay, and Unit $V_b$ (22-GC-7: 799-818 cm, 22-GC-3 790.5-816 cm) consisting of alternations of brownish gray clay with beige coccolith marl. Within Unit $V_b$ TOC-rich sapropelic clay layers are interrupted by thin carbonate layers. Seven finely laminated intervals may be distinguished by color changes.

1) brownish gray clay (22-GC-7: 799-802.8 cm, 22-GC-3: 790.5-792 cm),

2) beige coccolith marl (22-GC-7: 802.8-803 cm, 22-GC-3: 792-798 cm),

3) dark brown clay (22-GC-7: 803-808.1 cm, 22-GC-3: 798-803 cm),

4) light beige coccolith marl (22-GC-7: 808.1-808.5 cm, 22-GC-3: 803-804 cm),

5) brownish black clay (22-GC-7: 808.5-813.7 cm, 22-GC-3: 804-810.8 cm),

6) light beige coccolith marl (22-GC-7: 813.7-814 cm, 22-GC-3: 810.8-812 cm) and

7) brownish gray clay (22-GC-7: 814-818 cm, 22-GC-3: 812-816 cm).

The TOC-rich sapropelic clay layers are interrupted by thin carbonate layers. Analogous to Unit III gray clay is deposited in Unit VI below the sapropel (22-GC7: 818-963 cm, 22-GC-3: below 816 cm). Unit VI in core 22-GC-7 is interrupted by a porous, dark black layer containing pyrite (864.5-866.5 cm).

### 4.3.2. Age model

The change from the lacustrine stage to the present-day brackish Black Sea happened synchronously throughout the whole Black Sea basin over a time period of less than 900 a based on the replacement of the lacustrine by brackish/marine biota (SOULET et al., 2011). Due to this relatively fast paleoenvironmental change, it seems reasonable to

establish an age model valid for the deep Holocene Black Sea. This is based on the average thickness of each unit and the average ages of the Unit I/II and Unit II/III boundaries in six different cores across the whole Black Sea taken from the literature (Tab. 4-1). The mean ages of around 2.8 and 7.6 ka B.P. for the boundaries of Unit I/II and II/III, respectively, are valid for the whole basin (Tab. 4-1). Based on this age model sedimentation rates of 7.6 cm/ka and 7.1 cm/ka were calculated for Unit I and Unit II of core 22-GC-7, respectively.

The age of the Eemian sapropel in cores 22-GC-3/7 ranges from 130.4 to 121.8 ka based on correlations with dated pollen and $\delta^{18}O$ records (ALLEN and HUNTLEY, 2009; BADERTSCHER et al., 2011; TZEDAKIS et al., 2003). The turbidite might have eroded a sediment package that represented approx. 7 ka. This supports our interpretation that the transition from interglacial to glacial conditions in the geological record of our cores might not be fully preserved. The sedimentation rate within the Eemian sapropel (Unit V) is on average 4.0 cm/ka (not corrected for consolidation).

### 4.3.3. Redox-sensitive elements and their isotopes

The depth profiles of the Holocene section exclusively consist of samples from one core (22-GC-7; Abb. 4-3). Instead, for the Eemian section, samples from both cores (22-GC-3 and -7) were adjusted to the same depth scale and combined to one composite geochemical record for data presentation. The original data of both cores show the same chemical trends and values are in the same range, justifying this approach (see appendix for details).

In the Holocene section the depth profiles of Fe/Al ratios (from bottom to top) initially show average shale values (Fe/Al: 0.55, WEDEPOHL, 1991) in upper Unit III followed by two peaks at the Unit II/III boundary with Fe/Al ratios of 0.91 and 1.00 at 57.5 cm and 52.5 cm depth, respectively. After a slight decrease a broad peak occurs in the central part of Unit $II_b$ with a Fe/Al maximum of 0.78. In Unit I we observe small variation in Fe/Al ratios (0.57-0.63).

The Fe/Al ratio in the Eemian sapropel is elevated (0.62 to 0.84) compared to average shale with values of 0.63 at the bottom of the Eemian sapropel increasing upcore to 0.79, followed by a decrease to 0.62 in the central part of Unit V, increasing again to the

maximum of 0.84 at 796 cm depth. After this maximum we observe a steep decrease to average shale values.

The vertical distribution of $\delta^{56}$Fe in the Holocene as well as in the Eemian sapropel broadly mirrors the Fe/Al depth profile. Low $\delta^{56}$Fe values (minimum -0.22 ‰) coincide with iron enrichments (high Fe/Al ratios) and vice versa (Abb. 4-3). In the Eemian section Fe-Isotopes gradually shift upcore from heavier (maximum 0.11 ‰) towards lighter values (minimum -0.23 ‰ at 796 cm) followed by a sharp shift back to heavier $\delta^{56}$Fe (to 0.09 ‰) within the turbidite-affected post-sapropel sediment layers.

In the Holocene section the Mo/Al background (Unit III) is close to the average shale value (Mo/Al: 0.15) and starts to increase shortly below the Unit II/III boundary (Abb. 4-3). In the central part of Unit II we observe a gradual increase in Mo/Al to a broad maximum (Mo/Al = 16 to 18) and decreasing values towards the Unit I/II boundary (Mo/Al of 4 to 7). In Unit I the vertical Mo/Al distribution stays essentially constant.

Molybdenum/Al ratios stay around the average shale value of 0.15 at the bottom of the Eemian sapropel (Unit V/VI; Abb. 4-3) and increase almost linearly upcore to a maximum of 35 at 798.5 cm, followed by a steep but consistent decrease to background values towards the base of the turbidite.

The Holocene section of these cores has not been analyzed for Mo isotope ratios, but the literature offers many values for Black Sea Unit I (average $\delta^{97}$Mo ≈ 1.6 ‰) and II (average $\delta^{97}$Mo ≈ 1.1 ‰) sediments for comparison (e.g. ARNOLD et al., 2004a; BARLING et al., 2001; DAHL et al., 2010; NÄGLER et al., 2005; NEUBERT et al., 2008; POULSON et al., 2006; SCHEIDERICH et al., 2010; SIEBERT et al., 2003). However, $\delta^{97}$Mo values of the Eemian sapropel are around 1.08 ‰ at the bottom (Abb. 4-3), then decrease to values of 0.71 ‰, and finally increase to almost seawater values of 1.46 ‰ (BARLING et al., 2001).

**Tab. 4-1** Assumed averaged age model for the Black Sea and calculated sedimentation rates (SR) for core 22-GC-7 using average boundary ages.

| Age Unit I/II boundary [cal. ka BP] | Age Unit II/III boundary [cal. ka BP] | SR Unit I [cm/ka] | SR Unit II [cm/ka] | References |
|---|---|---|---|---|
| 2.044 ± 7 | 7.869 ± 237 | 25.7 | 20.0 | ARTHUR and DEAN, 1998 |
| | 7.607 ± 40 | | 4.5 | BAHR et al., 2006; 2005 |
| 2.720 ± 160 | 7.540 ± 130 | 18.5 | 13.1 | JONES and GAGNON, 1994 |
| 2.760 ± 35 | 7.995 ± 55 | 117.0 | 70.6 | LAMY et al., 2006 |
| 3.330 ± 108 | 7.160 ± 108 | 5.4 | 6.0 | MAJOR et al., 2002 |
| 3.090 ± 140 | 7.090 ± 180 | 6.4 | 9.2 | ROSS and DEGENS, 1974 |
| 3.050 ± 35 | 8.140 ± 50 | 126.2 | 48.5 | VERLEYE et al., 2009 |
| **2.760 ± 287** | **7.607 ± 316** | **22.1** | **13.1** | **Median** |
| | | 7.6 | 7.1 | Calculated for 22-GC-7 |

The vertical distribution of U/Al in the Holocene sapropel shows average shale values (0.42) at the Unit III/II boundary and increases slightly to 2.5 in Unit II (Abb. 4-3). After decreasing to values of about 0.5 at the Unit II/I boundary, ratios increase again and stay constant around 2 in Unit I. In the Eemian section the initial U/Al ratio is at average shale level at the base of the sapropel (Abb. 4-3). Within the sapropel the vertical U/Al distribution is much higher and shows three maxima: at 804 cm, at 800 cm, and at 796 cm with U/Al ratios of 9, 16, and 12, respectively. Beyond the uppermost peak U/Al ratios drop sharply back to average shale values within the tubidite. U isotope ratios were not measured in the Holocene part of the cores, but other studies (MONTOYA-PINO et al., 2010; WEYER et al., 2008) determined $\delta^{238}U$ values of ~0.02 ‰ and ~0.24 ‰ for Unit I and Unit II samples, respectively. The U $\delta^{238}U$ values in the Eemian samples range between -0.29 ‰ and 0.14 ‰ (Abb. 4-3). The vertical distribution of $\delta^{238}U$ starts with 0.06 ‰ at the bottom of the Eemian section followed by the maximum value of 0.14 ‰. $\delta^{238}U$ values between -0.08 ‰ and 0.10 ‰ are found in the center of the sapropel. This distribution gives no clear trend. The carbonate-rich top layer of the sapropel and the turbidite layer are enriched in the light U isotopes.

### 4.3.4. Organic markers for photic zone euxinia and $\delta^{13}C_{TOC}$

Organic molecular markers for photic zone euxinia were measured in selected samples of the sediment cores. The compounds tentatively identified and quantified are predominantly di-unsaturated isorenieratane (3 isomers) and to a minor extent di-unsaturated, cyclized isorenieratane (2 isomers). These compounds were first described from an Eastern Mediterranean sapropel, and structures have been proposed based on their mass spectra and chemical behavior upon hydrogenation (BOSCH et al., 1998). Isorenieratene can undergo various diagenetic reactions, that lead to a great variety of cyclized or aromatized derivatives found in sediments and sedimentary rocks of various ages (KOOPMANS et al., 1996).

In the Holocene part of core 22-GC-7 isorenieratene derivatives were found in the central part of Unit II, in layers enriched in TOC and Mo (Abb. 4-3) at concentrations between 1 and 6 µg/g TOC. In Unit I, Unit III and the lower part of Unit II no isorenieratene derivatives could be detected.

In the Eemian sapropel of cores 22-GC-3 and 7 isorenieratene derivatives were found in the central part of the sapropel, while they are absent in the lower section and the uppermost layer of Unit V, and also in the turbidite. Here, the concentrations of isorenieratane released by desulfurization and hydrogenation of polar fractions show a similar depth trend compared to that of Mo/Al, with concentration between 4 and 13 µg/g TOC. The concentrations of free isorenieratene derivatives show almost the same trend, with concentrations between 8 and 28 µg/g TOC, except for the sample at 807 cm depth. Here, the free isorenieratane-di-en concentration in the apolar fraction is much higher (42 µg/g TOC) compared to desulfurized isorenieratane (5 µg/g TOC).

**Abb. 4-3** Depth profiles of Ca*, TOC, Fe/Al, $\delta^{56}$Fe, Mo/Al, $\delta^{97}$Mo, U/Al, $\delta^{238}$U, $\delta^{13}$C, and isorenieratene derivatives
(filled squares: free; open squares: released from polar fraction by desulfurization); Unit boundaries after ARTHUR and DEAN (1998); brown hatched area: turbidite above Unit V; vertical dotted lines represent the average shale values for the element to Al ratios (WEDEPOHL, 1991); the error bars represent 2σ; Ca* represents the Ca content corrected for apatite. The Holocene part (Unit I-III) is based on data from core 22-GC-7, the Eemian part consists of composite depth profiles of cores 22-GC-3 and 22-GC-7.

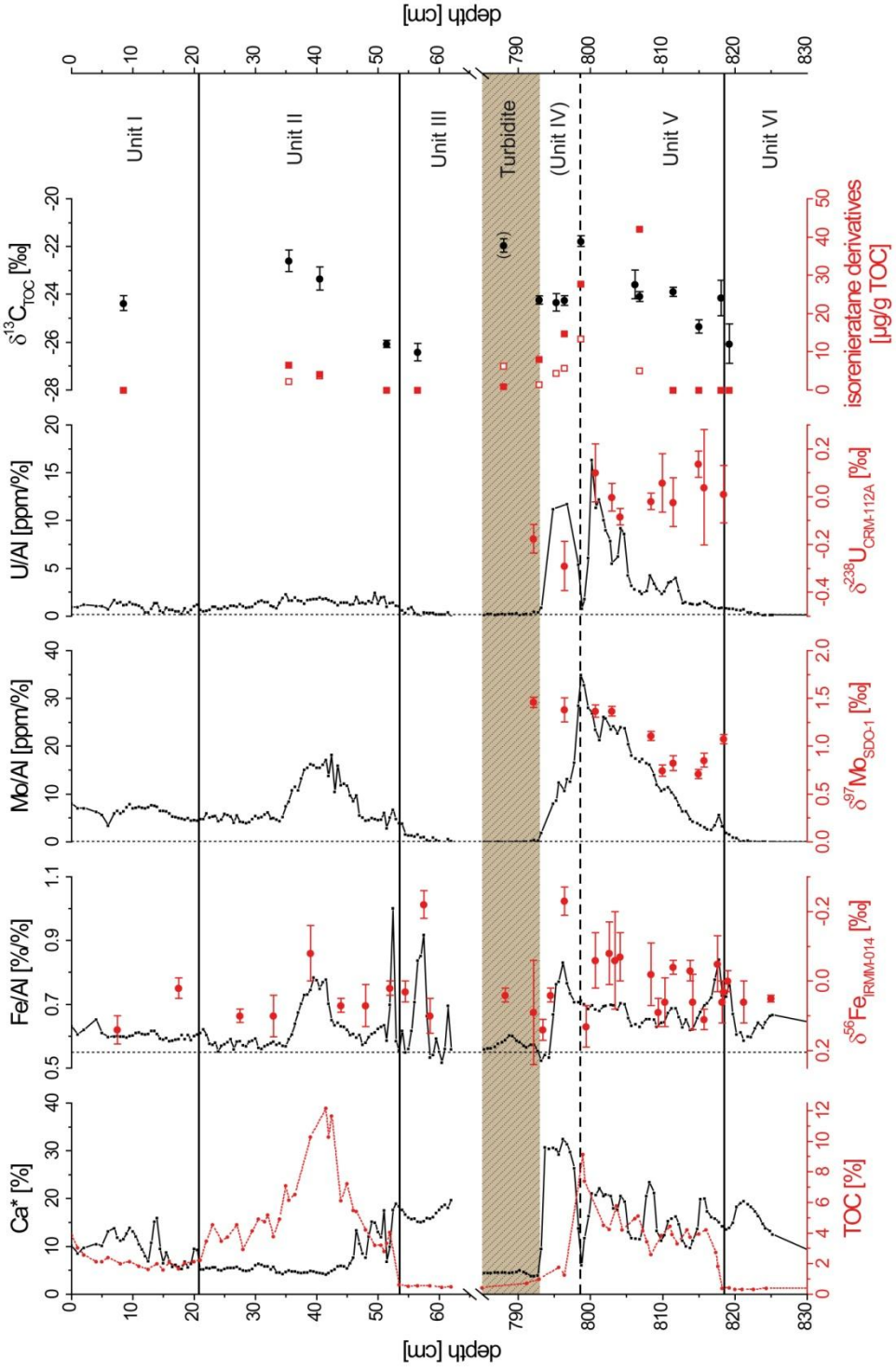

The carbon isotope composition of the bulk organic matter in the Holocene and Eemian sapropels follows the trend of the TOC and Mo/Al depth profiles. The $\delta^{13}C_{TOC}$ values in Unit III samples are low (~ -26 ‰), but increase to -22 ‰ in the central Unit II. After this maximum the $\delta^{13}C_{TOC}$ values decrease to -24 ‰ in Unit I.

Similarly, Unit VI is most depleted in $^{13}C$, and the most enriched samples occur in the central and upper part of the sapropel in Unit V with $\delta^{13}C_{TOC}$ values of ~ -24 ‰ and -21 ‰, respectively. The latter maximum $\delta^{13}C$ value coincides with the Mo/Al maximum.

To conclude, lithostratigraphy and geochemical composition of the two Eemian sapropel sections show similar vertical element patterns and compare very well with those of the Holocene sapropel.

## 4.4. Discussion

### 4.4.1. Marine ingression during the Holocene and Eemian interglacial

The change from a limnic to a brackish/marine Black Sea during the Holocene is a highly disputed topic in the literature. While many authors favor the continuous inflow model with an initial spillover of Mediterranean seawater over the Bosporus sill (AKSU et al., 2002; YANKO-HOMBACH et al., 2007), some authors argue for a rapid flooding with seawater (MAJOR et al., 2002; RYAN et al., 2003; RYAN et al., 1997).

Here we compare the geochemistry of Holocene and Eemian sapropels and their depositional history to provide geochemical arguments for the "inflow model" discussion. In addition to the results presented in this work we use a previously published composite geochemical core log (CGCL) for interpretation, which provides average geochemical concentration profiles for the Holocene Black Sea sapropel (ECKERT et al., 2013). The application of the same proxies used for the interpretation of the Holocene sapropel to the Eemian allows us to directly compare the marine ingression during both interglacials based on geochemical signatures in the Black Sea basin.

#### 4.4.1.1. Tracing seawater inflow and nature of organic material

High-resolution distributions of selected elements from the geological record should reflect changes in water column chemistry resulting from the ingression events. As mentioned above, sedimentary Mo may be used as a tracer for seawater intrusion in an euxinic environment. The Mo/Al depth profiles in Abb. 4-3 and in the CGCL (ECKERT et al., 2013) show a slight Mo enrichment at the Unit III/II boundary compared to the lithological background in Unit III. This points to the initial inflow of Mediterranean seawater into the limnic Black Sea before the transition sapropel was deposited. This slight initial Mo enrichment may indicate a better unit boundary definition regarding the change from limnic to brackish marine, anoxic conditions, than lithology, TOC and $CaCO_3$ records. The maximum Mo enrichment in the central part of the transition sapropel (~5.3 ka) at site 22 is not as pronounced as in the CGCL because the sampling site is located at the slope of the eastern Black Sea and not in the deep basin. Owing to higher sedimentation rates the sediment is more diluted by terrigenous input. At the same time the overlying euxinic water column provides a shorter pathway for the Mo reduction cascade.

The TOC depth profiles in Abb. 4-3 and in the CGCL (ECKERT et al., 2013) look rather similar to each other, even though TOC concentrations are generally lower at site 22. Furthermore an increasing influence of the primary production and preservation of marine organic matter compared to the fluvial input of terrestrial organic matter is indicated by the shift towards higher $\delta^{13}C$ values of bulk TOC upcore in the Holocene record, with maximum values in the organic-rich Unit II (RULLKÖTTER, 2006). The $\delta^{13}C$ maximum is accompanied by Mo and TOC maxima implying euxinic conditions in the water column with a high preservation potential for marine organic matter.

Our data document a continuous change from limnic to increasingly marine conditions within ~2 ka (ECKERT et al., 2013). After the first spillover of seawater into the freshwater lake a pycnocline has developed stratifying the limnic/brackish and marine water masses due to density differences. This stratification prevents mixing of oxic surface water with deep water, which becomes depleted in oxygen with time. Finally an anoxic/euxinic water column develops where the pycno-/chemocline forms the suboxic transition zone.

Ratios of Mo/Al in the Eemian sapropel start to increase at the Unit VI/V boundary, indicating the continuing ingression of seawater from the Mediterranean Sea into the Black Sea and the establishment of a chemocline separating oxic from euxinic waters (Abb. 4-3). From here on Mo/Al increases almost linearly to the top of Unit V with a maximum, which is comparable to the one found in Unit II of the Holocene CGCL. In both cases the Mo/Al depth profiles document the continuous ingression of seawater and synchronous Mo-removal under euxinic conditions due to water column stratification (and a rising pycno-/chemocline).

The vertical distribution of $\delta^{13}C_{TOC}$ and TOC parallels the Mo/Al depth profile and shows low values of $\delta^{13}C_{TOC}$ at the bottom of the Eemian section indicating the dominance of terrigenous organic matter, which is comparable to the Holocene situation at the Unit III/II boundary. The following decrease in $\delta^{13}C_{TOC}$ may results from the introduction of isotopically heavier organic matter due to enhanced primary production and/or better preservation of marine OM, analogous to the findings in the Holocene sapropel. The maxima in TOC, $\delta^{13}C_{TOC}$ and Mo/Al in the Holocene as well as the Eemian depth profiles indicate that the seawater ingression and the chemocline rise may have reached its maximum at this point.

#### 4.4.1.2. Tracing the rise of the chemocline

We try to trace the development and rise of the chemocline by using the sedimentary Fe content and Fe isotopic composition. Fe/Al ratios and $\delta^{56}Fe$ values, clearly indicate an active shelf to basin Fe shuttle during deposition of the central Unit II in core 22-GC-7 during the Holocene (ECKERT et al., 2013; SEVERMANN et al., 2008).

The Fe/Al ratios in Unit I are only slightly elevated compared to the CGCL (ECKERT et al., 2013) pointing to a less efficient Fe shuttle (Abb. 4-3). But the CGCL, which was created based on different sampling locations in the Black Sea, shows high Fe/Al ratios in combination with low $\delta^{56}Fe$ values (ECKERT et al., 2013; SEVERMANN et al., 2008). The lower ratios of the core shown here might be due to the different topography of the sampling location. While the northern and western Black Sea are characterized by a large, gently inclining shelf area, the Anatolian coast features a steep slope and a narrow shelf, resulting in a higher sediment accumulation masking the chemocline signal by

terrigeneous material (LYONS and SEVERMANN, 2006). Hence, suboxic waters impinge only on a small surface area at the Anatolian coast and Fe mobilization is reduced compared to the north-western Black Sea basin.

The three Fe/Al peaks at the Unit III/II boundary are considered as secondary in origin. They indicate the transition from oxic to euxinic conditions in the sediment column and early diagenetic trapping of Fe, which was mobilized in the suboxic sediment layers below. WILKIN et al. (1997) have shown as well that secondary, post-depositional Fe sulfide formation (e.g. greigite) occurred. Due to the downward migration of this $Fe^{2+}_{aq}/S^{2-}_{aq}$ redox-boundary, an overprinting of the Fe distribution pattern in the younger units is less likely (JØRGENSEN et al., 2004) and we assume that Fe/Al ratios in the sapropel remained unchanged and represent the primary signature originating from processes within the water column.

The vertical distribution of Fe/Al ratios, which track the rise of the chemocline, show values above average shale across the whole Eemian section, but distinctive maxima, such as seen in the Holocene section, are missing (Abb. 4-3). This implies that the position of the chemocline has varied much less in the Eemian than in the Holocene and may have reached its shallowest position around the Unit IV/V boundary.

Combining the information from the Eemian Fe/Al, $\delta^{56}Fe$, and the Mo/Al depth profiles with findings from the Holocene sapropel leads to the hypothesis that the chemocline developed and started to rise at the beginning of the Eemian interglacial. The constant increase of the Mo/Al ratio may indicate the continuous ingression of seawater and the concomitant development of anoxic/euxinic conditions in the water column. The slight Fe enrichment right below the turbidite base and above the Mo/Al maximum may indicate a shallow chemocline but reduced inflow of seawater (Mo source).

The vertical distribution of U/Al in the Holocene Unit II section at site 22 is similar to the U/Al profile of the CGCL, but differs in Unit I at site 22. Therefore, our Eemian U/Al depth profile with its high values seems to be more comparable to the CGCL of Unit I than to Unit II. Like in Unit I enrichments of U in the Eemian sapropel (Unit V) seem to be associated with high $CaCO_3$ (Ca*) concentrations, suggesting that some relationship between the U reduction and fixation process and the presence of carbonate surfaces does exist (KELLY et al., 2003; KELLY et al., 2006; STURCHIO et al., 1998;

TATSUMOTO and GOLDBERG, 1959). The Ca* concentrations in Unit V exceed those in Unit I at site 22 by a factor of two, which may results from haptophyte blooms (HAY et al., 1991) and the lower sedimentation rate during the Eemian Units VI and V (~4 cm/ka) compared to the Holocene Unit I (~8 cm/ka) at this location.

The Holocene depth profile of $\delta^{13}C_{TOC}$ is paralleled by the distribution of isorenieratene derivatives (Abb. 4-3). Photic zone euxinia must have persisted during deposition of the central Unit II (HUANG et al., 2000; KOOPMANS et al., 1996; REPETA, 1993; SINNINGHE DAMSTÉ et al., 1993). The occurrence of isorenieratene derivatives in the central and upper Eemian sapropel implies that the chemocline was positioned in the photic zone and therefore on the shelf during the time of deposition, too. Also the gradually decreasing $\delta^{56}Fe$ values indicate an increase in microbially mobilized Fe, transported via the shelf-to-basin Fe shuttle (Abb. 4-3). The information given by those two proxies leads to the conclusion that the Eemian sapropel compares well with the Holocene Unit I, as already indicated by U/Al. The chemocline must have been located within the photic zone and the shelf break. The more or less constant enrichment in Fe is related to the sampling location at the south-eastern slope, where only a small suboxic surface area may serve as a source for the Fe shuttle, as discussed above.

The proxies used here indicate a gradual rise of the chemocline from the sediment-water interface to the shelf break during deposition of Unit II sediments. The stratification maximum is attained in the central Unit II. The geochemical record of the Holocene section of core 22-GC-7 favors the continuous inflow model by DEGENS and ROSS (1972) or DEUSER (1974) in combination with a fluctuating pycno-/chemocline (Abb. 4-3) as elucidated in ECKERT et al. (2013). Independent of the depth of the Bosporus sill (MAJOR et al., 2002), a rapid and catastrophic flooding as proposed by RYAN et al. (1997) seems less compatible with our geochemical proxies. The geological record of the Eemian shows a gradual rise of the chemocline indicating also a continuous inflow of Mediterranean seawater, but without a significant fluctuation of the pycno-/chemocline.

### 4.4.2. Paleoenvironmental condition of sapropel deposition during the Eemian compared to the Holocene interglacial

As mentioned in the previous chapter, the Fe and Mo enrichments in the geological record are reliable proxies for euxinic conditions. For the reconstruction of the paleoenvironmental conditions in a restricted basin, the distribution of different isotopes of Mo and U also may serve as powerful tools (ARNOLD et al., 2012; BARLING et al., 2001; DAHL et al., 2010; MONTOYA-PINO et al., 2010; NÄGLER et al., 2011; NÄGLER et al., 2005; NEUBERT et al., 2008; POULSON BRUCKER et al., 2009; POULSON et al., 2006; SCHEIDERICH et al., 2010; SIEBERT et al., 2003; WEYER et al., 2008 and references therein).

Abb. 4-4 shows $\delta^{238}U$ versus $\delta^{97}Mo$ for Eemian sapropel samples and the empirically determined boundary conditions for different paleoenvironmental situations (e.g. Holocene Black Sea sapropel, ancient black shale; MONTOYA-PINO et al., 2010; WEYER et al., 2008). The deviation of $\delta^{238}U$ from the seawater value (~ -0.4 ‰) is due to the fractionation of U isotopes during redox reactions. In this case isotopically heavier U is removed from the water column and deposited in the underlying sediment, due to volume dependent fractionation effects (SCHAUBLE, 2007; WEYER et al., 2008). The $\delta^{238}U$ values in Abb. 4-3 and Abb. 4-4 indicate that the Eemian sapropel was deposited under oxygen depleted conditions right from the onset of lithological Unit V. The roughly constant $\delta^{238}U$ values, from the bottom of Unit V to its top, show that the whole Eemian sapropel was deposited under anoxic conditions.

Two samples close to the turbidite with low $\delta^{238}U$ values deviate from the trend. Most probably the uppermost sample is affected by the turbidite layer, which may consist of isotopically lighter continental source rock material, which is also present in the glacial clay sediments. The second uppermost sample has a high carbonate and uranium content, suggesting an association of U with $CaCO_3$ surfaces. This may indicate a more quantitative removal of U from the water column, leading to reduced isotope fractionation relative to the seawater U source, compared to samples with lower carbonate contents. Therefore, these two samples may not be diagnostic in terms of paleoredox reconstruction.

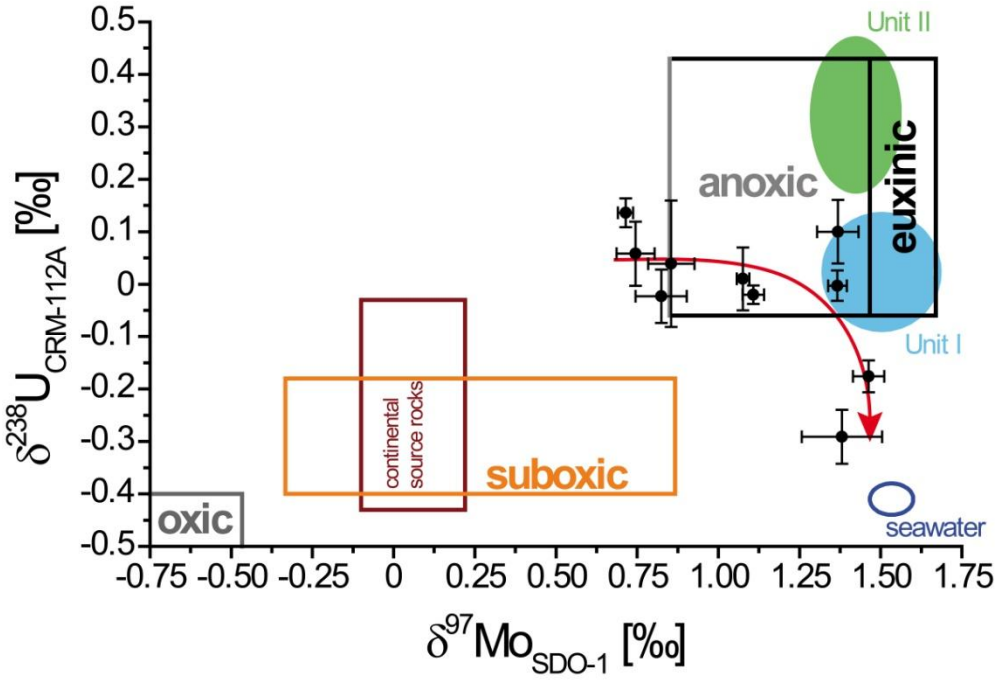


**Abb. 4-4** Isotopic map of $\delta^{238}U$ versus $\delta^{97}Mo$.
The error bars represent 2σ. The boundaries are according to BARLING et al. (2001), POULSON et al. (2006), WEYER et al. (2008), POULSON-BRUCKER et al. (2009), and MONTOYA-PINO et al. (2010). The red arrow pictures the chronological order (upcore) of the samples.

On basis of $\delta^{97}Mo$ values a change from suboxic conditions during deposition of the bottom layers of the Eemian sapropel to almost euxinic conditions during deposition of the top layers can be identified (Abb. 4-3 and Abb. 4-4). The Mo isotope composition of the sapropel continuously increases from the onset of the Eemian interglacial (with $\delta^{97}Mo$ of 0.5 to 1) to the top of the sapropel (with $\delta^{97}Mo$ of almost 1.5, i.e. close to the present seawater $\delta^{97}Mo$). These findings indicate the almost quantitative removal of Mo from the water column at the end of the Eemian sapropel formation. In contrast to the Holocene Unit I, quantitative Mo removal was not fully achieved. This may have the following reasons:

a) the semi-quantitative removal of Mo from the water column into the sediment,

b) a different water column chemistry (seawater to fresh water ratio) or

c) a different Mo isotopic composition in the Eemian water column of the Black Sea compared to the Holocene.

We will discuss these three options in detail in the following section.

a) One reason for the lower $\delta^{97}$Mo values of the Eemian compared to the Holocene samples might be weaker euxinic conditions, i.e. lower $H_2S_{aq}$ concentrations in the water column, resulting in an incomplete reaction pathway from $MoO_4^{2-}$ to $MoS_4^{2-}$. Using the recent data of NEUBERT et al. (2008), a linear correlation of sedimentary authigenic $\delta^{98}$Mo and water column $H_2S_{aq}$ can be recognized in Black Sea sediment samples between 150 and 500 mbsl, which represents the transition layer of anoxic conditions (with zero to low $H_2S_{aq}$ concentration) to fully euxinic conditions (with $H_2S_{aq}$ concentrations above APS) in the water column. Thus, the slope of the linear regression can be used to estimate the $H_2S_{aq}$ concentration in the Eemian water column on basis of the sedimentary authigenic $\delta^{98}$Mo values (modified after ARNOLD et al., 2012). These estimates presume that the Eemian sapropel was initially deposited at sulfide concentrations between 10 and 19 µM above the APS, but $H_2S_{aq}$ values did not reach the Holocene level (> 300 µM), and that the thiomolybdate reaction cascade did not reach the $MoS_4^{2-}$ stage (NÄGLER et al., 2011). Based on this hypothesis our Mo/Al data indicate an almost quantitative removal but with a shift towards lower $\delta^{97}$Mo values probably due to the incomplete reaction cascade.

b) The second possibility to explain the Eemian $\delta^{97}$Mo values is related to the water column chemistry, especially the seawater/river water ratio during the Eemian interglacial, which was possibly different to the ratios throughout the Holocene. The inflowing seawater ($\delta^{98}$Mo ~2.3 ‰) was presumably more diluted with fresh water ($\delta^{98}$Mo 0-0.7 ‰) from the adjacent rivers during the Eemian transgression compared to the Holocene (NÄGLER et al., 2011). The Mo concentration in seawater depends on salinity, while the riverine input of Mo is two orders of magnitude below the seawater value and is considered to be negligible in this case. Assuming almost quantitative removal of Mo from a euxinic water column during the interglacial transgressions (lower Units II and V) the sedimentary Mo inventory can be calculated and rates of marine inflow over the Bosporus sill for a defined time span can be estimated. Marine inflow rates are calculated in the first step by using the sedimentary Mo content, an average sediment density of 1.5 g/cm³, and a porosity of 60 % to calculate the absolute amount of Mo in each 1 cm³ surface sediment. Secondly, the Mo mass is multiplied with the assumed Black Sea brackish water Mo concentration (6.7 µg/l; conservative mixing model), the sedimentation rate (Eemian: 4.0 cm/ka; Holocene: 8.0 cm/ka) and

the basin's area covered by the anoxic water column (413,000 km²). The Mo concentration for the inflowing Eemian seawater is considered to be the same as for the Holocene seawater, because of the long ocean residence time of 800 ka for Mo (MORFORD and EMERSON, 1999). Thus, the composition of Mediterranean seawater and the dilution due to fresh water is assumed to be similar in both interglacials. The calculation shows that inflow rates of the Eemian interglacial are lower (up to 145 km³/a) compared to the Holocene (up to 250 km³/a) for this location. Consequently the salinity in the Eemian water column must have been lower.

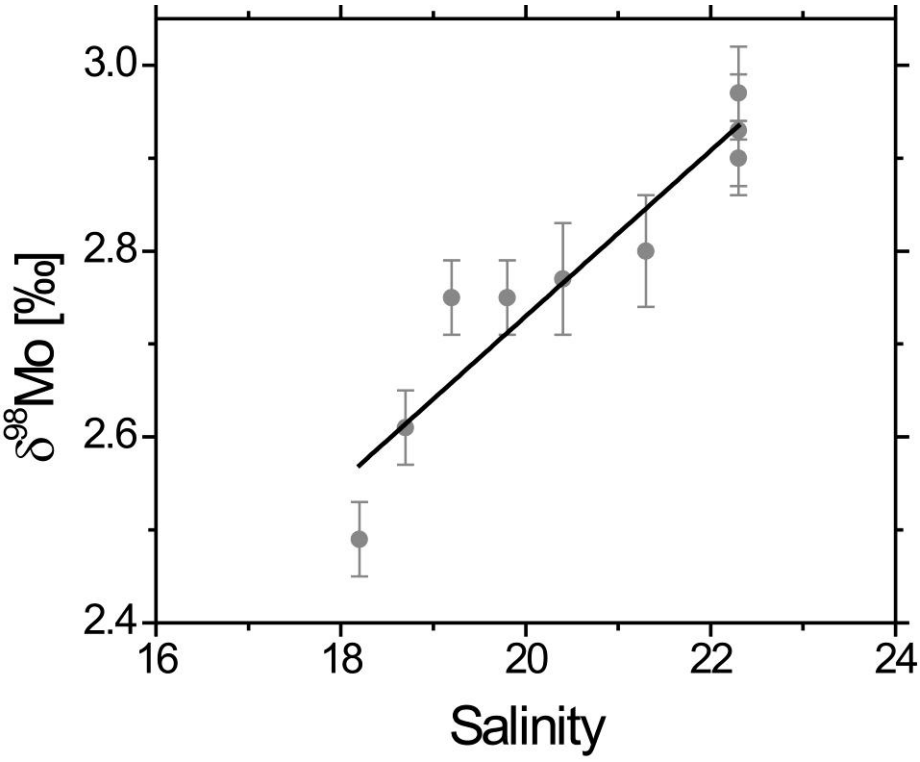


**Abb. 4-5** $\delta^{98}$Mo as a function of salinity
results in a linear relationship defined as: $\delta^{98}$Mo = 0.0891 (± 0.0119) × salinity + 0.9481 (± 0.2436); $r^2$ = 0.8898. Data are taken from the south-eastern site samples published in NÄGLER et al. (2011). The error bars represent 2σ.

To confirm this inventory calculation, the paleosalinity of the Eemian Black Sea can be estimated by Mo isotopes. Salinity and $\delta^{98}$Mo data for water column samples were taken from NÄGLER et al. (2011) and show a reasonable linear correlation (Abb. 4-5). Applying this regression to our sedimentary authigenic $\delta^{98}$Mo data of the Eemian samples results in lower salinities (up to 15) during the Eemian transgression compared to the Holocene (up to 22). We assume an almost quantitative removal of Mo from the

water column, which leads to almost the same isotopic composition of the sediment and water column after correcting for lithogenic Mo (modified after ARNOLD et al., 2012).

c) A third explanation may be that not the Eemian had lower but the Holocene had higher $\delta^{97}$Mo values. This may be due to the strong (almost complete) transfer of Mo from the Eemian water column into the sediment. This may results in higher $\delta^{97}$Mo values in the water column compared to lower $\delta^{97}$Mo values of Mo deposited in the sediment owing to the mass-dependent isotope fractionation (NÄGLER et al., 2011). Assuming the basin is fully restricted during the last interglacial and it shifts back from euxinic to oxic conditions a small reservoir of dissolved Mo with elevated isotopic composition is left. This may lead to higher $\delta^{97}$Mo values in the Holocene water column even before the quantitative removal of Mo was initiated in Unit II. A global change of the seawater $\delta^{97}$Mo (and $\delta^{238}$U) value can be ruled out, because the residence time of Mo (and U) and other factors affecting isotopic composition of the oceans, e.g. a global euxinic draw-down of Mo, are not documented for the last 130.000 years. The only possibility left might be that Mo deposition into the Mediterranean *S5* sapropel was sufficiently high to produce a Mo depletion in the remaining seawater, which flows into the Eemian Black Sea basin. But a rough inventory calculation shows that the Mo depletion in the Mediterranean water column was balanced by the high inflow of Atlantic seawater: On average $20.8 \cdot 10^6$ t of Mo is deposited in the *S5* sapropels, taking the following chemical and physical parameters for the *S5* sapropel: An average Mo content of 85 mg/kg (Tab. 4-2), a dry bulk density of 1.4 g/cm³ (EMEIS and SAKAMOTO, 1998), a porosity of 80 % (MOLLER et al., 2012), an average sapropel thickness of 35 cm (MOLLER et al., 2012) and a basin area of $2.5 \cdot 10^6$ km². But with a seawater inflow over the Strait of Gibraltar of 30,000 km³/a and a Mo concentration of 10.6 µg/l, resulting in 318,000 t/a of Mo. Hence, it would take a seawater intrusion period of 0.065 ka to outbalance the loss of Mo from the water column into the sediment, which is in good agreement with the findings of Nijenhuis et al. (1999) for Pliocene eastern Mediterranean sapropels of 0.089 ka for supplying enough excess Mo.

In summary, the Mo and U isotopes of the sediment column at site 22, combined with redox-sensitive proxies, show euxinic conditions in the water column of the Black Sea during the Holocene and Eemian interglacials. The isotopic signatures indicate less

intense euxinia and lower seawater intrusion for the Eemian compared to today's Black Sea.

### 4.4.3. Changes of the elemental distribution patterns due to turbidite deposition

The transition between the sediments deposited during the Eemian interglacial and the Würm/Weichselian glacial is interrupted by a turbidite as indicated by distinct peaks in the Si/Al, Ti/Al and Zr/Al depth profiles mentioned in chapter 4.1.

The *S1* sapropel of the Mediterranean Sea with oxic sediment on top (REITZ et al., 2006; THOMSON et al., 1993; THOMSON et al., 1995; THOMSON et al., 1999) may be well suited for comparison and interpretation of the elemental depth profiles in these transition layers, because the geochemical pattern of the turbidite on top of the sapropelic layer is in line with the average Unit III and VI sediments suggesting that the turbidite originated from above-lying limnic clay sediments. But the shape of the elemental depth profiles presented here differs from the ones of the Mediterranean *S1* sapropels (REITZ et al., 2006; THOMSON et al., 1995; THOMSON et al., 1999). Redox sensitive elements like Fe, Mn, and Mo are mobilized in the upper *S1* sediments, due to oxidation by the overlying sediment, which results in diffusion-like elemental profiles. Such profiles are not found in the Eemian elemental depth distribution. The sharp decreases in Ca* and U/Al at the top of the Eemian sapropel may indicate a hiatus caused by a turbidite. But since we do not see any indication of mobilization and diffusion of redox sensitive elements in the transition zone, it can be assumed that this event might have happened within the glacial stage.

The Fe/Al depth profile also shows a sharp decrease to values slightly below the average shale ratio. This drop in Fe enrichment might be a primary signal because comparable values are found 1 cm below the turbidite base. The Fe/Al ratios increase to average shale (or Unit III) values at the depth of the turbidite base indicating a different origin of the sediment layer and the absence of Fe mobilization. Fe/Al ratios less than the lithogenic background, combined with low $\delta^{56}$Fe values, reflect a shutdown of the Fe shuttle and the deposition of sediments depleted in reactive Fe.

**Tab. 4-2** Comparison of various sapropels from different locations and interglacials. Holocene Black Sea sapropels include Unit I and II. The data of the Eemian Black Sea sapropel is from Unit V samples. Mediterranean *S5* sapropels samples of ODP Leg 160 are extracted from WARNING and BRUMSACK (2000).

| | Avg. Black Sea Holocene (n = 656) | | Site 22 Holocene (n = 102) | | Site 22 Eemian (n = 157) | | DSDP 42B 379A Eemian (n = 15) | | Mediterranean *S5* (n = 10) | |
|---|---|---|---|---|---|---|---|---|---|---|
| | [wt. %] | element/Al | [wt. %] | element/Al | [wt. %] | element/Al | [wt. %] | element/Al | [wt. %] | element/Al |
| $SiO_2$ | 31.0 ± 12.3 | 2.8 ± 0.5 | 36.9 ± 4.8 | 2.6 ± 0.1 | 29.5 ± 9.1 | 2.7 ± 0.2 | 48.7 ± 1.1 | 3.3 ± 0.1 | 24.7 ± 4.4 | 3.3 ± 1.1 |
| $TiO_2$ | 0.43 ± 0.17 | 0.050 ± 0.003 | 0.61 ± 0.08 | 0.055 ± 0.002 | 0.43 ± 0.16 | 0.054 ± 0.004 | 0.30 ± 0.17 | 0.052 ± 0.003 | 0.41 ± 0.17 | 0.062 ± 0.005 |
| $Al_2O_3$ | 9.7 ± 3.6 | | 12.6 ± 1.7 | | 8.9 ± 3.0 | | 6.5 ± 3.5 | | 7.3 ± 2.6 | |
| $Fe_2O_3$ | 4.3 ± 1.2 | 0.6 ± 0.2 | 5.8 ± 0.7 | 0.6 ± 0.1 | 4.4 ± 1.4 | 0.7 ± 0.1 | 3.1 ± 1.4 | 0.7 ± 0.1 | 5.4 ± 1.4 | 1.0 ± 0.2 |
| MgO | 2.3 ± 0.8 | 0.29 ± 0.13 | 3.7 ± 0.4 | 0.34 ± 0.03 | 2.5 ± 0.9 | 0.32 ± 0.05 | 1.5 ± 0.8 | 0.28 ± 0.03 | 2.8 ± 0.5 | 0.47 ± 0.13 |
| CaO | 16.4 ± 10.7 | 3.9 ± 5.5 | 11.6 ± 5.4 | 1.3 ± 0.9 | 22.9 ± 9.4 | 5.0 ± 5.7 | 7.2 ± 2.3 | 1.8 ± 1.2 | 19.9 ± 3.3 | 4.3 ± 2.2 |
| $Na_2O$ | 3.0 ± 1.3 | 0.55 ± 0.43 | 2.7 ± 0.7 | 0.30 ± 0.11 | 1.1 ± 0.2 | 0.18 ± 0.06 | 0.8 ± 0.6 | 0.17 ± 0.03 | 3.0 ± 0.7 | 0.71 ± 0.44 |
| $K_2O$ | 1.7 ± 0.6 | 0.28 ± 0.02 | 2.1 ± 0.3 | 0.27 ± 0.01 | 1.5 ± 0.5 | 0.27 ± 0.02 | 1.0 ± 0.4 | 0.25 ± 0.02 | 1.1 ± 0.2 | 0.24 ± 0.05 |
| $P_2O_5$ | 0.16 ± 0.05 | 0.017 ± 0.011 | 0.13 ± 0.03 | 0.009 ± 0.002 | 0.18 ± 0.10 | 0.019 ± 0.014 | 0.14 ± 0.05 | 0.022 ± 0.014 | 0.13 ± 0.04 | 0.017 ± 0.011 |
| S | 1.6 ± 0.6 | 0.38 ± 0.24 | 1.6 ± 0.4 | 0.24 ± 0.08 | 1.2 ± 0.3 | 0.26 ± 0.08 | 0.8 ± 0.4 | 0.29 ± 0.22 | 2.2 ± 0.9 | 0.66 ± 0.38 |
| TOC | 6.9 ± 5.4 | 1.73 ± 1.35 | 4.1 ± 2.7 | 0.64 ± 0.45 | 3.9 ± 2.0 | 0.91 ± 0.36 | 1.6 ± 0.5 | 0.23 ± 0.08 | 5.6 ± 2.4 | 1.85 ± 1.37 |
| TIC | 3.5 ± 2.4 | 1.28 ± 1.71 | 2.4 ± 1.1 | 0.39 ± 0.25 | 4.8 ± 2.0 | 1.53 ± 1.88 | 1.70 ± 0.03 | 0.244 ± 0.004 | 4.2 ± 0.8 | 1.25 ± 0.63 |
| | [ppm] | | [ppm] | | [ppm] | | [ppm] | | [ppm] | |
| As | 15 ± 7 | 3.4 ± 2.2 | 20 ± 10 | 3.1 ± 2.3 | 55 ± 13 | 12 ± 5 | 32 ± 19 | 13 ± 11 | 35 ± 8 | 10 ± 4 |
| Ba | 615 ± 787 | 147 ± 211 | 439 ± 139 | 66 ± 18 | 292 ± 61 | 69 ± 32 | 217 ± 90 | 69 ± 22 | 1792 ± 962 | 616 ± 530 |
| Cd | 0.66 ± 0.37 | 0.19 ± 0.16 | 0.51 ± 0.26 | 0.079 ± 0.045 | 0.46 ± 0.22 | 0.12 ± 0.08 | 0.36 ± 0.18 | 0.15 ± 0.10 | 1.1 ± 0.4 | 0.27 ± 0.14 |
| Co | 20 ± 8 | 4.9 ± 3.8 | 24 ± 6 | 3.7 ± 1.0 | 17 ± 6 | 3.8 ± 0.7 | 16 ± 7 | 6 ± 4 | 36 ± 11 | 10 ± 5 |
| Cr | 80 ± 38 | 15 ± 5 | 142 ± 22 | 21 ± 2 | 89 ± 43 | 18 ± 5 | 58 ± 27 | 17 ± 3 | 78 ± 13 | 22 ± 7 |
| Cu | 63 ± 32 | 14 ± 9 | 69 ± 11 | 10 ± 2 | 57 ± 17 | 13 ± 3 | 60 ± 29 | 23 ± 17 | 83 ± 16 | 24 ± 10 |
| Mn | 423 ± 125 | 99 ± 58 | 227 ± 51 | 86 ± 12 | 864 ± 785 | 362 ± 323 | 925 ± 1005 | 37 ± 533 | 760 ± 188 | 242 ± 97 |
| Mo | 58 ± 45 | 13 ± 11 | 48 ± 22 | 7 ± 4 | 53 ± 37 | 12 ± 9 | 26 ± 25 | 11 ± 12 | 85 ± 35 | 28 ± 19 |
| Ni | 81 ± 42 | 17 ± 8 | 142 ± 36 | 21 ± 5 | 89 ± 35 | 19 ± 4 | 64 ± 24 | 23 ± 14 | 124 ± 20 | 37 ± 18 |
| Pb | 16 ± 7 | 3.4 ± 1.9 | 19 ± 7 | 2.8 ± 1.1 | 15 ± 7 | 3.3 ± 1.8 | 9 ± 3 | 3.0 ± 0.9 | 9 ± 3 | 2.6 ± 1.2 |
| Rb | 76 ± 28 | 15 ± 1 | 91 ± 13 | 14 ± 1 | 67 ± 23 | 14 ± 1 | 39 ± 13 | 12 ± 3 | 43 ± 11 | 12 ± 2 |
| Re | 0.055 ± 0.032 | 0.014 ± 0.009 | 0.054 ± 0.037 | 0.008 ± 0.005 | 0.059 ± 0.063 | 0.014 ± 0.011 | 0.035 ± 0.037 | 0.015 ± 0.017 | 0.18 ± 0.07 | 0.044 ± 0.021 |
| Sr | 658 ± 467 | 215 ± 296 | 501 ± 480 | 83 ± 95 | 1357 ± 1175 | 418 ± 699 | 581 ± 364 | 240 ± 255 | 726 ± 257 | 225 ± 151 |
| U | 11 ± 6 | 3.1 ± 3.2 | 8 ± 3 | 1.2 ± 0.4 | 16 ± 13 | 3.9 ± 4.0 | 5 ± 3 | 1.9 ± 1.7 | 30 ± 14 | 10 ± 8 |
| V | 143 ± 59 | 30 ± 13 | 168 ± 39 | 25 ± 6 | 124 ± 35 | 27 ± 5 | 86 ± 26 | 28 ± 10 | 298 ± 76 | 89 ± 46 |
| Y | 22 ± 15 | 5.3 ± 5.7 | 19 ± 2 | 2.8 ± 0.2 | 18 ± 9 | 4.0 ± 1.3 | 11 ± 4 | 3.5 ± 0.9 | 22 ± 3 | 6.5 ± 2.5 |
| Zn | 84 ± 51 | 21 ± 27 | 88 ± 12 | 13 ± 2 | 66 ± 20 | 14 ± 1 | 49 ± 16 | 16 ± 4 | 65 ± 12 | 18 ± 4 |
| Zr | 84 ± 28 | 17 ± 4 | 99 ± 12 | 15 ± 1 | 75 ± 30 | 16 ± 2 | 57 ± 26 | 17 ± 2 | 90 ± 37 | 23 ± 2 |

The decreasing Mo/Al ratios from the Unit V maximum to the turbidite base, combined with the fact that the maximum of the Mo/Al depth profile is below the Fe/Al maximum, indicates a decrease of the authigenic Mo precipitation from the water column, possibly related to the decrease of the seawater inflow (Mo source). Thus, the decreases in Mo/Al and Fe/Al may indicate the transition from marine back to limnic conditions in the basin accompanied by a lowering of the chemocline and not an oxidation effect by the turbidite. Hence, the turbidite event in our view took place after sapropel deposition and at most erased part of the transition layer in the core presented here.

### 4.4.4. Comparison with the time-equivalent Mediterranean *S5* sapropel

The Black Sea is not the only anoxic marginal basin where sapropels were deposited during the Eemian. The adjacent Eastern Mediterranean Sea is known for its numerous occurrences of sapropels in its geological record (EMEIS et al., 2000; NIJENHUIS et al., 1998; PASSIER et al., 1999; RINNA et al., 2002; WARNING and BRUMSACK, 2000; WEHAUSEN and BRUMSACK, 1998). The *S5* sapropel deposited during MIS 5e may serve as a time-equivalent analog for the Eemian sapropel in the Black Sea. By contrast the *S1* sapropel, which was deposited between 6 and 11 ka, does not represent a suitable time-equivalent analog for the Holocene Black Sea sapropel.

In Tab. 4-2 mean values of various elements for the Holocene and Eemian sapropels of site 22 and DSDP Leg 42B site 379 and various *S5* sapropels sampled during ODP Leg 160 (extracted from original data of WARNING and BRUMSACK, 2000) are compared. On basis of element to aluminum ratios the paleoenvironmental conditions during the deposition of the different sapropels may be distinguished (Tab. 4-2). The high enrichments in Mo, TOC, and sulfur combined with the moderate enrichments of Fe- and sulfide-bound elements (e.g. As, Co, Cu, Ni) indicate euxinic conditions in both basins during the Holocene and Eemian interglacials. The enrichment of these elements results from sulfide precipitation processes, redox reactions and associated scavenging processes in the water column as described above. Depending on the sampling location the sedimentation rates of *S5* sapropels vary between 2 and 30 cm/ka with an average rate of ~7 cm/ka (KRAAL et al., 2010; MELKI et al., 2010; MOLLER et al., 2012;

ROHLING et al., 2006; WELDEAB et al., 2003a; WELDEAB et al., 2003b). Therefore the sedimentation rates are much higher during *S5* deposition compared to the Eemian Black Sea sapropel. We know from our detailed study of the Holocene Black Sea sapropel, that sedimentation rates can strongly differ across the basin (ECKERT et al., 2013). On basis of the enrichment of these redox-sensitive elements (Tab. 4-2) and the sedimentation rates, euxinia in the Mediterranean Sea were possibly stronger compared to the Black Sea, as it seems to be indicated by organic markers for photic zone euxinia (ROHLING et al., 2006).

The terrestrial input influencing the Black Sea sampling location site 22, represented by Cr, K, Mg, Rb, Ti, and Zr, was more or less identical during both interglacials. Only the different enrichments in Mg may indicate a shift from illite- to chlorite-dominated fluvial input (WEHAUSEN and BRUMSACK, 1998). The higher Ti enrichment in the *S5* sapropel shows the influence of an aeolian component to the sediments, most probably from the Sahara desert (MOLLER et al., 2012; SANGIORGI et al., 2006; WEHAUSEN and BRUMSACK, 1999; WELDEAB et al., 2003b).

Paleoproductivity proxies, like phosphorous and biogenic carbonates, show higher enrichments in all Mediterranean *S5* sapropels compared to the Holocene Black Sea sapropel, indicating a higher nutrient flux during times of deposition, which fits to the argument of a warmer Eemian interglacial (ROHLING et al., 2008). Especially Ba is very abundant in the Mediterranean Sea during MIS 5e compared to the Black Sea, indicating a high primary productivity (DYMOND et al., 1992; MOLLER et al., 2012; WEHAUSEN and BRUMSACK, 1999; WELDEAB et al., 2003a). The occurrence of isorenieratene derivatives in the Mediterranean *S5* sapropels implies the establishment of a GSB community, and hence, a chemocline positioned in the photic zone, very similar to the Black Sea Eemian sapropel (ROHLING et al., 2006).

The comparison of Mediterranean and Black Sea Eemian sapropels by means of element to aluminum ratios shows various similarities, but the local characteristics of site 22 seems to have more impact on the geochemical patterns than the global conditions during the Eemian interglacial. This explains that there are more chemical similarities between the Eemian and Holocene Black Sea sapropels compared to those between the Eemian Black Sea and the Mediterranean *S5* sapropel.

### 4.5. Conclusions

In this study we provide for the first time a geochemical characterization of the Eemian sapropel from the Black Sea. The Eemian sapropel retrieved from two adjacent sediment cores (site 22, R/V *Meteor* expedition M72/5) has been compared with the recent (Holocene) sapropel at the same site, the average Holocene sapropel (CGCL), and the time-equivalent *S5* sapropel from the Mediterranean Sea. On basis of major and trace element abundances in combination with stable isotope data of C, Fe, Mo, and U and selected organic markers of photic zone euxinia (isorenieratene derivatives), the following conclusions may be drawn:

- Three new units (IV to VI) are proposed for the Eemian sapropel, and the antecedent glacial, in analogy to the Holocene Units I, II, and III. The lithological units of both, the Holocene and Eemian Black Sea sapropels are geochemically defined by Ca* ($CaCO_3$) and TOC contents.
- A pycno-/chemocline in the water column of the Black Sea developed after ingression of Mediterranean seawater during both interglacials. The chemocline, dividing (sub-)oxic from anoxic/euxinic water masses did reach the photic zone in both cases. This is documented by element/Al ratios of Fe, Mo, and U, the occurrence of isorenieratene derivatives and carbon as well as Fe isotopes.
- Geochemical proxies favor the gradual inflow of seawater into the basin. The pycno-/chemocline fluctuated during the Holocene but not during the Eemian interglacial.
- $\delta^{97}$Mo and $\delta^{238}$U values indicate stronger euxinic and marine conditions in the Holocene compared to the Eemian interglacial in the Black Sea.
- Paleoproductivity was generally enhanced during deposition of both, the Eastern Mediterranean *S5* and the Eemian Black Sea sapropel. Productivity proxies are slightly more elevated in the Mediterranean *S5* record, suggesting higher productivity in the Eastern Mediterranean.
- The terrigenous input at Black Sea site 22 was rather constant during the last 130 ka and shows less aeolian input compared to the Eastern Mediterranean location.

*Acknowledgements.*

We are grateful to the crew of R/V *Meteor* and to the Deutsche Forschungsgemeinschaft (DFG) for funding this project (IODP SPP Br 775/26-1). We are indebted to C. Montoya-Pino, A.-K. Meinhardt, E. Gründken, C. Lehners and M. Schulz for analytical assistance.

## 4.6. Appendix

### 4.6.1. Construction of the Eemian composite geochemical core log

The geochemical pattern of the two Eemian sapropels from cores 22-GC-3 and 22-GC-7 were visually inspected. After recognizing several similarities of the vertical distribution of geochemical proxies in both sapropels adjustment points for the depth correlation were chosen. The adjustment points are the tubidite base (peaks in Ti/Al and Zr/Al depth profile), the Mo/Al maximum, and several peaks and troughs in the Ca/Al depth profile. The depth scale of the shorter sapropel (core 22-GC-7) was adjusted to core 22-GC-3 by linear interpolation between these adjustment points. The proxy data was combined and mean values were calculated for each interpolated 0.5 cm depth interval by a custom made MATLAB routine (according to ECKERT et al., 2013). The resulting composite profiles underwent a two-point-average smoothing to remove scatter.

**Tab. 4-3** Accuracy and precision of the analysis stated as pooled relative standard deviation (%pRSD), pooled relative deviation from the reference value (%r), and the number of measurements (n). GSR-5, GSR-6, SDO-1, and five in-house standards were used for references.

| | **XRF** | | **ICP-OES** | | **HR-ICP-MS** | |
|---|---|---|---|---|---|---|
| | n = 40 | | n = 88 | | n = 57 | |
| | %pRSD | %r | %pRSD | %r | %pRSD | %r |
| $SiO_2$ | 3.3 | -2.3 | | | | |
| $Ti_2O$ | 2.8 | 0.4 | 3.6 | -3.6 | | |
| $Al_2O_3$ | 3.3 | -3.4 | 3.6 | -3.1 | | |
| $Fe_2O_3$ | 2.9 | -1.7 | 4.7 | -1.1 | | |
| MnO | 2.1 | 1.6 | 3.4 | -0.6 | | |
| MgO | 3.6 | -1.2 | 3.2 | -3.3 | | |
| CaO | 3.0 | -2.1 | 4.9 | -0.9 | | |
| $Na_2O$ | 6.2 | -1.9 | 13.7 | -2.6 | | |
| $K_2O$ | 4.0 | -4.0 | 4.7 | 2.8 | | |
| $P_2O_5$ | 3.3 | -5.7 | 5.1 | -1.4 | | |
| | | | | | | |
| As | 4.6 | 6.3 | 14.8 | -2.0 | | |
| Ba | 4.0 | 1.1 | 2.7 | -3.9 | 3.2 | -1.6 |
| Cd | | | 16.5 | -0.8 | 5.5 | -3.8 |
| Co | 6.5 | 7.9 | 4.9 | -2.8 | 4.0 | 0.3 |
| Cr | 9.0 | -11.2 | 9.0 | -4.4 | 3.2 | -0.6 |
| Cu | 5.5 | -2.1 | 5.7 | -3.3 | 4.2 | -1.0 |
| Mo | 5.4 | -6.2 | 6.9 | 2.1 | 6.8 | 2.3 |
| Ni | 4.0 | 0.6 | 3.9 | -3.5 | 2.6 | -1.2 |
| Pb | 25.4 | -8.3 | 11.7 | 0.9 | 4.7 | 1.0 |
| Rb | 3.2 | 3.1 | | | 2.8 | -0.4 |
| Re | | | | | 4.4 | 3.6 |
| Sr | 2.7 | -0.3 | 3.1 | -3.1 | 3.0 | -0.1 |
| U | 15.1 | -6.0 | | | 4.6 | 1.7 |
| V | 3.4 | -3.3 | 6.1 | 0.3 | 3.4 | 1.1 |
| Y | 3.9 | 7.6 | 4.7 | -1.8 | 1.9 | -1.1 |
| Zn | 3.3 | 2.0 | 3.1 | -3.7 | 7.9 | -1.1 |
| Zr | 3.8 | -2.0 | 5.7 | -1.2 | 3.8 | -1.2 |

**Tab. 4-4** Mean values and precision of the U, Mo, and Fe isotopes analyses stated as double relative standard deviation (2σ), and the number of measurements (n) for the associated delta notation. $\delta^{238}U$ was calculated using CRM-112A; $\delta^{97}Mo$ and $\delta^{98}Mo$ was calculated using Mo-STD; $\delta^{56}Fe$ was calculated using IRMM-14.

| Standard (n) | $\delta^{238}U$ mean [‰] | $\delta^{238}U$ 2σ [‰] |
|---|---|---|
| IRMM-184 (9) | -1.19 | 0.11 |
| REIMEP-18A (9) | -0.11 | 0.12 |
| | $\delta^{97}Mo$ mean [‰] | $\delta^{97}Mo$ 2σ [‰] |
| SDO-1 (3) | 0.78 | 0.02 |
| SDO-1, spiked (3) | -0.20 | 0.07 |
| Grav-Mo-STD (4) | -1.02 | 0.12 |
| | $\delta^{98}Mo$ mean [‰] | $\delta^{98}Mo$ 2σ [‰] |
| SDO-1 (3) | 1.13 | 0.04 |
| SDO-1, spiked (3) | 0.16 | 0.05 |
| Grav-Mo-STD (4) | -1.05 | 0.19 |
| | $\delta^{56}Fe$ mean [‰] | $\delta^{56}Fe$ 2σ [‰] |
| SDO-1 (22) | 0.08 | 0.09 |
| BIR-1 (19) | 0.10 | 0.11 |
| SCo-1 (11) | 0.07 | 0.11 |
| IRMM-grav-1 (31) | -1.04 | 0.06 |
| MAG-1 (10) | 0.18 | 0.12 |

# 5. The uranium carbonate association in Holocene Black Sea sediments

Authors:

Sebastian Eckert, Mikrobiogeochemie, Institut für Chemie und Biologie des Meeres (ICBM), Carl von Ossietzky Universität, 26111 Oldenburg

Bernhard Schnetger, Mikrobiogeochemie, Institut für Chemie und Biologie des Meeres (ICBM), Carl von Ossietzky Universität, 26111 Oldenburg

Hans-Jürgen Brumsack, Mikrobiogeochemie, Institut für Chemie und Biologie des Meeres (ICBM), Carl von Ossietzky Universität, 26111 Oldenburg

## Abstract

Uranium is one of the most abundant trace metal in seawater, but its depositional pathway under reducing conditions is poorly known. While under oxic conditions dissolved U is present as a uranyl carbonate complex [$U^{VI}O_2(CO_3)_4^{2-}$], it eventually precipitates as $U^{IV}O_2$ under reducing conditions. For anoxic conditions with enhanced preservation and thus deposition of organic matter, the association of $U^{IV}$ with organic matter is the presumed pathway of U deposition. In this work we try to follow the question what alternative deposition mechanism exists for $U^{IV}$, if organic carbon ($C_{org}$) does not form one of the major biogenic sediment matrix components.

Based on the geochemical data from seven sediment cores from the late Holocene Black Sea we discuss the possibility that carbonate minerals may serve as reduction surfaces for U. The sediment cores investigated consist of lithological units with high $C_{org}$ and low carbonate contents (Unit II) and units with high carbonate and medium $C_{org}$ concentrations (Unit I). The results of cluster analysis and adjusted coefficients of determination ($\overline{R^2}$) for U vs. $C_{org}$, and carbonate show a correlation of U and $C_{org}$ for Unit II samples and a correlation of U and $C_{carb}$ for Unit I samples. This behavior of U in the presence of carbonate-rich anoxic sediments was also recognized in black shale layers of OAE 2 from Demerara Rise. These observations may indicate that the behavior of U depends on the major component of the sediment matrix and highlight the possible association of U with carbonate under euxinic conditions.

## 5.1. Introduction

The geochemical characteristics of U and its economic value has been in the interest of geoscientists for decades. Uranium is not only important for energy production, but also for dating of geo- and cosmochemical samples by means of the U-Th-method and besides being used as a paleoredox proxy in sediment cores. Furthermore uranium is the second most abundant trace metal in ocean seawater (MARTIN and WHITFIELD, 1983).

Uranium is present in oxic seawater as a uranyl carbonate complex $U^{VI}O_2(CO_3)_4^{2-}$ and behaves conservatively throughout the oxic water column (LANGMUIR, 1978). However, in suboxic to anoxic environments the conservative behavior of uranium changes to a complex particle surface reactive behavior, most likely due to microbially mediated reduction processes forming $U^{IV}O_2$ and monomeric $U^{IV}$ (ANDERSON et al., 1989; BARGAR et al., 2013; KLINKHAMMER and PALMER, 1991). Unlike Fe or Mo, which can be reduced by sulfide in a euxinic water column and precipitate as sulfides accumulation in sediments, U may diffuse into the upper sediment layer, where it gets reduced, most likely mediated by mineral surfaces of sediment particles. As shown by KLINKHAMMER and PALMER (1991) the reduction takes place following Fe reduction in the diagenetic redox sequence, mostly enhanced by sulfate reducing bacteria, but without being influenced by Fe and Mn redox cycling (ALGEO and MAYNARD, 2004). Recently BARGAR et al. (2013) showed that FeS minerals in combination with microbially produced phosphate can favor U reduction under sulfate reducing conditions.

However, this special reduction pathway, and the known removal without involving scavenging, seems to explain the well-known correlation of U with organic matter (OM) under oxygen limited conditions (ALGEO and MAYNARD, 2004; ANDERSON, 1982; CHAILLOU et al., 2002; CRUSIUS and THOMSON, 2000; KLINKHAMMER and PALMER, 1991; MCMANUS et al., 2005; ZHENG et al., 2002a; ZHENG et al., 2002b). This is especially true for the Black Sea, the type location of an anoxic basin with high capability of OM preservation (ANDERSON, 1987; ANDERSON et al., 1989; BARNES and COCHRAN, 1991; CAGATAY et al., 1990; COLODNER et al., 1995; DEGENS et al., 1977). As KLINKHAMMER and PALMER (1991) could show correctly, this observation is complex and controversial, partly because of the not fully understood coupling of U and OM, or specific functional groups within OM. Indeed the functionality of OM may lead

to the assumption that U, like other redox-sensitive trace metals (e.g. Cu, Ni, V), forms organic complexes in regions with high OM rain rates. But what happens if OM is not the most abundant sediment component besides the more or less inert terrigenous fraction? How, for example, does the U reduction and removal process operate in carbonate rich anoxic sediment layers?

Uranium in carbonates has often been analyzed, but never discussed in terms of reduction processes in reducing, organic-rich sediments. It was shown that U can be incorporated in calcite (and as well as aragonite) as oxygenated $U^{VI}$ and reduced $U^{IV}$ by exchanging the Ca and carbonate ions (KELLY et al., 2003; KELLY et al., 2006; RUSSELL et al., 1994; STURCHIO et al., 1998; SWART and HUBBARD, 1982; TATSUMOTO and GOLDBERG, 1959).

To answer the question of a possible connection between U and the predominant sediment matrix we analyzed U and carbonate contents and statistically averaged the data for different cores of the Black Sea in the marine, coccolith-rich layer (Unit I) and in the transitional, brackish, OM-rich layer (Unit II).

The Black Sea is a textbook example of a restricted marine basin with a stratified water column leading to anoxic to euxinic deep water masses. The 2000 m thick anoxic water column and the high productivity of haptophytes in the oxic photic zone provide excellent conditions to test different scenarios of U reduction with different dominating sediment components.

Additionally, we compared these samples with ancient black shale samples of the Cenomanian/Turonian oceanic anoxic event (OAE 2) from the Demerara Rise (off Suriname, South America) consisting of alternating carbonate-rich and OM-rich layers.

In this work we offer a new perspective on the U reduction pathway in a marine anoxic environment which may be helpful for interpreting the carbonate-U association.

## 5.2. Material and Methods

### 5.2.1. Sampling

The material used for this study was sampled on the western Black Sea shelf (GeoB 7604, 7607, 7608, 7609, 7610 and 8-GC-1) and north of the Anatolian coast in the south-eastern Black Sea (22-GC-7) (Abb. 5-1). The samples were recovered by gravity

corers (GC) and associated short corers (Multicorer, MUC) during R/V *Meteor* expeditions M51/4 (2001) and M72/5 (2007). The GCs were cut on board in one-meter sections, stored in a cold-storage room (4 °C) and continuously sub-sampled on centimeter to millimeter scale in the laboratory of the ICBM, Oldenburg. The MUCs were continuously sub-sampled at 1-5 cm intervals on board and stored at 4 °C as well.

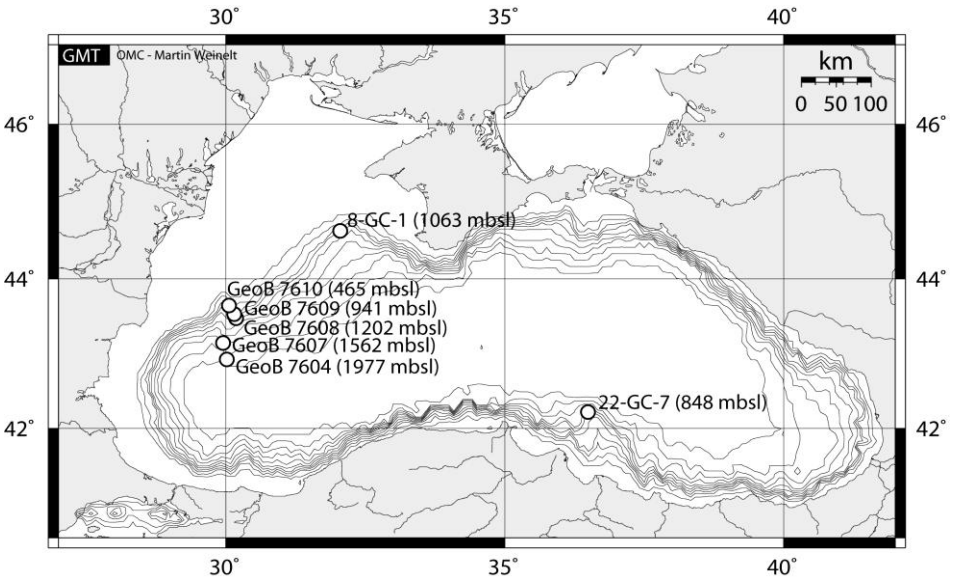


**Abb. 5-1** Map of the Black Sea with sampling locations.
Sampling water depth is noted in brackets. (created by OMC, copyright: M. Weinelt)

### 5.2.2. Geochemical analysis

The samples were freeze-dried and ground with an agate planetary ball mill before they were analyzed by XRF for major and minor elements, by IR-Spectroscopy for total carbon ($C_{tot}$) and by $CO_2$-Coulometry for total inorganic carbon ($C_{carb}$). The amount of total organic carbon ($C_{org}$) was calculated as the difference between $C_{tot}$ and $C_{carb}$.

For XRF analysis 0.7 g of dried and ground sample were mixed with 4.2 g $Li_2B_4O_7$ and 1.0 g $(NH_4)_2NO_3$ (oxidizing agent) and fused to borate glass beads at 1350 °C. These beads were measured with a Philips Panalytical PW-2400 WD-XRF spectrometer (calibrated with 53 geostandards and controlled by random measurements of acid digestions of samples with ICP-OES (Thermo Scientific iCap 6000) and ICP-MS (Thermo Finnigan Element 2)).

For the $C_{tot}$ analyses a given amount of dried and ground sample (50-100 mg) was mixed with $V_2O_5$ (oxidizing agent) and combusted in an $O_2$ stream. The resulting $CO_2$

was measured with an ELTRA CS-500 IR-spectrometer. For $C_{carb}$ analysis 5 ml 2 M $HClO_4$ were added to 50-100 mg of dried and ground sample, and the evolving $CO_2$ was measured in a coulometric cell (UIC CM-5012; carrier gas: $N_2$).

All analytical results were confirmed by parallel analysis of in-house and international reference materials (GSR-3, GSR-6 and SDO-1). The relative standard deviation (RSD) for the XRF-measurements are < 4 % for Calcium and < 9 % for Uranium, while the RSD for $C_{tot}$, $C_{carb}$ and hence $C_{org}$ is < 1 %.

### 5.2.3. Combining surface and deep sediment cores

Whereas MUCs recover undisturbed sediment surfaces, but often do not reach greater depths, GCs do not always recover surface sediments or are disturbed in the surficial layers. Ideally both core types, if available from the same location, are combined to one single core. This has been done for the cores used in this study based on depth profiles of various geochemical parameters.

### 5.2.4. Stratigraphy

Based on lithology of the seven cores three stratigraphic Units were defined (ARTHUR and DEAN, 1998; ARTHUR et al., 1994; HAY et al., 1991; JONES and GAGNON, 1994; ROSS and DEGENS, 1974). The uppermost recent Unit I was deposited under fully marine and euxinic conditions after the final establishment of coccolithophorida populations, resulting in finely laminated alternating gray-greenish and white sediment layers of coccolith ooze. Unit II is a dark brownish to black sapropel, formed during the brackish transition period from a limnic lake to a marine basin. This Unit II is subdivided into Units IIa and IIb. Due to higher $C_{org}$ content Unit IIb has a darker color and a diagnostic aragonite layer at the bottom. Unit III consists mainly of gray glacial marly clay, partly containing diagenetically formed black iron sulfides.

Unit boundaries were determined by the varying $C_{org}$ and $CaCO_3$ contents of the sediments according to ARTHUR and DEAN (1998).

### 5.2.5. Cluster analysis

The R-mode cluster analysis was performed using the software R (Version: 2.12.2; R-DEVELOPMENT-CORE-TEAM, 2011). The method *agnes*, an agglomerative computation based on a correlation matrix and hierarchical clustering, was used for data processing. This method merges the two nearest clusters to a bigger one until only one large cluster is left (MAECHLER et al., 2005). Dendrograms were created with the average linkage calculation method, where the distance between two clusters is the average of the dissimilarities between a point in one cluster and a point in the second cluster (MAECHLER et al., 2005).

Because a cluster analysis is more a qualitative way of data processing depending on the procedure the user applied, the method *pvclust* was performed as well, which is also based on a correlation matrix and hierarchical clustering, but uses p-value calculations via multiscale bootstrap resampling (SUZUKI and SHIMODAIRA, 2011). Additionally, different linkage calculation methods were tested: The complete linkage method calculates the largest dissimilarity between a point in the first cluster and a point in the second cluster (furthest neighbor method) (MAECHLER et al., 2005). The single linkage method calculates the smallest dissimilarity between a point in the first cluster and a point in the second cluster (nearest neighbor method) (MAECHLER et al., 2005).

These methods show almost the same clusters as the agnes method with average linkage calculation and therefore can verify the correlation of our data in the clusters of the agnes method.

## 5.3. Results

The geochemistry of the major components within each lithological unit is comparable between the seven sediment cores. The enrichment of the authigenic elements depends on the local sedimentation rate and thus on dilution with terrigenous material. The $C_{org}$ contents vary between 3 to 14 wt. % for Unit I and 4 to 23 wt. % for Unit II. In all cores we see a gradual increase of $C_{org}$ from the Unit III/II boundary to a maximum in the centre of Unit II followed by a decrease upcore and almost constant values in Unit I. The vertical distribution of $C_{carb}$ shows an opposite profile, with elevated concentrations at the Unit III/II boundary (up to 7 wt. %), a minimum in Unit II with ~0.5 wt. %, and

higher values up to 10 wt. % in Unit I. The absolute U concentrations vary between 5 and 25 ppm. The concentration range was more or less the same in all individual cores, but they could be differentiated by the profile shape. The absolute U concentration of Unit I is higher than in Unit II for GeoB 7607, while the opposite is true for GeoB 7604, 7608, 7609, and 8-GC-1. In cores 22-GC-7 and GeoB 7610 the U concentrations in Unit I and II are almost the same.

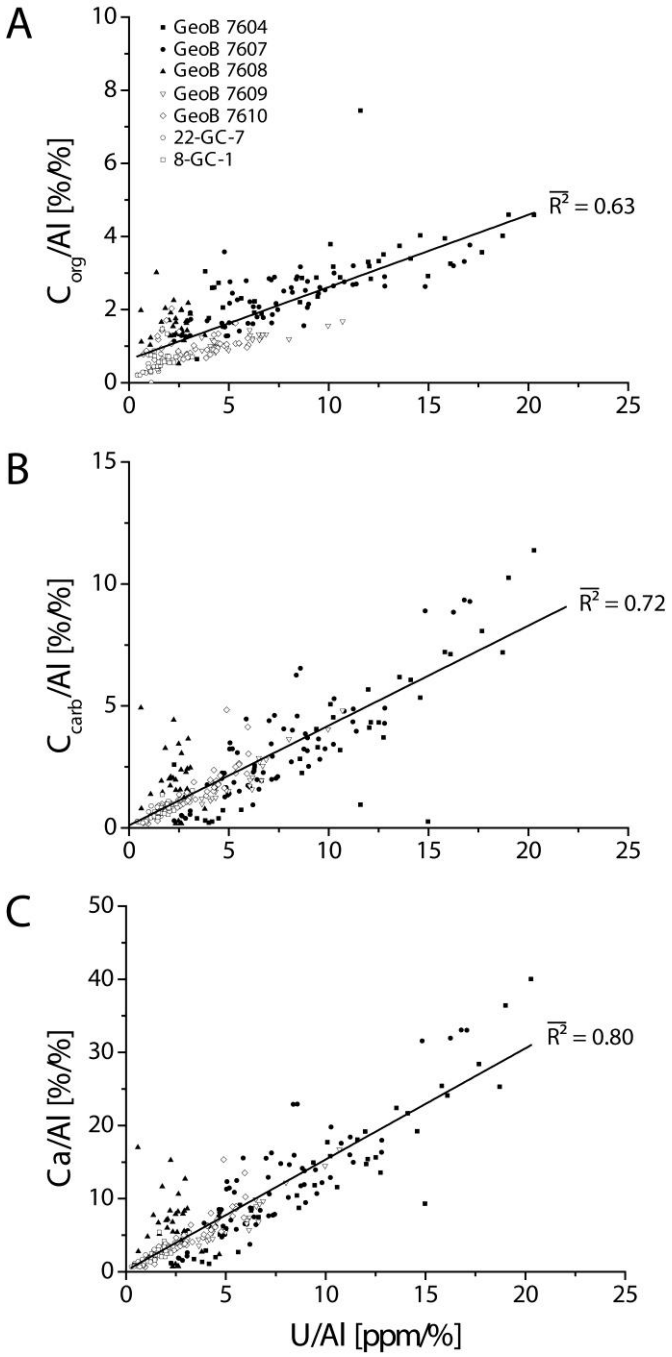


**Abb. 5-2** Element/Al ratios of $C_{org}$, $C_{carb}$, and Ca versus U/Al for Unit I samples. Solid lines represent the adjusted coefficients of determination ($\overline{R^2}$ ).

Normalization to Al was used to compensate for dilution effects of detrital matter. This procedure shows no change in the vertical trend of $C_{org}$ and $C_{carb}$ indicating a clear water column signal without influence of terrigenous material. The U/Al ratio shows values of 1 to 3 at the Unit III/II boundary increasing to a broad but shallow peak in Unit II with ratios up to 6. After a slight decrease we find an enrichment of U in Unit I with U/Al values up to 22. It is worthwhile mentioning that the vertical distribution of U/Al follows $C_{org}$ in Unit II, but it parallels $C_{carb}$ in Unit I. The Ca/Al depth profile matches perfectly with the $C_{carb}$/Al profile.

These similarities in the depth profiles are also found in the adjusted coefficients of determination of U/Al of Unit I samples with $C_{org}$/Al ($\overline{R^2}$ = 0.63), $C_{carb}$/Al ($\overline{R^2}$ = 0.72), and Ca/Al ($\overline{R^2}$ = 0.80) (Abb. 5-2). In Unit II we find only a rough correlation of U/Al with $C_{org}$/Al ($\overline{R^2}$ = 0.50), while $C_{carb}$/Al and Ca/Al show no correlation ($\overline{R^2}$ = 0.09 and $\overline{R^2}$ = 0.13) (Abb. 5-3).

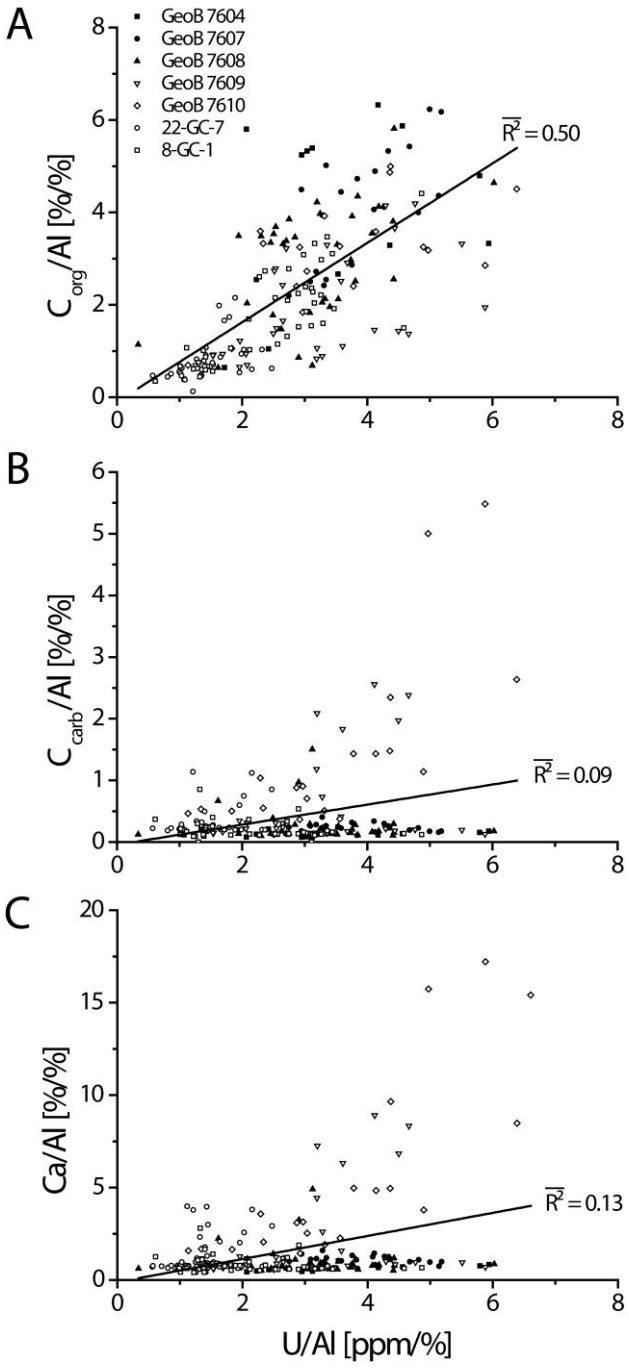


**Abb. 5-3** Element/Al ratios of $C_{org}$, $C_{carb}$, and Ca versus U/Al for Unit II samples. Solid lines represent the adjusted coefficients of determination ($\overline{R^2}$ ).

The cluster analysis for Unit I samples shows a direct connection of the Ca carbonate cluster ($C_{carb}$, Ca and Sr) with U (Abb. 5-4). The Unit II samples show a connection of the carbonate cluster with U over five branches and over the whole height of the dendrogram (Abb. 5-4). The carbonate cluster is also separated from all the other nodes with the highest branch. The connection of uranium with $C_{org}$ goes over seven branches, but is closer in terms of height compared to $C_{carb}$ (Abb. 5-4). In the cluster analysis

another distinctive cluster was recognized. It consists of Al, K, Rb, Si, Ti, and Zr and represents the terrigenous component of the sediment matrix (e.g. quartz, aluminosilicates, clay minerals, etc.) (Abb. 5-4).

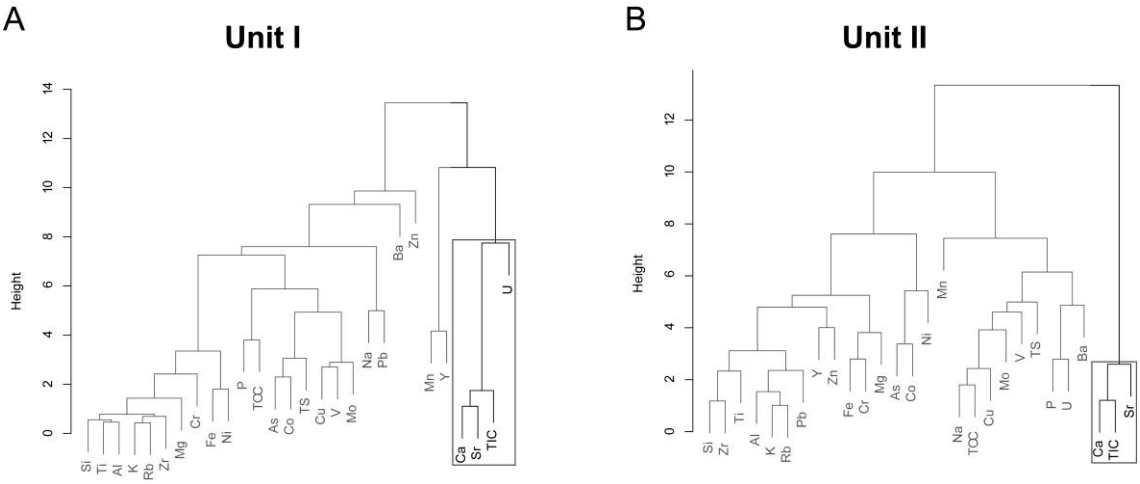


**Abb. 5-4** Dendrograms of *agnes* cluster analyses with average linkage calculation for A) Unit I and B) Unit II samples. Carbonate clusters are highlighted.

To get an overview about the geological record we show exemplarily the depth profile of core GeoB 7604, which originates from the deepest location in the northwestern transect with lowest sedimentation rates and hence lowest dilution by terrigenous matter (Abb. 5-5). In this depth plot the normalization of U to different major components of the sediment (Al for clay minerals, Ca for carbonate and $C_{org}$ for organic matter) indicates to whta degree U enrichment depends on the sediment matrix. If one of these major components is present in higher amounts, it will dilute the U content resulting in lower U to sediment component ratios. Carbonate accounts for most of the dilution in Unit I, while $C_{org}$ is the major diluting component in Unit II (Abb. 5-5). Normalization to all three major sediment components results in an almost vertical line, which indicates that U is associated with all three components, but the fractions differ depending of the lithological unit (Abb. 5-5).

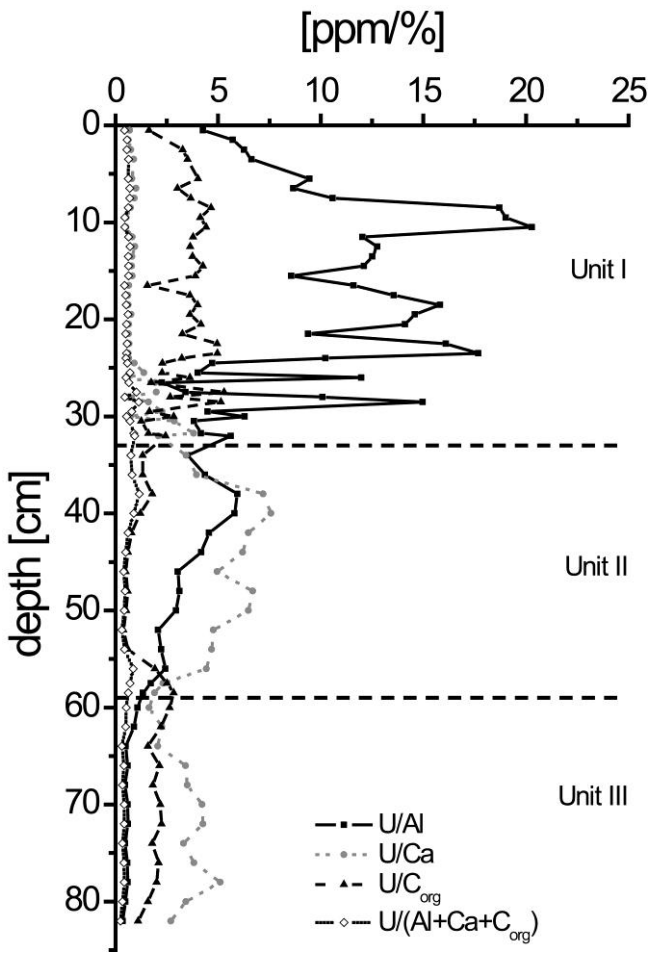


**Abb. 5-5** Depth profile of normalizations for different sediment components of core GeoB 7604. Dashed horizontal lines represent the Unit boundaries.

### 5.4. Discussion

The association of U with OM in natural marine systems is a long known fact (ANDERSON, 1982; BARNES and COCHRAN, 1990; MCMANUS et al., 2005; ZHENG et al., 2002a and references therein). But also the ability of U to couple to Ca carbonate is a topic that should be discussed (KELLY et al., 2003; KELLY et al., 2006; RUSSELL et al., 1994; STURCHIO et al., 1998; TATSUMOTO and GOLDBERG, 1959).

ANDERSON (1982) was one of the first authors discussing the association of U with $C_{org}$ or $CaCO_3$. He could show, that U contents are primarily correlated with $C_{org}$ in pelagic sediments of the Atlantic and Pacific Ocean using samples from sites STIE P (Pacific Ocean), and E (Atlantic Ocean). In this contribution U, Corg, and $CaCO_3$ data were for the first time published for a whole set of samples. Therefore, these data were taken to illustrate the U-$C_{org}$-$C_{carb}$ association from a different perspective.

Adjusted determination coefficients of the U and $C_{org}$ relation were calculated by taking Anderson's data resulting in $\overline{R^2}$ values of 0.27, 0.55, and 0.57 for sites STIE, E, and P, respectively. The overall adjusted determination coefficient for U and organic matter is $\overline{R^2}$ = 0.50. Under closer examination these $\overline{R^2}$ values show only more or less moderate correlations. In the same work ANDERSON (1982) also published a scatter plot of U versus $CaCO_3$. The overall weak correlation of these data serves him as additional evidence for his hypothesis. But when taking a closer look at the data and separating the single data sets of each sampling location, the adjusted determination coefficient of $\overline{R^2}$ = 0.87 for site E can be used as evidencing contrary. It has also to be mentioned that the sites STIE and P show only very weak correlations ($\overline{R^2}$ = -0.19 and -0.11, respectively) and hence, support the hypothesis of the association of U with $C_{org}$ in pelagic sediments of the Atlantic and Pacific Ocean. However, site STIE has low $CaCO_3$ (between 20 and 40 %), while the $C_{org}$ content is exceeding 15 % and on the contrary site E contains more than 60 % $CaCO_3$ and almost the same $C_{org}$ content as site STIE. These data may indicate a connection of U to more than one (main) component of the sediment matrix. These observations could be the first hint to an association of U not only with $C_{org}$ but also with $C_{carb}$.

Other authors in support of the close U-$C_{org}$ association are MO et al. (1973), who found a direct proportionality in anoxic sediments of the Pettaquamscutt river estuary and marine sediments of the Atlantic and Pacific Oceans. But they had to admit, that samples from the Gulf of Mexico with high carbonate content have higher U concentration than samples with low carbonate content from the Altantic/Pacific Ocean. This observation matches the results above. Further the suggestion was made, that not only the organic-rich anoxic marine areas may be regarded as sinks for U, but that carbonate-rich sediments have to be taken into account to balance the worlds riverine U input (MO et al., 1973).

The above-mentioned observations from Atlantic and Pacific pelagic sediments regarding the behavior of U may be supported by samples from the Black Sea. The Holocene Black Sea sediment samples of this work show a strong correlation of U with $C_{org}$ in Units I and II (which are enriched in organic matter). But at the same time a correlation of U with $CaCO_3$ in Unit I, but not in Unit II (Abb. 5-2 and Abb. 5-3) seems evident. For Unit II samples our results match the findings of CAGATAY et al. (1990), who also found high U concentrations in sediments with high $C_{org}$ content and low

sedimentation rates, and hence low dilution by calcareous material. They calculated that in these sediments (mainly Unit II) 25-75 % of the total U is associated with OM with a correlation of r = 0.8. However, extraction experiments show no direct correlation of the organic U fraction with $C_{org}$ (CAGATAY et al., 1990). Further, the results differ for Unit I sediments, where CAGATAY et al. (1990) detected low U concentrations, which correlate also with $C_{org}$ but not with the carbonate content. Paradoxically they found also a good correlation of U and Sr in Unit I samples, which fits our results of the cluster analysis. RONA and JOENSU (1974), on the other hand, found higher U contents in Unit I compared to Unit II in an western-eastern transect of the central Black Sea.

In addition to the above mentioned correlations, Abb. 5-5, for example, shows some variability in the vertical distribution of U in the geological record of the samples of this work. The normalization of U with a specific carrier element results in ratios showing the proportion of association of U with the sediment component. For example, U/Al ratios demonstrate the significant enrichment in U above the terrigenous-detrital background in Units I and II. When U is associated with a specific carrier phase, like carbonate or $C_{org}$, the respective U/Ca or U/$C_{org}$ ratios should be rather constant and low. This indeed seems to be true (Abb. 5-5). These different U patterns may result from the variable $CaCO_3$ content in the different lithological units. Unit I samples have a twentyfold higher $CaCO_3$ concentration compared to Unit II, which is dominated by $C_{org}$. This carbonate enrichment in the late Holocene sediment layers combined with the results of the cluster analysis (Abb. 5-4) may not indicate a stochastic correlation of U with $CaCO_3$, but rather a causal coherence. Such association may provide an alternative pathway to enrich U in marine anoxic sediments besides organometallic complexation of U.

According to our observations and the results of the data analysis, we suggest the following mechanism of U deposition in the two Units: In Unit II, which represents the brackish transition stadium of the Holocene Black Sea, where oxic and limnic conditions changed to anoxic/euxinic and marine conditions, haptophytes, especially coccolithophorida (HAY et al., 1991) could not thrive. Under such conditions $U^{VI}$ (present as $U^{VI}O_2(CO_3)_3^{4-}$) may diffuse into the euxinic sediment, where it gets reduced to $U^{IV}$ and deposited either as $U^{IV}O_2$ or $U^{IV}$ organometallic complex (ALGEO and MAYNARD, 2004; KLINKHAMMER and PALMER, 1991; ZHENG et al., 2002a; ZHENG et al., 2002b). The reduction mechanism requires reaction surfaces for catalyzing electron

transport (ANDERSON, 1987). Bacteria, organic macromolecules, or minerals could provide such surfaces to enhance the reduction process (ANDERSON et al., 1989; BARGAR et al., 2013; KLINKHAMMER and PALMER, 1991). In Unit II sediments the main pathway of U deposition seems to be organometallic complexation after reduction due to low Eh conditions caused by the enrichment of $C_{org}$ and the presence of sulfide in the pore water. This seems to be the favored reduction and deposition mechanism for most anoxic or $C_{org}$-rich sediments (ANDERSON, 1987; CAGATAY et al., 1990 and references therein). Unit II sediments are more textbook-like examples for the U-$C_{org}$ association. Because of the low carbonate content in Unit II, the major component besides clay and siliclastic material is organic matter. Therefore, it is not surprising that only $C_{org}$ shows a correlation to U, while $C_{carb}$ and Ca do not (Abb. 5-3). Also the cluster analysis indicates no association between U and the $CaCO_3$ cluster in Unit II (Abb. 5-4).

Unit I sediments were deposited under marine and euxinic conditions dominated by coccolith ooze, which mainly consists of *Emiliania huxleyi* carbonate remains. The results of adjusted determination coefficients and cluster analysis of our samples indicate an association of U with $CaCO_3$ and to a lesser extent with $C_{org}$ in Unit I sediments (Abb. 5-2 and Abb. 5-4). This correlation may imply the involvement of carbonate into the U deposition pathway, which may take place at two instances during the transfer of U from the water column to the sediment: 1) The direct incorporation of U into biogenic calcareous matter, mainly coccoliths, during primary production in the surface waters (DEGENS et al., 1977). In this process the $U^{VI}O_2^{2+}$ ion replaces one $Ca^{2+}$ and/or two or more $CO_3^{2-}$ ions in the mineral structure of calcite, controlled by pH/Eh changes between seawater and cytoplasm (KELLY et al., 2003; KELLY et al., 2006; RUSSELL et al., 1994). Or 2) the exchange of one $U^{4+}$ for three $Ca^{2+}$ (and supposedly two $Na^{+}$) after the deposition of calcite under reducing conditions (STURCHIO et al., 1998).

For Unit I sediments all mentioned reduction mechanisms (the two $CaCO_3$ associated ones and the $C_{org}$ associated one) may be responsible for the U enrichment. Referring to the laminated structure of Unit I sediments, which consist of alternating white, calcareous and dark, $C_{org}$-rich layers, a seasonal deposition of calcareous layer seems obvious. As seen at the $\overline{R^2}$ values of Unit I both major sediment components ($CaCO_3$ and $C_{org}$) are associated with U (Abb. 5-2). The most likely explanation may be that U forms complexes with $C_{org}$ during deposition of the dark layers, while it is incorporated

into $CaCO_3$ during formation and precipitation of coccoliths. But also an association of U with the $C_{org}$ of the haptophytes, which provide the biogenic CaCO3 matrix may be a possible explanation for the high $\overline{R^2}$ values of Unit I. Degens et al. (1977) already proposed a fixation of U via uronic acids and polysaccharide sulfate within the haptophytes. An argument against the latter possibility could be seen in the anticorrelation of $C_{carb}$ with $C_{org}$ in Unit I (Abb. 5-6). This may indicate an additional origin of the $C_{org}$ besides marine primary production, presumably terrestrial input. A similar observation was made for coral skeletons, which contain the same amount of U independent from their $C_{org}$ content (SWART and HUBBARD, 1982).

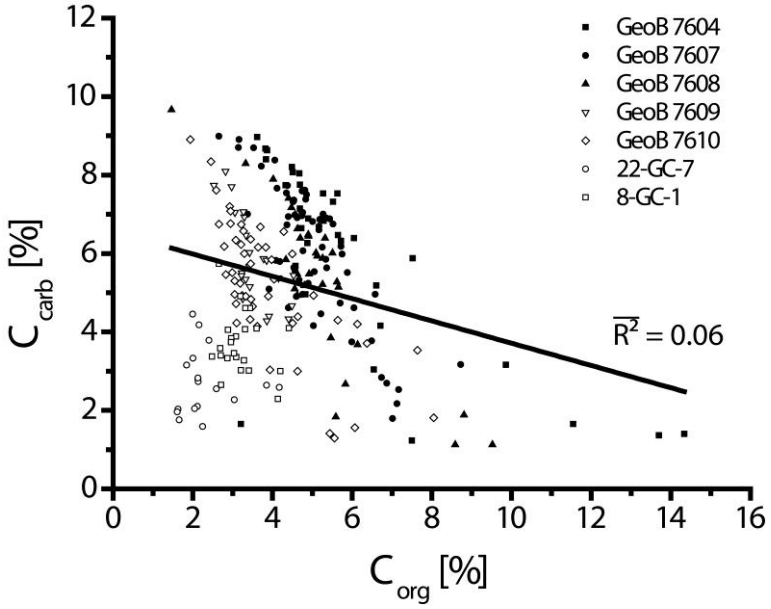


**Abb. 5-6** $C_{carb}$ versus $C_{org}$ for Unit I samples.
Solid line represents the adjusted coefficient of determination ($\overline{R^2}$ ).

To summarize, both carbonate and $C_{org}$, as the major components of the Unit I sediments, are possibly associated with U. Taking the observation from Unit II into account the above stated results indicate, that the U deposition depends on the dominating sediment components. But it should also be mentioned that this finding, as well as those from previous works are based on correlations. These may not always be indicating generic association, but rather serve as an indicator that the variables of a system may be controlled by the same external factors (CAGATAY et al., 1990).

The Black Sea is often used as modern analogue to widespread Cretaceous oceanic anoxic events (OAEs) to understand the deposition and diagenesis of these thick black

shale layers. Here, we will compare the recent Black Sea sapropels with black shale samples from ODP Leg 207 Site 1260 deposited during the Cenomanian/Turonian boundary event (CTBE; OAE 2) at the Demerara Rise (BUNTE, 2009; HETZEL et al., 2009; HETZEL et al., 2006). These ancient sediments are characterized as well by changes in carbonate and $C_{org}$ content. The $\overline{R^2}$ values of these OAE sediments show on the one hand a high correlation of U with Ca (0.76) and $C_{carb}$ (0.76) in sediment layers with $CaCO_3$ as dominating matrix component and on the other hand a moderate correlation with $C_{org}$ (0.56) in layers with low carbonate concentration but high $C_{org}$ content. This again points to an U-carbonate association during deposition of ancient black shales under reducing conditions, which is comparable with our results from Black Sea's Unit I.

### 5.5. Conclusions

In this work we have shown an association of U with Ca carbonate besides organic matter on basis of inorganic geochemical analysis and statistical data processing. The assumption of a exclusive U-$C_{org}$ correlation, hypothesized by several authors, was called into question, based on inconsistencies in sediment layers with high carbonate contents. Furthermore Holocene Black Sea sediments show a correlation of U with carbonate and $C_{org}$ in marine and euxinic Unit I samples, by means of adjusted coefficients of determination and hierarchical cluster analysis. Samples from the brackish and euxinic Unit II, which is depleted in carbonate, only show a correlation of U with $C_{org}$ and not with $C_{carb}$. This behavior of U in the presence of carbonate-rich anoxic sediments was also recognized in black shale layers of OAE 2 from Demerara Rise.

These observations may indicate that the behavior of U depends on the main components of the sediment matrix and show a possible association of U with carbonate under natural reducing conditions.

*Acknowledgements.*

We are grateful to the crew of R/V *Meteor* and to the Deutsche Forschungsgemeinschaft (DFG) for funding this project (IODP SPP Br 775/26-1). We are indebted to E. Gründken, C. Lehners and M. Schulz for analytical assistance. We thank P. Monien for the helpful discussions.

# 6. Manganese-rich brown layers in Arctic Ocean sediments: Composition, formation mechanisms, and diagenetic overprint

Authors:

Christian März, Mikrobiogeochemie, Institut für Chemie und Biologie des Meeres (ICBM), Carl von Ossietzky Universität, 26111 Oldenburg

Alexandra Stratmann, Mikrobiogeochemie, Institut für Chemie und Biologie des Meeres (ICBM), Carl von Ossietzky Universität, 26111 Oldenburg

Jens Matthiessen, Meeresgeologie und Paläontologie, Alfred Wegener Institut für Polar und Meeresforschung (AWI), 27568 Bremerhaven

Ann-Katrin Meinhardt, Mikrobiogeochemie, Institut für Chemie und Biologie des Meeres (ICBM), Carl von Ossietzky Universität, 26111 Oldenburg

Sebastian Eckert, Mikrobiogeochemie, Institut für Chemie und Biologie des Meeres (ICBM), Carl von Ossietzky Universität, 26111 Oldenburg

Bernhard Schnetger, Mikrobiogeochemie, Institut für Chemie und Biologie des Meeres (ICBM), Carl von Ossietzky Universität, 26111 Oldenburg

Christoph Vogt, Kristallographie/ZEKAM, Fachbereich Geowissenschaften, Universität Bremen, 28334 Bremen

Rüdiger Stein, Meeresgeologie und Paläontologie, Alfred Wegener Institut für Polar und Meeresforschung (AWI), 27568 Bremerhaven

Hans-Jürgen Brumsack, Mikrobiogeochemie, Institut für Chemie und Biologie des Meeres (ICBM), Carl von Ossietzky Universität, 26111 Oldenburg

## Abstract

We present inorganic geochemical analyses of pore waters and sediments of two Late Quaternary sediment cores from the western Arctic Ocean (southern Mendeleev Ridge, RV Polarstern Expedition ARK-XXIII/3), focusing on the composition and origin of distinct, brown-colored, Mn-rich sediment layers. Carbonate enrichments occur in association with these layers as peaks in Ca/Al, Mg/Al, Sr/Al and Sr/Mg, suggesting enhanced input of both ice-rafted and biogenic carbonate. For the first time, we show that the Mn-rich layers are also consistently enriched in the scavenged trace metals Co, Cu, Mo and Ni. Distinct bioturbation patterns, specifically well-defined brown burrows into the underlying sediments, suggest these metal enrichments formed close to the sediment–water interface. The geochemical signature of these metal- and carbonate-rich layers most probably documents formation under warmer climate conditions with an intensified continental hydrological cycle and only seasonal sea ice cover. Both rivers and sea ice delivered trace metals to the Arctic Ocean, while enhanced seasonal productivity exported reactive organic matter to the sea floor. The coeval deposition of organic matter, Mn (oxyhydr)oxides and trace metals triggered intense diagenetic Mn cycling at the sediment–water interface. These processes resulted in the formation of Mn and trace metal enrichments, and the degradation of labile organic matter. With the onset of cooler conditions, reduced riverine runoff and/or a solid sea ice cover terminated the input of riverine trace metal and fresh organic matter, resulting in deposition of grayish-yellowish, metal-poor sediments. Oxygen depletion of Arctic bottom waters under these cooler conditions is not supported by our data, and did not cause the sedimentary Mn distribution. While the original composition and texture of the brown layers resulted from specific climatic conditions and corresponding diagenetic processes, pore water data show that diagenetic Mn redistribution is still affecting the organic-poor deeper sediments. Given persistent steady state conditions, purely authigenic Mn-rich brown layers may form, while others may be partly or completely dissolved. The degree of diagenetic Mn redistribution largely depends on the depositional environment, the Mn and organic matter availability, and apparently affected the Co/Mo ratios of Mn-rich layers. Thus, brown Arctic layers are not necessarily synchronous features, and should not be correlated across the Arctic Ocean without additional age control.

# 7. Zusammenfassung

Das Schwarze Meer mit seiner komplexen Geobiochemie eignet sich für eine Vielzahl von wissenschaftlichen Fragestellungen, deren Antworten sich auch auf andere Gebiete der Erde (z.B. Norwegische Fjorde, Cariaco Graben, etc.) und auch in andere geologische Epochen (z.B. Schwarzschiefer des Mesozoikums und Paläozoikums) extrapolieren lassen.

In dieser Arbeit wurde der Frage nachgegangen in wie weit sich die jetzige Warmzeit, das Holozän, von der vorherigen Warmzeit, dem Eem, unterscheidet. Um eine Antwort auf diese Frage zu bekommen, wurden zunächst die Sedimentschichten untersucht, die während des Holozäns im Schwarzen Meer abgelagert wurden. Diese Sedimente sind in der Literatur gut bekannt und bilden die Datengrundlage für sämtliche bisherigen Theorien über die Entwicklung eines stratifizierten Meerbeckens mit oxischem Oberflächenwasser und euxinischem Tiefenwasser. Aus diesem Grund wurden in dieser Arbeit zuerst die Holozänen Sapropele untersucht und mit der Literatur verglichen um auf der Basis der Ergebnisse die Sedimente des Eem-Sapropels zu interpretieren.

Sämtliche Sedimentproben wurden auf Haupt- und Spurenelemente untersucht. An ausgewählten Proben wurde zudem noch der Gehalt an Selten Erden Elementen und organischen Biomarkern (Isorenieratanderivate) bestimmt. Des Weiteren, als besonderer Punkt in den geochemischen Analysen, wurden an ausgewählte Proben das Verhältnis von Fe-, Mo- und U-Isotopen bestimmt um eine Aussage über die Fraktionierung gegenüber den jeweiligen Elementquellen machen zu können.

Die hier untersuchten acht holozänen Sedimentkerne weisen die in der Literatur beschriebene Abfolge von lithologischen Units auf, welche den Wandel von Eiszeit zu Warmzeit dokumentieren. Aufgrund ihrer weiten Verteilung über das Schwarze Meer, der guten Erhaltung, der hochauflösenden Probenahme und der geochemischen Vergleichbarkeit können diese Kerne, zusammengefasst zu einem künstlichen Sedimentkern, diesen Wandel nicht nur lokal, sondern regional für das gesamte Schwarze Meer beschreiben. Die prägnanten Signale in diesem *composite geochemical core log* zeigen ubiquitäre und synchrone Prozesse an, da lokale Variationen aufgrund von variablen Sedimentationsraten durch eine Normierung auf eine Referenztiefe aufgehoben werden.

Ein wichtiger Punkt in dieser Arbeit, welcher erst die Idee zur Nutzung eines künstlichen Kerns lieferte, ist das Auftreten von zwei Eisenanreicherungen in allen untersuchten Sapropelen. Diese beiden Eisenanreicherungen wurden an der Grenze von Unit II und III, sowie in der zentralen Unit II gefunden. Diese Eisenanreicherungen sind durch die Mobilisierung von Fe aus den Schelfsedimenten bzw. den Beckensedimenten zu erklären, welche während der letzten Eiszeit abgelagert wurden. Die Eisenanreicherung an der Unit II/III Grenze repräsentiert das erste Auftreten von euxinischem Bodenwasser im Becken des Schwarzen Meeres. Die zweite Eisenanreicherung signalisiert einen aktiven Fe-Shuttle von der Schelfkante ins Innere des Beckens. Dieser Fe-Transport wird ermöglicht durch die suboxische Chemokline, die das mobilisierte Fe durch einen sich wiederholenden Reduktions-/Oxidationszyklus lateral transportiert. Anhand des Tiefenprofils des Fe/Al-Verhältnisses, kombiniert mit der Fe-Isotopenfraktionierung, lässt sich somit der Anstieg und das Absinken der Chemokline rekonstruieren. Gekoppelt mit dem Molybdäninventar des Sapropels konnte der Ablauf des Wechsels von limnischen zu marinen Bedingungen im Schwarzen Meer gezeigt und Paläoeinflussraten bestimmt werden. Zudem konnte gezeigt werden, wie wichtig die Rolle der Chemokline in diesem Zusammenhang ist. Schwankungen im Einstrom-/Ausstromverhältnis von Meerwasser ins Schwarze Meer haben eine Positionsänderung der Chemokline zur Folge, welche wiederum den Eisenkreislauf und die daran gebundenen geobiochemischen Prozesse beeinflusst. Wie in Kap. 3 vorgestellt, hat die Chemokline vor ca. 7.600 Jahren das Sediment verlassen und ist von da an in der Wassersäule angestiegen. Vor ca. 5.300 Jahren hat die Chemokline den Schelfbereich des Beckens erreicht und die Fe-Mobilisierung initiiert. Nach einem Absinken der Chemokline unterhalb des Schelfs wurden vor ca. 2.700 Jahren die heutigen geochemischen Bedingungen in der Wassersäule etabliert.

Diese Erkenntnisse über die Entwicklung des Holozänen Schwarzen Meeres wurden in Kap. 4 auf die Sedimente übertragen, die während der Eem-Warmzeit im Schwarzen Meer abgelagert wurden. Die hier vorgestellten Daten des Eem-Sapropels bilden die Grundlage für die erste hochauflösende geochemische Charakterisierung dieser Sedimentschicht seit der ersten Erwähnung durch CALVERT und BATCHELOR (1978). In dem in Kap. 4 vorgestellten Sapropel zeigen die Fe/Al-, $\delta^{56}$Fe- und Mo/Al-Tiefenprofile einen graduellen Anstieg der Chemokline an, ohne Regression wie während des Holozäns. Diese Erkenntnis wurde durch Isorenieratanderivate und $\delta^{13}$C-Messungen

verifiziert. Die Parameter-Palette wurde zudem noch um die Isotopenverhältnisse von Mo und U erweitert, die eine genauere Klassifizierung des biogeochemischen Regimes unter dem die Sapropele abgelagert wurden, möglich machte. Anhand einer Kartierung mittels $\delta^{97}$Mo und $\delta^{235}$U lässt sich der Verlauf der Redoxbedingungen von oxisch über suboxisch bis hin zu anoxisch/euxinisch verfolgen. Dabei konnte eine stärkere euxinische Ausprägung während des Holozäns gegenüber dem Eem beobachtet werden.

Die Nutzung eines *composite geochemical core log* birgt viele Vorteile bei einer Multiproxy-Analyse von verschiedenen Kernen eines Systems, vorausgesetzt die regionalen Unterschiede unterliegen keiner starken Schwankung. Weiterführend ist die Messung von zusätzlichen Sedimentkernen, die mehrere Units umfassen, aus verschiedenen Lokationen und Wassertiefen ratsam um die Standardabweichung innerhalb des Datensatzes zu reduzieren und ein exakteres Abbild des Systems "Schwarzes Meer" zu bekommen. Anknüpfende Untersuchungen wären unter anderem die Erstellung eines künstlichen Sedimentkernes für Porenwasserdaten um die Prozesse der einzelnen Proxy sowohl für die feste, also auch für die flüssige Phase in einem System darzustellen. Kombiniert mit δ-Werten einzelner Elemente, die über stabile Isotope verfügen, würde dies zu einem vollständigen Abbild der geochemischen Prozesse dieser Proxies in einem System über alle vier Dimensionen führen. Vereint in einer weiteren Multiproxy-Analyse würde ein geochemisches System (fast) komplett dargestellt werden können.

Diese Art der Datenpräsentation ist nicht nur für eine geochemische Charakterisierung in anoxischen Becken von Vorteil, sondern auch für Bilanzierungen über die Zeit, die Veränderung eines Systems im geobiochemischen Kontext und, bei der Gegenüberstellung von verschiedenen Systemen, zur Grundlagenforschung von einzelnen Prozessen/Proxy geeignet.

Einige wichtigen Fragen, die sich Wissenschaftler zu dem Thema "Anoxia und Schwarzes Meer" stellen, konnten auch mit dem hier präsentierten Datensatz von über 1.400 Proben und 56 gemessen Parametern nicht vollständig beantwortet werden. Ein Beispiel ist die Frage nach den physikalischen Ausmaßen der Chemo-/Pyknokline (Stärke, Form, Position) über die Zeit, ein weiteres Beispiel ist der exakte Zeitpunkt und Ort des Wechsels von oxischen zu anoxischen Bedingungen im Schwarzen Meer. Auch die Frage welcher Effekt bei der TOC-Anreicherung überwiegt, Primärproduktion oder

Erhaltung, ist noch nicht eindeutig geklärt. Genauso wie die Nutzbarkeit von einigen Paläoumweltproxies, die unter rein oxischen oder rein anoxischen Bedingungen funktionieren, aber in den Übergängen Fragen aufwerfen, weiter untersucht werden muss. Um solche geochemischen Prozesse die zur An- bzw. Abreicherung von bestimmten Proxies führen genauer zu untersuchen, würde sich das geologische Archiv des Schwarzen Meeres aufgrund seiner Wechsel von limnisch-oxischen zu marinen-euxinischen Verhältnissen, mit all seinen Zwischenphasen, bestens eignen.

# 8. Literaturverzeichnis

Aksu, A. E., Mudie, P. J., Rochon, A., Kaminski, M. A., Abrajano, T., and Yasar, D., 2002. Persistent holocene outflow from the Black Sea to the eastern Mediterranean contradicts Noah's flood hypothesis. *GSA Today* **12**, 3-10.

Algeo, T. J., 2004. Can marine anoxic events draw down the trace element inventory of seawater? *Geology* **32**, 1057-1060.

Algeo, T. J. and Lyons, T. W., 2006. Mo-total organic carbon covariation in modern anoxic marine environments: Implications for analysis of paleoredox and paleohydrographic conditions. *Paleoceanography* **21**, 1-23.

Algeo, T. J., Lyons, T. W., Blakey, R. C., and Over, D. J., 2007. Hydrographic conditions of the Devono-Carboniferous North American Seaway inferred from sedimentary Mo-TOC relationships. *Palaeogeogr. Palaeocl.* **256**, 204-230.

Algeo, T. J. and Maynard, J. B., 2004. Trace-element behavior and redox facies in core shales of Upper Pennsylvanian Kansas-type cyclothems. *Chem. Geol.* **206**, 289-318.

Allen, J. R. M. and Huntley, B., 2009. Last Interglacial palaeovegetation, palaeoenvironments and chronology: a new record from Lago Grande di Monticchio, southern Italy. *Quaternary Sci. Rev.* **28**, 1521-1538.

Anderson, R. F., 1982. Concentration, Vertical Flux, and Remineralization of Particulate Uranium in Sea-Water. *Geochim. Cosmochim. Acta* **46**, 1293-1299.

Anderson, R. F., 1987. Redox behavior of uranium in an anoxic marine basin. *Uranium* **3**, 145-164.

Anderson, R. F., Fleisher, M. Q., and Lehuray, A. P., 1989. Concentration, Oxidation-State, and Particulate Flux of Uranium in the Black-Sea. *Geochim. Cosmochim. Acta* **53**, 2215-2224.

Anderson, T. F. and Raiswell, R., 2004. Sources and mechanisms for the enrichment of highly reactive iron in euxinic Black Sea sediments. *Am. J. Sci.* **304**, 203-233.

Arnold, G. L., Anbar, A. D., Barling, J., and Lyons, T. W., 2004a. Molybdenum isotope evidence for widespread anoxia in mid-proterozoic oceans. *Science* **304**, 87-90.

Arnold, G. L., Lyons, T. W., Gordon, G. W., and Anbar, A. D., 2012. Extreme change in sulfide concentrations in the Black Sea during the Little Ice Age reconstructed using molybdenum isotopes. *Geology* **40**, 595-598.

Arnold, G. L., Weyer, S., and Anbar, A. D., 2004b. Fe isotope variations in natural materials measured using high mass resolution multiple collector ICPMS. *Anal. Chem.* **76**, 322-327.

Arthur, M. A. and Dean, W. E., 1998. Organic-matter production and preservation and evolution of anoxia in the Holocene Black Sea. *Paleoceanography* **13**, 395-411.

Arthur, M. A., Dean, W. E., Neff, E. D., Hay, B. J., King, J., and Jones, G., 1994. Varve Calibrated Records of Carbonate and Organic-Carbon Accumulation over the Last 2000 Years in the Black-Sea. *Glob. Biogeochem. Cycle* **8**, 195-217.

Arthur, M. A. and Sageman, B. B., 2005. Sea-level control on source-rock development: Perspectives from the Holocene Black Sea, the mid-Cretaceous Western Interior Basin of North America, and the Late Devonian Appalachian Basin. In: Harris, N. B. (Ed.), *Deposition of organic-carbon-rich sediments: Models, mechanisms, and consequences*. SEPM (Society for Sedimentary Geology) Special Publication.

Babu, C. P., Brumsack, H. J., and Schnetger, B., 1999. Distribution of organic carbon in surface sediments along the eastern Arabian Sea: a revisit. *Mar. Geol.* **162**, 91-103.

Badertscher, S., Fleitmann, D., Cheng, H., Edwards, R. L., Gokturk, O. M., Zumbuhl, A., Leuenberger, M., and Tuysuz, O., 2011. Pleistocene water intrusions from the Mediterranean and Caspian seas into the Black Sea. *Nat. Geosci.* **4**, 236-239.

Bahr, A., Arz, H. W., Lamy, F., and Wefer, G., 2006. Late glacial to Holocene paleoenvironmental evolution of the Black Sea, reconstructed with stable oxygen isotope records obtained on ostracod shells. *Earth Planet. Sci. Lett.* **241**, 863-875.

Bahr, A., Lamy, F., Arz, H., Kuhlmann, H., and Wefer, G., 2005. Late glacial to Holocene climate and sedimentation history in the NW Black Sea. *Mar. Geol.* **214**, 309-322.

Bahr, A., Lamy, F., Arz, H., Major, C., Kwiecien, O., and Wefer, G., 2008. Abrupt changes of temperature and water chemistry in the late Pleistocene and early Holocene Black sea. *Geochem. Geophy. Geosys.* **9**, 1-16.

Bargar, J. R., Williams, K. H., Campbell, K. M., Long, P. E., Stubbs, J. E., Suvorova, E. I., Lezama-Pacheco, J. S., Alessi, D. S., Stylo, M., Webb, S. M., Davis, J. A., Giammar, D. E., Blue, L. Y., and Bernier-Latmani, R., 2013. Uranium redox transition pathways in acetate-amended sediments. *PNAS* **110**, 4506-4511.

Barling, J., Arnold, G. L., and Anbar, A. D., 2001. Natural mass-dependent variations in the isotopic composition of molybdenum. *Earth Planet. Sci. Lett.* **193**, 447-457.

Barnes, C. E. and Cochran, J. K., 1990. Uranium removal in oceanic sediments and the oceanic U balance. *Earth Planet. Sci. Lett.* **97**, 94-101.

Barnes, C. E. and Cochran, J. K., 1991. Geochemistry of Uranium in Black-Sea Sediments. *Deep-Sea Res. Pt. A* **38**, S1237-S1254.

Bau, M., Moller, P., and Dulski, P., 1997. Yttrium and lanthanides in eastern Mediterranean seawater and their fractionation during redox-cycling. *Mar. Chem.* **56**, 123-131.

Beard, B. L., Johnson, C. M., Skulan, J. L., Nealson, K. H., Cox, L., and Sun, H., 2003. Application of Fe isotopes to tracing the geochemical and biological cycling of Fe. *Chem. Geol.* **195**, 87-117.

Bertine, K. K., 1972. The deposition of Molybdenum in anoxic waters. *Mar. Chem.* **1**, 43-53.

Bigeleisen, J., 1996. Nuclear Size and Shape Effects in Chemical Reactions. Isotope Chemistry of the Heavy Elements. *J. Am. Chem. Soc.* **118**, 3676-3680.

Bigeleisen, J. and Mayer, M. G., 1947. Calculation of Equilibrium Constants for Isotopic Exchange Reactions. *J. Chem. Phys.* **15**, 261-267.

Bosch, H. J., Sinninghé Damsté, J. S., and de Leeuw, J. W., 1998. Molecular palaeontology of Eastern Mediterranean sapropels: Evidence for photo zone euxinia. *Proc. Ocean Drill. Program. Sci. Results* **160**, 285-295.

Brückner, H., Kelterbaum, D., Marunchak, O., Porotov, A., and Vött, A., 2010. The Holocene sea level story since 7500 BP - lessons from the Eastern Mediterranean, the Black and the Azov Seas. *Quatern. Int.* **225**, 160-179.

Brumsack, H.-J., 1989a. Geochemistry of recent TOC-rich sediments from the Gulf of California and the Black Sea. *Geol. Rundsch.* **78**, 851-882.

Brumsack, H.-J., 1989b. Geochemistry of recent TOC-rich sediments from the Gulf of California and the Black Sea. *Geol. Rundsch.* **78**, 851-882.

Brumsack, H.-J., 2006a. The trace metal content of recent organic carbon-rich sediments: Implications for Cretaceous black shale formation. *Palaeogeogr. Palaeocl.* **232**, 344-361.

Brumsack, H. J., 2006b. The trace metal content of recent organic carbon-rich sediments: Implications for Cretaceous black shale formation. *Palaeogeogr. Palaeocl.* **232**, 344-361.

Brumsack, H. J. and Gieskes, J. M., 1983. Interstitial Water Trace-Metal Chemistry of Laminated Sediments from the Gulf of California, Mexico. *Mar. Chem.* **14**, 89-106.

Bunte, A., 2009. Geochemical signatures of black shales deposited during Oceanic Anoxic Event 2 (Cenomanian/Turonian) in the tropical Atlantic (Demerara Rise, ODP Leg 207) and in northern Germany (Wunstorf). PhD thesis, Carl von Ossietzky Universität Oldenburg.

Cagatay, M. N., Gedik, A., and Saltoglu, T., 1990. Geochemistry of uranium in the late Pleistocene-Holocene sediments from the southern part of the Black-Sea basin. *Chem. Geol.* **82**, 129-144.

Calvert, S. E., 1990. Geochemistry and Origin of the Holocene Sapropel in the Black Sea. In: V., I., Kempe, S., Michaels, W., and Spitzy, A. Eds.), *Facets of modern Biogeochemistry*. Springer, Berlin.

Calvert, S. E. and Batchelor, C. H., 1978. Major and minor element geochemistry of sediments from Hole 379A, Leg 42B, Deep Sea Drilling Project. In: Usher, J. L. and Supko, P. Eds.), *Initial Rep. Deep-Sea*. U.S. Government Printing office, Washington D.C.

Calvert, S. E. and Karlin, R. E., 1998. Organic carbon accumulation in the Holocene sapropel of the Black Sea. *Geology* **26**, 107-110.

Calvert, S. E. and Pedersen, T. F., 1993. Geochemistry of Recent Oxic and Anoxic Marine-Sediments - Implications for the Geological Record. *Mar. Geol.* **113**, 67-88.

Calvert, S. E., Vogel, J. S., and Southon, J. R., 1987. Carbon accumulation rates and the origin of the Holocene sapropel in the Black Sea. *Geology* **15**, 918-921.

Cane, T., Rohling, E. J., Kemp, A. E. S., Cooke, S., and Pearce, R. B., 2002. High-resolution stratigraphic framework for Mediterranean sapropel S5: defining temporal relationships between records of Eemian climate variability. *Palaeogeogr. Palaeocl.* **183**, 87-101.

Canfield, D. E., Lyons, T. W., and Raiswell, R., 1996. A model for iron deposition to euxinic Black Sea sediments. *Am. J. Sci.* **296**, 818-834.

Chaillou, G., Anschutz, P., Lavaux, G., and Schäfer, J., 2002. The distribution of Mo, U and Cd in relation to major redox species in muddy sediments of the Bay of Biscay. *Mar. Chem.* **80**, 41-59.

Colodner, D., Edmond, J., and Boyle, E., 1995. Rhenium in the Black Sea: comparison with molybdenum and uranium. *Earth Planet. Sci. Lett.* **131**, 1-15.

Colodner, D., Sachs, J., Ravizza, G., Turekian, K., Edmond, J., and Boyle, E., 1993. The Geochemical Cycle of Rhenium - a Reconnaissance. *Earth Planet. Sci. Lett.* **117**, 205-221.

Crusius, J., Calvert, S., Pedersen, T., and Sage, D., 1996. Rhenium and molybdenum enrichments in sediments as indicators of oxic, suboxic and sulfidic conditions of deposition. *Earth Planet. Sci. Lett.* **145**, 65-78.

Crusius, J. and Thomson, J., 2000. Comparative behavior of authigenic Re, U, and Mo during reoxidation and subsequent long-term burial in marine sediments. *Geochim. Cosmochim. Acta* **64**, 2233-2242.

Dahl, T. W., Anbar, A. D., Gordon, G. W., Rosing, M. T., Frei, R., and Canfield, D. E., 2010. The behavior of molybdenum and its isotopes across the chemocline and in the sediments of sulfidic Lake Cadagno, Switzerland. *Geochim. Cosmochim. Ac.* **74**, 144-163.

Degens, E. T., Khoo, F., and Michaelis, W., 1977. Uranium Anomaly in Black Sea Sediments. *Nature* **269**, 566-569.

Degens, E. T. and Ross, D. A., 1972. Chronology of the Black Sea over the last 25,000 years. *Chem. Geol.* **10**, 1-16.

Degens, E. T. and Ross, D. A., 1974. *The Black Sea - Geology, Chemistry, and Biology*. American Association of Petroleum Geologists, Tulsa, Oklahoma, U.S.A.

Dellwig, O., Leipe, T., Marz, C., Glockzin, M., Pollehne, F., Schnetger, B., Yakushev, E. V., Bottcher, M. E., and Brumsack, H. J., 2010. A new particulate Mn-Fe-P-shuttle at the redoxcline of anoxic basins. *Geochim. Cosmochim. Acta* **74**, 7100-7115.

Deuser, W. G., 1974. Evolution of anoxic conditions in Black Sea during Holocene. In: Degens, E. T. and Ross, D. A. Eds.), *The Black Sea - Geology, Chemistry, and Biology*. Memoirs of the American Association of Petroleum Geologists, Tulsa, U.S.A.

Dymond, J., Suess, E., and Lyle, M., 1992. Barium in deep-sea sediment: A geochemical proxy for paleoproductivity. *Paleoceanography* **7**, 163-181.

Eckert, S., Brumsack, H.-J., Schnetger, B., Fröllje, H., and Severmann, S., 2013. The establishment of euxinic conditions in the Holocene Black Sea. *Geology* **41**, 431-434.

Emeis, K.-C. and Sakamoto, T., 1998. The sapropel theme of Leg 160. *Proc. Ocean Drill. Program. Sci. Results* **160**, 29-36.

Emeis, K. C., Sakamoto, T., Wehausen, R., and Brumsack, H. J., 2000. The sapropel record of the eastern Mediterranean Sea - results of Ocean Drilling Program Leg 160. *Palaeogeogr. Palaeocl.* **158**, 371-395.

Erickson, B. E. and Helz, G. R., 2000. Molybdenum(VI) speciation in sulfidic waters: Stability and lability of thiomolybdates. *Geochim. Cosmochim. Ac.* **64**, 1149-1158.

Field, M. H., Huntley, B., and Muller, H., 1994. Eemian Climate Fluctuations Observed in a European Pollen Record. *Nature* **371**, 779-783.

Froelich, P. N., Klinkhammer, G. P., Bender, M. L., Luedtke, N. A., Heath, G. R., Cullen, D., Dauphin, P., Hammond, D., Hartman, B., and Maynard, V., 1979. Early Oxidation of Organic-Matter in Pelagic Sediments of the Eastern Equatorial Atlantic - Suboxic Diagenesis. *Geochim. Cosmochim. Acta* **43**, 1075-1090.

Fujii, T., Moynier, F., and Albarède, F., 2006. Nuclear field vs. nucleosynthetic effects as cause of isotopic anomalies in the early Solar System. *Earth Planet. Sci. Lett.* **247**, 1-9.

Giosan, L., Filip, F., and Constatinescu, S., 2009. Was the Black Sea catastrophically flooded in the early Holocene? *Quaternary Sci. Rev.* **28**, 1-6.

Hay, B. J., Arthur, M. A., Dean, W. E., Neff, E. D., and Honjo, S., 1991. Sediment deposition in the Late Holocene abyssal Black Sea with climatic and chronological implications. *Deep-Sea Res. Pt. A* **38**, S1221-S1235.

Helz, G. R., Bura-Nakic, E., Mikac, N., and Ciglenecki, I., 2011. New model for molybdenum behavior in euxinic waters. *Chem. Geol.* **284**, 323-332.

Helz, G. R. and Dolor, M. K., 2012. What regulates rhenium deposition in euxinic basins? *Chem. Geol.* **304**, 131-141.

Helz, G. R., Miller, C. V., Charnock, J. M., Mosselmans, J. F. W., Pattrick, R. A. D., Garner, C. D., and Vaughan, D. J., 1996. Mechanism of molybdenum removal from the sea and its concentration in black shales: EXAFS evidence. *Geochim. Cosmochim. Ac.* **60**, 3631-3642.

Henkel, S., Mogollon, J. M., Noethen, K., Franke, C., Bogus, K., Robin, E., Bahr, A., Blumenberg, M., Pape, T., Seifert, R., Marz, C., de Lange, G. J., and Kasten, S., 2012. Diagenetic barium cycling in Black Sea sediments - A case study for anoxic marine environments. *Geochim. Cosmochim. Acta* **88**, 88-105.

Hetzel, A., Böttcher, M. E., Wortmann, U. G., and Brumsack, H., 2009. Paleo-redox conditions during OAE 2 reflected in Demerara Rise sediment geochemistry (ODP Leg 207). *Palaeogeogr. Palaeocl.* **273**, 302-328.

Hetzel, A., Brumsack, H.-J., Schnetger, B., and Böttcher, M., 2006. Inorganic geochemical characterization of lithologic units recovered during ODP Leg 207 (Demerara Rise). *Proc. Ocean Drill. Program. Sci. Results* **207**.

Huang, Y. S., Freeman, K. H., Wilkin, R. T., Arthur, M. A., and Jones, A. D., 2000. Black Sea chemocline oscillations during the Holocene: molecular and isotopic studies of marginal sediments. *Org. Geochem.* **31**, 1525-1531.

Huerta-Diaz, M. A. and Morse, J. W., 1990. A quantitative method for determination of trace metal concentrations in sedimentary pyrite. *Mar. Chem.* **29**, 119-144.

Huerta-Diaz, M. A. and Morse, J. W., 1992. Pyritization of trace metals in anoxic marine sediments. *Geochim. Cosmochim. Acta* **56**, 2681-2702.

Ivanova, E. V., Murdmaa, I. O., Chepalyga, A. L., Cronin, T. M., Pasechnik, I. V., Levchenko, O. V., Howe, S. S., Manushkina, A. V., and Platonova, E. A., 2007. Holocene sea-level oscillations and environmental changes on the Eastern Black Sea shelf. *Palaeogeogr. Palaeocl.* **246**, 228-259.

Jones, G. A. and Gagnon, A. R., 1994. Radiocarbon chronology of Black Sea sediments. *Deep-Sea Res. Pt. I* **41**, 531-557.

Jørgensen, B. B., Böttcher, M. E., Lüschen, H., Neretin, L. N., and Volkov, I. I., 2004. Anaerobic methane oxidation and a deep $H_2S$ sink generate isotopically heavy sulfides in Black Sea sediments. *Geochim. Cosmochim. Ac.* **68**, 2095-2118.

Karabanov, E. B., Propenko, A. A., Williams, D. F., and Khursevich, G. K., 2000. Evidence for mid-Eemian cooling in continental climatic record from Lake Baikal. *J. Paleolimnol.* **23**, 365-371.

Kelly, S. D., Newville, M. G., Cheng, L., Kemner, K. M., Sutton, S. R., Fenter, P., Sturchio, N. C., and Spotl, C., 2003. Uranyl incorporation in natural calcite. *Environ. Sci. Technol.* **37**, 1284-1287.

Kelly, S. D., Rasbury, E. T., Chattopadhyay, S., Kropf, A. J., and Kemner, K. M., 2006. Evidence of a stable uranyl site in ancient organic-rich calcite. *Environ. Sci. Technol.* **40**, 2262-2268.

Kenison Falkner, K., Klinkhammer, G. P., Bowers, T. S., Todd, J. F., Lewis, B. L., Landing, W. M., and Edmond, J. M., 1993. The behavior of barium in anoxic marine waters. *Geochim. Cosmochim. Acta* **57**, 537-554.

Klinkhammer, G. P. and Palmer, M. R., 1991. Uranium in the Oceans: Where it goes and why. *Geochim. Cosmochim. Acta* **55**, 1799-1806.

Konovalov, S., Samodurov, A., Oguz, T., and Ivanov, L., 2004. Parameterization of iron and manganese cycling in the Black Sea suboxic and anoxic environment. *Deep-Sea Res. Pt. I* **51**, 2027-2045.

Koopmans, M. P., Köster, J., van Kaam-Peters, H. M. E., Kenig, F., Schouten, S., Hartgers, W. A., de Leeuw, J. W., and Sinninghé Damsté, J. S., 1996. Diagenetic and catagenetic products of isorenieratene: Molecular indicators for photic zone anoxia. *Geochim. Cosmochim. Ac.* **60**, 4467-4496.

Kopp, R. E., Simons, F. J., Mitrovica, J. X., Maloof, A. C., and Oppenheimer, M., 2009. Probabilistic assessment of sea level during the last interglacial stage. *Nature* **462**, 863-U51.

Kraal, P., Slomp, C. P., and de Lange, G. J., 2010. Sedimentary organic carbon to phosphorus ratios as a redox proxy in Quaternary records from the Mediterranean. *Chem. Geol.* **277**, 167-177.

Lamy, F., Arz, H. W., Bond, G. C., Bahr, A., and Patzold, J., 2006. Multicentennial-scale hydrological changes in the Black Sea and northern Red Sea during the Holocene and the Arctic/North Atlantic oscillation. *Paleoceanography* **21**, 11.

Langmuir, D., 1978. Uranium solution-mineral equilibria at low temperatures with applications to sedimentary ore deposits. *Geochim. Cosmochim. Acta* **42**, 547-569.

Lewis, B. L. and Landing, W. M., 1991. The biogeochemistry of manganese and iron in the Black Sea. *Deep-Sea Res. Pt. A* **38**, S773-S803.

Lyons, T. W., Berner, R. A., and Anderson, R. F., 1993. Evidence for large pre-industrial pertubations of the Black Sea chemocline. *Nature* **365**, 538-540.

Lyons, T. W. and Severmann, S., 2006. A critical look at iron paleoredox proxies: New insights from modern euxinic marine basins. *Geochim. Cosmochim. Ac.* **70**, 5698-5722.

Maechler, M., Rousseeuw, P., Struyf, A., and Hubert, M., 2005. Cluster Analysis Basics and Extensions. CRAN R-Projekt.

Major, C., Ryan, W., Lericolais, G., and Hajdas, I., 2002. Constraints on Black Sea outflow to the Sea of Marmara during the last glacial-interglacial transition. *Mar. Geol.* **190**, 19-34.

Martin, J.-M. and Whitfield, M., 1983. The significance of the river input of chemical elements to the ocean. In: Wong, C. S., Boyle, E., Bruland, K. W., Burton, J. D., and Goldberg, E. D. Eds.), *Trace Metals in Sea Water*. Plenum Press, New York.

März, C., Poulton, S. W., Beckmann, B., Küster, K., Wagner, T., and Kasten, S., 2008. Redox sensitivity of P cycling during marine black shale formation: Dynamics of sulfidic and anoxic, non-sulfidic bottom waters. *Geochim. Cosmochim. Acta* **72**, 3703-3717.

McManus, J., Berelson, W. M., Klinkhammer, G. P., Hammond, D. E., and Holm, C., 2005. Authigenic uranium: Relationship to oxygen penetration depth and organic carbon rain. *Geochim. Cosmochim. Acta* **69**, 95-108.

McManus, J. F., Bond, G. C., Broecker, W. S., Johnsen, S., Labeyrie, L., and Higgins, S., 1994. High-Resolution Climate Records from the North-Atlantic during the Last Interglacial. *Nature* **371**, 326-329.

Melki, T., Kallel, N., and Fontugne, M., 2010. The nature of transitions from dry to wet condition during sapropel events in the Eastern Mediterranean Sea. *Palaeogeogr. Palaeocl.* **291**, 267-285.

Mo, T., Suttle, A. D., and Sackett, W. M., 1973. Uranium concentrations in marine sediments. *Geochim. Cosmochim. Acta* **37**, 35-51.

Moller, T., Schulz, H., Hamann, Y., Dellwig, O., and Kucera, M., 2012. Sedimentology and geochemistry of an exceptionally preserved last interglacial sapropel S5 in the Levantine Basin (Mediterranean Sea). *Mar. Geol.* **291-294**, 34-48.

Montoya-Pino, C., Weyer, S., Anbar, A. D., Pross, J., Oschmann, W., van de Schootbrugge, B., and Arz, H. W., 2010. Global enhancement of ocean anoxia

during Oceanic Anoxic Event 2: A quantitative approach using U isotopes. *Geology* **38**, 315-318.

Morford, J. L. and Emerson, S., 1999. The geochemistry of redox sensitive trace metals in sediments. *Geochim. Cosmochim. Ac.* **63**, 1735-1750.

Morford, J. L., Martin, W. R., and Carney, C. M., 2012. Rhenium geochemical cycling: Insights from continental margins. *Chem. Geol.* **324**, 73-86.

Murray, J. W., Jannasch, H. W., Honjo, S., Anderson, R. F., Reeburgh, W. S., Top, Z., Friederich, G. E., Codispoti, L. A., and Izdar, E., 1989. Unexpected Changes in the Oxic Anoxic Interface in the Black-Sea. *Nature* **338**, 411-413.

Murray, J. W., Top, Z., and Özsoy, E., 1991. Hydrographic properties and ventilation of the Black Sea. *Deep-Sea Res. Pt. A* **38**, S663-S689.

Nägler, T. F., Neubert, N., Böttcher, M. E., Dellwig, O., and Schnetger, B., 2011. Molybdenum isotope fractionation in pelagic euxinia: Evidence from the modern Black and Baltic Seas. *Chem. Geol.* **289**, 1-11.

Nägler, T. F., Siebert, C., Lüschen, H., and Böttcher, M. E., 2005. Sedimentary Mo isotope record across the Holocene fresh–brackish water transition of the Black Sea. *Chem. Geol.* **219**, 283-295.

Nakamura, N., 1974. Determination of REE, Ba, Fe, Mg, Na and K in carbonaceous and ordinary chondrites. *Geochim. Cosmochim. Acta* **38**, 757-775.

Neretin, L. N., Böttcher, M. E., Jörgensen, B. B., Volkov, II, Lüschen, H., and Hilgenfeldt, K., 2004. Pyritization processes and greigite formation in the advancing sulfidization front in the Upper Pleistocene sediments of the Black Sea. *Geochim. Cosmochim. Ac.* **68**, 2081-2093.

Neubert, N., Nägler, T. F., and Böttcher, M. E., 2008. Sulfidity controls molybdenum isotope fractionation into euxinic sediments: Evidence from the modern Black Sea. *Geology* **36**, 775-778.

Nijenhuis, I. A., Bosch, H. J., Sinninghe Damsté, J. S., Brumsack, H.-J., and De Lange, G. J., 1999. Organic matter and trace element rich sapropels and black shales: a geochemical comparison. *Earth Planet. Sci. Lett.* **169**, 277-290.

Nijenhuis, I. A., Brumsack, H.-J., and De Lange, G. J., 1998. The trace element budget of the eastern Mediterranean during Pliocene sapropel formation. *Proc. Ocean Drill. Program. Sci. Results* **160**, 199-206.

Östlund, H. G., 1974. Expedition "Odysseus 65": Radiocarbon age of Black Sea deep water. In: Degens, E. T. and Ross, D. A. Eds.), *The Black Sea - Geology, Chemistry, and Biology*. Memoirs of the American Association of Petroleum Geologists, Tulsa, U.S.A.

Özsoy, E. and Ünlüata, Ü., 1997. Oceanography of the Black Sea: a review of some recent results. *Earth-Sci. Rev.* **42**, 231-272.

Pakhomova, S. V., Hall, P. O. J., Kononets, M. Y., Rozanov, A. G., Tengberg, A., and Vershinin, A. V., 2007. Fluxes of iron and manganese across the sediment-water interface under various redox conditions. Elsevier Science Bv.

Passier, H. F., Bosch, H.-J., Nijenhuis, I. A., Lourens, L. J., Böttcher, M. E., Leenders, A., Sinnignghe Damsté, J. S., de Lange, G. J., and de Leeuw, J. W., 1999.

Sulphidic Mediterranean surface waters during Pliocene sapropel formation. *Nature* **397**, 146-149.

Piper, D. Z. and Calvert, S. E., 2011. Holocene and late glacial palaeoceanography and palaeolimnology of the Black Sea: Changing sediment provenance and basin hydrography over the past 20,000 years. *Geochim. Cosmochim. Acta* **75**, 5597-5624.

Planavsky, N., Bekker, A., Rouxel, O. J., Kamber, B., Hofmann, A., Knudsen, A., and Lyons, T. W., 2010. Rare Earth Element and yttrium compositions of Archean and Paleoproterozoic Fe formations revisited: New perspectives on the significance and mechanisms of deposition. *Geochim. Cosmochim. Acta* **74**, 6387-6405.

Poulson Brucker, R. L., McManus, J., Severmann, S., and Berelson, W. M., 2009. Molybdenum behavior during early diagenesis: Insights from Mo isotopes. *Geochem. Geophy. Geosys.* **10**, 1-25.

Poulson, R. L., Siebert, C., McManus, J., and Berelson, W. M., 2006. Authigenic molybdenum isotope signatures in marine sediments. *Geology* **34**, 617-620.

R-Development-Core-Team, 2011. R: Language and Environment for Statistical Computing. R Foundation for Statistical Computing, Vienna, Austria.

Reitz, A., Thomson, J., de Lange, G. J., and Hensen, C., 2006. Source and development of large manganese enrichments above eastern Mediterranean sapropel S1. *Paleoceanography* **21**, 17.

Repeta, D. J., 1993. A High-Resolution Historical Record of Holocene Anoxygenic Primary Production in the Black-Sea. *Geochim. Cosmochim. Acta* **57**, 4337-4342.

Repeta, D. J. and Simpson, D. J., 1991. The Distribution and Recycling of Chlorophyll, Bacteriochlorophyll and Carotenoids in the Black-Sea. *Deep-Sea Res. Pt. A* **38**, S969-S984.

Rinna, J., Warning, B., Meyers, P. A., Brumsack, H.-J., and Rullkotter, J., 2002. Combined organic and inorganic geochemical reconstruction of paleodepositional conditions of a Pliocene sapropel from the eastern Mediterranean Sea. *Geochim. Cosmochim. Ac.* **66**, 1969-1986.

Rohling, E. J., Grant, K., Hemleben, C., Siddall, M., Hoogakker, B. A. A., Bolshaw, M., and Kucera, M., 2008. High rates of sea-level rise during the last interglacial period. *Nat. Geosci.* **1**, 38-42.

Rohling, E. J., Hopmans, E. C., and Damste, J. S. S., 2006. Water column dynamics during the last interglacial anoxic event in the Mediterranean (sapropel S5). *Paleoceanography* **21**.

Rona, E. and Joensu, O., 1974. Uranium geochemistry in Black Sea. In: Degens, E. T. and Ross, D. A. Eds.), *The Black Sea - Geology, Chemistry, and Biology*. Memoirs of the American Association of Petroleum Geologists, Tulsa, Oklahoma, U.S.A.

Ross, D. A. and Degens, E. T., 1974. Recent sediments of the Black Sea. In: Degens, E. T. and Ross, D. A. Eds.), *The Black Sea - Geology, Chemistry, and Biology*.

Memoirs of the American Association of Petroleum Geologists, Tulsa, Oklahoma, U.S.A.

Ross, D. A., Uchupi, E., Prada, K. E., and MacIlvane, J. C., 1974. Bathymetry and microtopography of Black Sea. In: Degens, E. T. and Ross, D. A. Eds.), *The Black Sea - Geology, Chemistry, and Biology*. Memoirs of the American Association of Petroleum Geologists, Tulsa, Oklahoma, U.S.A.

Ruddiman, W. F., Cline, R. M. L., Hays, J. D., Prell, W. L., Moore, T. C., Kipp, N. G., Molfino, B. E., Denton, G. H., Hughes, T. J., Balsam, W. L., Brunner, C. A., Duplessy, J.-C., Fastook, J. L., Imbrie, J., Keigwin, L. D., Kellogg, T. B., McIntyre, A., Matthews, R. K., Mix, A. C., Morley, J. J., Shackleton, N. J., Streeter, S. S., and Thompson, P. R., 1984. The last interglacial ocean. *Quaternary Res.* **21**, 123-224.

Rullkötter, J., 2006. Organic Matter: The Driving Force for Early Diagenesis. In: Schulz, H. and Zabel, M. Eds.), *Marine Geochemistry*. Springer, Berlin.

Russell, A. D., Emerson, S., Nelson, B. K., Erez, J., and Lea, D. W., 1994. Uranium in Foraminiferal Calcite as a Recorder of Seawater Uranium Concentrations. *Geochim. Cosmochim. Acta* **58**, 671-681.

Ryan, W. B. F., Major, C. O., Lericolais, G., and Goldstein, S. L., 2003. Catastrophic flooding of the Black Sea. *Annu. Rev. Earth Planet. Sci.* **31**, 525-554.

Ryan, W. B. F., Pitman, W. C., Major, C. O., Shimkus, K., Moskalenko, V., Jones, G. A., Dimitrov, P., Gorur, N., Sakinc, M., and Yuce, H., 1997. An abrupt drowning of the Black Sea shelf. *Mar. Geol.* **138**, 119-126.

Sangiorgi, F., Dinelli, E., Maffioli, P., Capotondi, L., Giunta, S., Morigi, C., Principato, M. S., Negri, A., Emeis, K. C., and Corselli, C., 2006. Geochemical and micropaleontological characterisation of a Mediterranean sapropel S5: A case study from core BAN89GCO9 (south of Crete). *Palaeogeogr. Palaeocl.* **235**, 192-207.

Schauble, E. A., 2007. Role of nuclear volume in driving equilibrium stable isotope fractionation of mercury, thallium, and other very heavy elements. *Geochim. Cosmochim. Acta* **71**, 2170-2189.

Scheiderich, K., Zerkle, A. L., Helz, G. R., Farquhar, J., and Walker, R. J., 2010. Molybdenum isotope, multiple sulfur isotope, and redox-sensitive element behavior in early Pleistocene Mediterranean sapropels. *Chem. Geol.* **279**, 134-144.

Schnetger, B., 1997. Trace element analysis of sediments by HR-ICP-MS using low and medium resolution and different acid digestions. *Fresen. J. Anal. Chem.* **359**, 468-472.

Schnetger, B., Brumsack, H. J., Schale, H., Hinrichs, J., and Dittert, L., 2000. Geochemical characteristics of deep-sea sediments from the Arabian Sea: a high-resolution study. *Deep-Sea Res. Pt. II* **47**, 2735-2768.

Severmann, S., Johnson, C. M., Beard, B. L., and McManus, J., 2006. The effect of early diagenesis on the Fe isotope compositions of porewaters and authigenic minerals in continental margin sediments. *Geochim. Cosmochim. Acta* **70**, 2006-2022.

Severmann, S., Lyons, T. W., Anbar, A., McManus, J., and Gordon, G., 2008. Modern iron isotope perspective on the benthic iron shuttle and the redox evolution of ancient oceans. *Geology* **36**, 487-490.

Sholkovitz, E. R., Landing, W. M., and Lewis, B. L., 1994. Ocean Particle Chemistry - the Fractionation of Rare-Earth Elements between Suspended Particles and Seawater. *Geochim. Cosmochim. Acta* **58**, 1567-1579.

Siebert, C., Nagler, T. F., von Blanckenburg, F., and Kramers, J. D., 2003. Molybdenum isotope records as a potential new proxy for paleoceanography. *Earth Planet. Sci. Lett.* **211**, 159-171.

Sinninghe Damsté, J. S., Rijpstra, W. I. C., Deleeuw, I. W., and Schenck, P. A., 1988. Origin of Organic Sulfur-Compounds and Sulfur-Containing High Molecular-Weight Substances in Sediments and Immature Crude Oils. *Org. Geochem.* **13**, 593-606.

Sinninghe Damsté, J. S., Wakeham, S. G., Kohnen, M. E. L., Hayes, J. M., and Deleeuw, J. W., 1993. A 6,000-year sedimentary molecular record of chemocline excursions in the Black Sea. *Nature* **362**, 827-829.

Soulet, G., Ménot, G., Lericolais, G., and Bard, E., 2011. A revised calendar age for the last reconnection of the Black Sea to the global ocean. *Quaternary Sci. Rev.* **30**, 1019-1026.

Stanev, E. V., 1990. On the Mechanisms of the Black-Sea Circulation. *Earth-Sci. Rev.* **28**, 285-319.

Sturchio, N. C., Antonio, M. R., Saderholm, L., Sutton, S. R., and Brannon, J. C., 1998. Tetravalent uranium in calcite. *Science* **281**, 971-973.

Suzuki, R. and Shimodaira, H., 2011. pvclust. CRAN R-Projekt.

Swart, P. K. and Hubbard, J. A. E. B., 1982. Uranium in Scleractinian Coral Skeletons. *Coral Reefs* **1**, 13-19.

Tatsumoto, M. and Goldberg, E. D., 1959. Some Aspects of the Marine Geochemistry of Uranium. *Geochim. Cosmochim. Ac.* **17**, 201-208.

Taylor, S. R. and McLennan, S. M., 1985. *The continental crust: its composition and evolution*. Blackwell, Oxford.

Thomson, J., Higgs, N. C., Croudace, I. W., Colley, S., and Hydes, D. J., 1993. Redox zonation of elements at an oxic/post-oxic boundary in deep-sea sediments. *Geochim. Cosmochim. Ac.* **57**, 579-595.

Thomson, J., Higgs, N. C., Wilson, T. R. S., Croudace, I. W., de Lange, G. J., and van Santvoort, P. J. M., 1995. Redistribution and geochemical behaviour of redox-sensitive elements around S1, the most recent eastern Mediterranean sapropel. *Geochim. Cosmochim. Ac.* **59**, 3487-3501.

Thomson, J., Jarvis, I., Green, D. R. H., Green, D. A., and Clayton, T., 1998. Mobility and immobility of redox-sensitive elements in deep-sea turbidites during shallow burial. *Geochim. Cosmochim. Acta* **62**, 643-656.

Thomson, J., Mercone, D., De Lange, G. J., and Van Santvoort, P. J. M., 1999. Review of recent advances in the interpretation of eastern Mediterranean sapropel S1 from geochemical evidence. *Mar. Geol.* **153**, 77-89.

Torres, M. E., Brumsack, H.-J., Bohrmann, G., and Emeis, K.-C., 1996. Barite fronts in continental margin sediments: A new look at barium remobilization in the zone of sulfate reduction and formation of heavy barites in diagenetic fronts. *Chem. Geol.* **127**, 125-139.

Triantaphyllou, M. V., Antonarakou, A., Dimiza, M., and Anagnostou, C., 2010. Calcareous nannofossil and planktonic foraminiferal distributional patterns during deposition of sapropels S6, S5 and S1 in the Libyan Sea (Eastern Mediterranean). *Geo-Mar. Lett.* **30**, 1-13.

Tribovillard, N., Algeo, T. J., Lyons, T., and Riboulleau, A., 2006. Trace metals as paleoredox and paleoproductivity proxies: An update. *Chem. Geol.* **232**, 12-32.

Turner, C., 2000. The Eemian interglacial in the North European plain and adjacent areas. *Geol. Mijnbouw - N. J. G.* **79**, 217-231.

Turon, J. L., 1984. Direct Land Sea Correlations in the Last Interglacial Complex. *Nature* **309**, 673-676.

Tzedakis, P. C., Frogley, M. R., and Heaton, T. H. E., 2003. Last Interglacial conditions in southern Europe: evidence from Ioannina, northwest Greece. *Global Planet. Change* **36**, 157-170.

Usher, J. L. and Supko, P., 1978. Initial Reports of the Deep Sea Drilling Project

U.S. Government Printing office, Washington D.C.

van der Meer, M. T. J., Sangiorgi, F., Baas, M., Brinkhuis, H., Damste, J. S. S., and Schouten, S., 2008. Molecular isotopic and dinoflagellate evidence for Late Holocene freshening of the Black Sea. *Earth Planet. Sci. Lett.* **267**, 426-434.

Verleye, T. J., Mertens, K. N., Louwye, S., and Arz, H. W., 2009. Holocene Salinity Changes in the Southwestern Black Sea: A Reconstruction Based on Dinoflagellate Cysts. *Palynology* **33**, 77-100.

Warning, B. and Brumsack, H.-J., 2000. Trace metal signatures of eastern Mediterranean sapropels. *Palaeogeogr. Palaeocl.* **158**, 293-309.

Wedepohl, K. H., 1991. Chemical composition and fractionation of the continental crust. *Geol. Rundsch.* **80**, 207-223.

Wehausen, R. and Brumsack, H.-J., 1999. Cyclic variations in the chemical composition of eastern Mediterranean Pliocene sediments: a key for understanding sapropel formation. *Mar. Geol.* **153**, 161-176.

Wehausen, R. and Brumsack, H. J., 1998. The formation of pliocene Mediterranean sapropels: constraints from high-resolution major and minor element studies. *Proc. Ocean Drill. Program. Sci. Results* **160**, 207-217.

Weldeab, S., Emeis, K. C., Hemleben, C., Schmiedl, G., and Schulz, H., 2003a. Spatial productivity variations during formation of sapropels S5 and S6 in the Mediterranean Sea: evidence from Ba contents. *Palaeogeogr. Palaeocl.* **191**, 169-190.

Weldeab, S., Siebel, W., Wehausen, R., Emeis, K. C., Schmiedl, G., and Hemleben, C., 2003b. Late Pleistocene sedimentation in the Western Mediterranean Sea: implications for productivity changes and climatic conditions in the catchment areas. *Palaeogeogr. Palaeocl.* **190**, 121-137.

Westerhausen, L., Poynter, J., Eglinton, G., Erlenkeuser, H., and Sarnthein, M., 1993. Marine and Terrigenous Origin of Organic-Matter in Modern Sediments of the Equatorial East Atlantic - the Delta-C-13 and Molecular Record. *Deep-Sea Res. Pt. I* **40**, 1087-1121.

Weyer, S., Anbar, A. D., Gerdes, A., Gordon, G. W., Algeo, T. J., and Boyle, E. A., 2008. Natural fractionation of U-238/U-235. *Geochim. Cosmochim. Acta* **72**, 345-359.

Wijsman, J. W. M., Middelburg, J. J., and Heip, C. H. R., 2001. Reactive iron in Black Sea sediments: implications for iron cycling. *Mar. Geol.* **172**, 167-180.

Wilkin, R. T. and Arthur, M. A., 2001. Variations in pyrite texture, sulfur isotope composition, and iron systematics in the Black Sea: Evidence for Late Pleistocene to Holocene excursions of the O-2-H2S redox transition. *Geochim. Cosmochim. Acta* **65**, 1399-1416.

Wilkin, R. T., Arthur, M. A., and Dean, W. E., 1997. History of water-column anoxia in the Black Sea indicated by pyrite framboid size distributions. *Earth Planet. Sci. Lett.* **148**, 517-525.

Yanko-Hombach, V., Gilbert, A. S., and Dolukhanov, P., 2007. Controversy over the great flood hypotheses in the Black Sea in light of geological, paleontological, and archaeological evidence. *Quatern. Int.* **167**, 91-113.

Zheng, Y., Anderson, R. F., Van Geen, A., and Fleisher, M. Q., 2002a. Preservation of particulate non-lithogenic uranium in marine sediments. *Geochim. Cosmochim. Acta* **66**, 3085-3092.

Zheng, Y., Anderson, R. F., Van Geen, A., and Fleisher, M. Q., 2002b. Remobilization of authigenic uranium in marine sediments by bioturbidation. *Geochim. Cosmochim. Acta* **66**, 1759-1772.

# Danksagung

Als erstes möchte ich Prof. Dr. Hans-Jürgen Brumsack dafür danken, dass er es mir ermöglicht hat in einem so spannenden Bereich der Geochemie zu arbeiten und unter seiner Leitung diese Arbeit zu verfassen. Des Weiteren gilt mein Dank Dr. Bernhard Schnetger, der mir immer mit Rat, Tat und konstruktiver Kritik zur Seite stand und mich in die Geheimnisse der instrumentellen Analytik eingeweiht hat.

Zudem möchte ich Prof. Dr. Stefan Weyer für die freundliche Übernahme des zweiten Gutachtens und die Gastfreundschaft in seiner Arbeitsgruppe danken.

Des Weiteren danke ich Dr. Jürgen Köster und Dr. Silke Severmann, sowie allen anderen Kooperationspartnern für die gute Zusammenarbeit. Darüber hinaus danke ich der DFG (IODP SPP) für die finanziellen Unterstützung.

Mein besonderer Dank gilt der gesamten Arbeitsgruppe Mikrobiogeochemie und der Arbeitsgruppe Organische Geochemie für die tolle gemeinsame Zeit und die tägliche Unterstützung bei diesem Projekt. Und für die Unterstützung über den Alltag hinaus danke ich der selbsternannten "Geochemischen Familie", die sich über die Jahre in eine Richtige verwandelt hat. Was wäre ich nur ohne euch: Dr. Thomas Riedel, Ann-Katrin Meinhard, Patrick Monien, Dr. Christian März, Angelika Klugkist, Jörn Logemann, Dr. Melanie Beck, Tanja Badewien, Dr. Donata Monien, Dr. Michael Seidel und Dr. Philipp Böning.

Dr. Martina Nullmeier danke ich für ihre starken Nerven, da sie über die Jahre immer zu mir gehalten, an mich geglaubt und mir mein Leben versüßt hat.

Ein großer Dank gilt auch allen meinen Freunden, insbesondere Gordon Schroeder und Carsten Wendt, die dafür gesorgt haben, dass ich nicht komplett an dieser Arbeit eingehe.

Ganz besonders danke ich meinen Eltern und meiner Oma dafür, dass sie immer für mich da waren, mich gefördert haben und mich in allen Lebenslagen unterstützt haben.

Danke!

# Curriculum vitae

Persönliche Daten

| | |
|---|---|
| Name | Sebastian Eckert |
| Geburtstag | 22.08.1982 |
| Staatsangehörigkeit | deutsch |
| Anschrift | Hermannshof 1, 36251 Bad Hersfeld |
| Email | s.eckert@uni-oldenburg.de |

Schulbildung

| | |
|---|---|
| 1995 - 2002 | Gymnasium an der Willmsstraße in Delmenhorst<br>Abschluss: Allgemeine Hochschulreife |
| 1993 - 1995 | Orientierungsstufe West in Delmenhorst |
| 1989 - 1993 | Grundschule Beethovenstraße in Delmenhorst |

Akademischer Werdegang

| | |
|---|---|
| Seit Mai 2008 | Promotionsstudium am Institut für Chemie und Biologie des Meeres, Carl von Ossietzky Universität Oldenburg<br>Thema: "The past and present trace metal budget of the Black Sea – A comparison of the Holocene and Eemian marine ingression" |
| Okt. 2003 – April 2008 | Carl von Ossietzky Universität in Oldenburg, Studienfach „Diplom Chemie“<br>Diplomarbeit: "Ein geochemischer Vergleich von Holozän- und Eem-Sapropelen aus dem Schwarzen Meer"<br>Abschluss: Diplom |

Erklärung:

Hiermit versichere ich, dass ich die vorliegende Arbeit selbstständig angefertigt und keine anderen als die angegebenen Quellen und Hilfsmittel verwendet habe. Zusätzlich erkläre ich, dass diese Dissertation weder in ihrer Gesamtheit noch in Teilen einer anderen wissenschaftlichen Hochschule zur Begutachtung in einem Promotionsverfahren vorliegt oder vorgelegen hat.

Oldenburg, den 11.07.2014

Sebastian Eckert